NTNU – Trondheim
Norwegian University of
Science and Technology

Physical investigation of slamming loads on a 2D body

Pauline Kværnes Øien

Marine Technology
Submission date: June 2015
Supervisor: Marilena Greco, IMT

Norwegian University of Science and Technology
Department of Marine Technology

ABSTRACT

In this thesis a physical investigation of the slamming loads on a two-dimensional body is performed. It includes an experimental analysis of a drop test performed at MARINTEK's laboratories on a wedge shaped section in two-dimensional flow conditions. Due to confidentiality, the experiment will only be referred to as 'the MARINTEK experiment'. From a former analysis of the experimental results at MARINTEK, deviations between measurements and theoretically predicted impact loads were found. The need for a further investigation of the involved features was announced. A search for an explanation for these deviations is the motivation behind this thesis. This task is demanding, and experienced researchers have already made an attempt of explaining the observed behaviour.

A rigid wedge with a mass of 170 kg and a deadrise angle of 10° was dropped from three drop heights: 0.1, 0.25 and 0.5 m. Pressure, force and position were measured. The accelerometers were not set up during the experiments so the acceleration data files proved to be empty. Velocity derived from position measurements was used instead. The pressure sensors are mounted on the force panel.

All data from the tests have been available and analysed in Matlab. Features of the measured pressure and force for different drop heights were analysed. The observed features are compared to theoretical predictions. Measurement techniques and applicability limits of theoretical models were studied as a background for the discussion of deviations between theory and measurements. Other slamming experiments were also studied to be aware of common challenges and for comparison with results from the MARINTEK experiment.

Differences between measured data and theoretically predicted results were found. Wagner's theory (1932) was used for comparison. Spatial distribution of maximum pressures and pressure coefficients showed values differing from the prediction by Wagner. A discrepancy between integrated pressure and force measurements over the panel was found. This occurred for the lowest drop height only. It was found that the lowest drop height showed the largest deviations from theoretical predictions in most of the analyses made.

Various effects that can affect the results were assessed. The change in velocity was investigated, but it was concluded that the small changes in velocity are not capable of causing the observed behaviour. Hydroelasticity was considered, but no indications of it occurring were found in the analyses. Three-dimensional effects are also considered, but from the test set-up they are not likely to occur. As a last solution, total error estimates for the peak pressure and maximum pressure coefficient were made. The deviations from the theoretical predictions were found to be inside this error range. For the discrepancy between force and integrated pressure, the results from the performed analyses indicated

that it is a combination of measurement errors from force and pressure sensors. It is suspected that the force measurements for 0.1 m drop height show values above the true ones.

Negative pressures reoccurred before the rise to peak pressure for all drop heights. It is concluded that this is most likely due to air being trapped in the curvature of the sensor front. A small increase in pressure was observed before the negative drop. This can be explained by the air being compressed initially (causing the rise in pressure), and when the cavity collapses, it causes the negative pressure.

The repeatability of pressure and force measurements for all drops at each drop height was investigated. It was found that the peak pressures are of a stochastic nature, which is expected. The repeatability of the force measurements was satisfying for 0.5 and 0.25 m drop height. A better repeatability is expected for the force measurements as they are not as sensitive to small changes in local quantities as the pressure. For 0.1 m drop height, a poor repeatability was found for the force measurements. This supports the hypothesis of an error in the force measurements for this drop height. Linear or non-linear dependence on drop height was evaluated for different slamming parameters. A non-linear dependency was observed for the pressure coefficient, slamming pressure duration and rise time of the pressure.

The data from the MARINTEK experiment were compared to the results of another experiment with a 10° wedge. It was discovered that the experiment used for comparison was performed with three-dimensional flow conditions. The comparison indicated that three-dimensional effects cause a large decrease in peak pressure as well as a quicker decrease in impact velocity.

Different theoretical models were evaluated to reproduce the main features of the MARINTEK experiment. The deadrise angle will not set a limitation for the choice of theoretical model. Including variation in velocity was not considered necessary. Including gravity was considered beneficial, as it will give realistic results for a longer time scale. The most efficient model to meet these requirements is the generalized Wagner method (Zhao et al. 1996). Wagner's theory (1932) is recommended as a conservative estimate for peak pressures. This argues that the theoretical model is not the reason for the observed differences between measured pressure peaks and Wagner's estimates.

Possibilities for a further study are considered limited, as all available information from the MARINTEK experiment is already gathered. If flow visualization of a drop test with the same sensor type (Kulite CT-190) is available, the explanation for negative pressures may be verified. It is also suggested that a more in depth error analysis is carried out. This would increase the understanding of the measurement errors assumed to be the explanation for the differences between theoretical predictions and experimental results.

SAMMENDRAG

I denne oppgaven vil en undersøkelse av slamming laster under todimensjonale forhold bli presentert. Hovedfokuset er en eksperimentell analyse av en drop test av en stiv kile, utført av MARINTEK. Grunnet konfidensialitet vil eksperimentet kun bli referert til som "MARINTEKs eksperiment". Data fra forsøket har tidligere blitt evaluert av forskere ved MARINTEK. De fant avvik mellom målte resultater og forventede resultater fra teoretiske modeller. Grunnet dette er det et behov for en videre analyse av data fra forsøket. Å finne forklaringer på de observerte avvikene fra teorien er hovedmålet med denne oppgaven.

En stiv kile med en vekt på 170 kg og angrepsvinkel på 10° ble sluppet fra høyder på 0,1, 0,25 og 0,5 m. Trykk, kraft og posisjon ble målt under slippet. Det viste seg at datafilene som skulle inneholde akselerasjonsmålingene var tomme, da akselerometre ikke var festet på kilen. Hastigheten til kilen er derfor brukt isteden. Trykk- og kraftsensorer er festet på kilens høyre side.

All data fra forsøket har vært tilgjengelig, og har blitt analysert ved hjelp av programvaren Matlab. Karakteristiske verdier for trykk og kraft har blitt analysert for de forskjellige slipp-høydene. Verdiene ble deretter sammenliknet med forventede verdier fra teoretiske modeller. Mulige feilkilder, både for eksperimentelle målinger og for bruk av teoretiske modeller, har blitt studert for videre drøfting av avvik mellom teori og målte resultater. Andre slammingeksperimenter har blitt studert for å øke kunnskapen om typiske utfordringer og for sammenlikning med MARINTEKs eksperiment.

Det ble funnet avvik mellom teori og målinger for MARINTEKs eksperiment. Teorien valgt for sammenlikning var Wagners teori (1932). Fordelingen av maksimum trykk og trykk-koeffisient over kilen viste avvik fra teorien. Integrert trykk over kraftpanelet ble sammenliknet med kraftmålingene. For den laveste slipphøyden ble det observert et stort avvik mellom de to. Generelt sett var det den laveste slipp-høyden som viste størst avvik fra teoretiske estimater.

Flere mulige effekter ble vurdert som grunn til de observerte avvikene. En endring i hastighet ble vurdert, men det ble konkludert med at avvikene ikke kunne forklares med en hastighetsendring. Hydroelastisitet og tredimensjonale effekter ble vurdert, men ingen tegn på påvirkning fra disse effektene ble funnet i analysene som ble gjort. Til sist ble feil i målingene vurdert. Et estimat for den totale målefeilen på maksimum trykk og trykk-koeffisient ble utarbeidet. Avvikene mellom teori og målinger viste seg å være innenfor intervallet av mulig målefeil. For avviket mellom integrert trykk og målt kraft antydet resultatene fra analysene at det er en kombinasjon av målefeil i trykk- og kraftsensorer. Det kan virke som om kraftmålingene for 0,1 m slipp-høyde er over de virkelige verdiene.

Negative trykk gjentok seg før trykket steg til maksimum trykk for alle slipp-høyder. Den beste forklaringen på dette er luft som blir fanget i den buede formen på trykksensorens overflate. Før trykkfallet ble det observert en liten økning i trykk. Dette kan forklares ved at luften blir komprimert i det sensoren treffer vannoverflaten (som fører til en trykkøkning), før luftboblen kollapser og fører til det negative trykket.

Repeterbarheten til trykk- og kraftmålinger ble undersøkt. Verdien for maksimalt trykk viste seg å være stokastisk. Repeterbarheten til kraftmålingene var tilfredsstillende for 0,5 og 0,25 m slipp-høyde. Det var forventet at repeterbarheten til kraftmålingene skulle være bedre enn for trykket. Trykktoppene er veldig følsomme for små endringer i lokale parametere, hvilket ikke kraften på kilen er i samme grad. For 0,1 m slipp-høyde var repeterbarheten for kraften ikke tilfredsstillende. Dette underbygger hypotesen om feilmålinger av kraft for den laveste slipp-høyden. Ikke-lineær oppførsel av målte parametere ble undersøkt. En ikke-lineær sammenheng med slipp-høyde ble funnet for trykk-koeffisient, varighet av slamming-trykk og stigningstiden til trykktoppene.

Dataene fra MARINTEKs eksperiment ble sammenliknet med resultater fra en annen drop test av en kile med 10° angrepsvinkel. Underveis i analysen ble det klart at dette eksperimentet var tredimensjonalt. Sammenlikningen viste at trykktoppene ble kraftig redusert av tredimensjonale effekter.

Forskjellige teoretiske modeller ble undersøkt for å vurdere hvilken som best kunne gjenskape resultatene fra MARINTEKs eksperiment. Det ble fastsatt at angrepsvinkelen ikke vil sette en grense for hvilken teori som kan bli brukt. Mulighet for å inkludere en variasjon i hastighet ble heller ikke vurdert som nødvendig. Derimot ble det konkludert å være gunstig å kunne inkludere tyngdekraften i den teoretiske modellen. Dette kan gi realistiske resultater for et lenger tidsintervall. Den mest effektive modellen som kan møte disse kravene er den generaliserte Wagner-teorien av Zhao et al. (1996). Wagners teori (1932) er anbefalt hvis konservative estimater for trykktoppene er ønsket.

Det er ikke store muligheter for videre arbeid på denne oppgaven. All data fra forsøket har allerede blitt mottatt og analysert. Om det hadde blitt gjort filmopptak av et annet forsøk med den samme typen trykksensorer (Kulite CT-190), kunne kanskje hypotesen om årsaken til de negative trykkene blitt verifisert. Det foreslås også at en mer grundig feilanalyse av trykk- og kraftmålinger blir gjort. Dette vil kunne bedre forståelsen for feilmålingene som til nå er den beste forklaringen funnet på avvikene mellom målinger og forventede verdier fra teorien.

SCOPE OF WORK

NTNU Trondheim
Norwegian University of Science and Technology
Faculty of Engineering Science and Technology
Department of MarineTechnology

MASTER THESIS IN MARINE TECHNOLOGY

SPRING 2015

FOR

Pauline Øien

Physical investigation of slamming loads on a 2D body
(Fysisk undersøkelse av slamming last på et 2D legeme)

Slamming is a nonlinear phenomenon connected with liquid-structure impact. It can be dangerous for the local structural integrity but also have consequences on the global elastic behavior of the body. It is important both for ships and offshore structures, as well as in coastal engineering. Its occurrence depends on the local structure-fluid relative motion and its features are affected by the local geometry in the impact region, as well as on the kinematic and dynamic conditions at the impact. In the case of ships, the cross-sections are mostly U/V shaped. Therefore it is relevant to study the slamming of 2D circular/wedge shapes to understand the physics. The project thesis has investigated the available literature on theoretical, experimental and numerical investigations carried out along the years with emphasis on 2D cases but also accounting for 3D studies. The classical Wagner theory was compared against available experiments in 2D conditions. Present master thesis will further examine those experiments and possibly others so to discuss relevant features of the phenomena on the basis of an in-depth analysis.

Objective
The aim of the thesis is to investigate the features connected with slamming by means of the analysis of available model tests in 2D flow conditions.

The work should be carried out in steps as follows:

1. Summarize major findings/outcomes from the project thesis.
2. Perform a literature investigation of measurement techniques and sensors used within experimental studies and discuss advantages and issues connected with accuracy and errors.

3. Perform the analysis of the 2D experiments on a wedge in free falling conditions identified during the project thesis. Use information from local pressures and integrated loads and water-entry conditions (velocities) of the body. Examine the features of pressure peaks, rises and duration of high pressures for different impact velocities and other parameters modified in the tests. Discuss comparatively integrated pressures and force measurements.
4. Taking the experiments in item 3, investigate repeatability of the different parameters and possible stochastic behaviour of the local quantities and discuss these aspects in the context of previous available physical studies. Examine nonlinear features in the slamming phenomena.
5. Discuss available 2D wedge experiments in similar conditions as in the studies at items 3 and 4 and compare the two physical studies in terms of general features of involved body accelerations during the water entry phase and of the local pressures measured along the body. Using the data from the two tests, make an attempt of an explanation of the phenomena relevant for the recorded features also on the basis of what studied from the literature during the project thesis.
6. Using findings from item 5, discuss theoretical model/s needed to properly reproduce the main features of the observed phenomena with the attempt of preserving as much as possible efficiency.

The work may show to be more extensive than anticipated. Some topics may therefore be left out after discussion with the supervisor without any negative influence on the grading.

The candidate should in her report give a personal contribution to the solution of the problem formulated in this text. All assumptions and conclusions must be supported by mathematical models and/or references to physical effects in a logical manner.

The candidate should apply all available sources to find relevant literature and information on the actual problem.

The thesis should be organised in a rational manner to give a clear presentation of the work in terms of exposition of results, assessments, and conclusions. It is important that the text is well written and that tables and figures are used to support the verbal presentation. The thesis should be complete, but still as short as possible. In particular, the text should be brief and to the point, with a clear language. Telegraphic language should be avoided.

The thesis must contain the following elements: the text defining the scope (i.e. this text), preface (outlining project-work steps and acknowledgements), abstract (providing the summary), table of contents, main body of thesis, conclusions with recommendations for further work, list of symbols and acronyms, references and (optional) appendices. All figures, tables and equations shall be numerated.

The supervisor may require that the candidate, in an early stage of the work, present a written plan for the completion of the work. The plan should include budget for the use of computer and laboratory resources that will be charged to the department. Overruns shall be reported to the supervisor.

From the thesis it should be possible to identify the work carried out by the candidate and what has been found in the available literature. It is important to give references to the original source for theories and experimental results.

Supervisor :Marilena Greco
Submitted :16 January 2015
Deadline :10 June 2015

Marilena Greco
Supervisor

PREFACE

This thesis is a result of the individual work carried out in the spring of 2015, January 16^{th} to June 10^{th}. It is a required part of the degree Master of Science with specialization in Hydrodynamics at the Norwegian University of Science and Technology (NTNU). The work is conducted with Professor Marilena Greco as supervisor.

The topic for this thesis was proposed by involved engineers from the industry during the spring of 2014. An experimental investigation of a drop test from MARINTEK is the main focus of this thesis. Differences between predicted impact loads and experimental results have been found by researchers at MARINTEK.

Searching for explanations for the observed differences has been challenging and time consuming, but also very interesting and educational. Both researchers at MARINTEK and engineers from the industry have concluded that the differences need to be studied further. No explanation have yet been established by these experienced researchers. The continued search for such explanations have therefore proved to be demanding. Regardless, the process has provided me with valuable experience and I hope that my contribution can help increase the understanding of the deviations from theoretical models.

I would like to thank Kjetil Berget at MARINTEK for answering my questions regarding the experiment and Claudio Lugni from CNR-INSEAN for sharing his valuable experience with slamming experiments. A special thanks is given to my supervisor Marilena Greco. I am very grateful for all the help and guidance she has given me throughout my last year at NTNU. She has been inspiring, shown interest in my work and supported me through this whole process.

At last I would like to thank my friends and family. They have been a great support and a source of motivation.

Pauline Kværnes Øien
Trondheim, June 10^{th}, 2015

Contents

List of Figures

List of Tables

List of Abbreviations

2D	: Two-dimensional
3D	: Three-dimensional
BEM	: Boundary Element Method
FFT	: Fast Fourier Transform
LP	: Low Pass
MARINTEK	: Norsk Marinteknisk Forskningsinstitutt
ms	: millisenconds

List of Symbols

Greek

Ω	: volume of submerged body
β	: deadrise angle
μ	: mean of N measurements
ρ	: mass density of water.
ϕ	: velocity potential
σ	: standard deviation

Latin

A_{33}	: high frequency added mass in heave
B	: breadth of body at instantanous intersection of body and free surface
C_p	: pressure coefficient
$C_{p_{\max}}$	: pressure coefficient at maximum pressure
F_3	: total vertical hydrodynamic force
F_3^{2D}	: two-dimensional vertical hydrodynamic force
$F_{3_{\max}}$	: maximum vertical slamming force
L	: length of body at instantanous intersection of body and free surface
$H(f)$	: transfer function
ΔS_s	: spatial extent of slamming pressure
N	: number of repeated tests
T	: total time of measurement recording
V	: vertical velocity of the wedge
V_0	: initial impact velocity

b_n	: bits used to store each data sample
$c(t)$	: wetted length
f_{3D}	: cut-off frequency
f_c	: cut-off frequency
f_N	: Nyquist frequency
f_s	: sampling frequency
g	: gravitational accleration
h	: drop height
h_s	: interval between samples
m	: body mass
p	: pressure
p_0	: atmospheric pressure
$p_{\max}$	: maximum pressure
$p_{\min}$	: minimum pressure
t	: time
x, y, z	: coordinates on wedge surface
x_a	: horizontal coordinate of start of force panel on wedge surface
x_b	: horizontal coordinate of end of force panel on wedge surface
$y_{\max}$	: y-coordinate of maximum pressure
$z_{\max}$	: z-coordinate of maximum pressure

1

INTRODUCTION

Slamming (water impact) is important in the design of both ships and offshore structures. It is defined by impulse loads with high localised pressure peaks. Examples of situations where slamming occur can be a ship bottom hitting water with high velocity, waves breaking upon platform columns or blunt transom sterns hitting waves. It has caused many serious accidents and damages, also in the recent years. This may be part of the motivation behind the large amount of papers written on the subject.

Both analytical and numerical methods have been developed throughout time to estimate the slamming loads. The first paper presented on the topic was the publication of von Karman in 1929. A few years later (1932), Wagner presented a paper with what is probably the most well-known theory on slamming. His method is still used today, both as a basis for other theories and for relatively simple estimates. After the pioneering work by von Karman and Wagner, several other methods have been presented. Among these is the similarity solution by Dobrovol'skaya (1969). She used a similarity flow to solve the two-dimensional impact on a symmetric body. Zhao and Faltinsen (1993) used a boundary element method to solve the problem. In the later time, computational fluid dynamics has also been applied to water impact problems. As for most theories within hydrodynamics, model testing is needed for validation. Model testing is also important to gain increased understanding of the involved features of the slamming phenomenon.

The most frequently applied experiment is the drop test of a body onto an initially flat free surface. When the body is blunt, the pressure peaks become very high and localised in both time and space. The time scale of the impact loads on a rigid body entering water is typically in the range of milliseconds. Many difficulties can be encountered during such experiments. The small spatial extent and short time duration of the pressure peaks set a high level of requirements for the measurement system and the sensors. Influence of vibrations of the test rig and a varying impact velocity have also proved to be difficult to avoid. Despite these challenges drop tests have been performed for over 60 years (Kapsenberg 2011).

The focus of this thesis is an experimental investigation of a drop test performed at MARINTEK's laboratories on a two-dimensional wedge shaped section. Due to confidentiality, the experiment will not be referred to as other than 'MARINTEK's drop test/experiment'. Both force and pressure on the wedge surface was measured. These quantities, as well as the velocity development during impact will be studied with the aim of increasing the understanding of the involved features. All data from the drop tests have been available and investigated with use of Matlab.

Prior to this work, the experimental results from MARINTEK's drop test have been assessed by researchers at MARINTEK. They observed a difference between the measured and theoretically predicted impact loads. From this observation, the need

for a further investigation of the involved features was announced. An analysis will be carried out, evaluating the correspondence with theoretical predictions. The intent of this thesis is to investigate different effects that might cause the deviations that are found.

Many effects can lead to deviations from theoretically predicted impact loads. The theoretical model used will have limits that may not apply to the experiment. There can also be errors in the instruments used for measurements, in the test set-up or in the experimental procedure carried out. Possible error sources and challenges will be studied on the basis of the available literature on theoretical models for impact loads, slamming experiments and measurement techniques.

The thesis consists of seven more chapters containing, in short, the following:

- **Chapter 2:** A presentaion of previous theoretical and experimental studies on slamming.
- **Chapter 3:** A literature study on measurement techniques and challenges met when performing a drop test.
- **Chapter 4:** An analysis of the two-dimensional drop test of a wedge shaped section performed at MARINTEK's laboratories.
- **Chapter 5:** An investigation of the repeatability and behaviour of measured local quantities of the drop test from MARINTEK.
- **Chapter 6:** A comparison with a similar drop test performed by Yang et al. (2007).
- **Chapter 7:** A discussion of theoretical models suited to reproduce the main features of the drop test from MARINTEK.
- **Chapter 8:** Conclusions and recommendations for further work.

2

THEORETICAL AND EXPERIMENTAL STUDIES

In experimental research, the compliance between theory and experiment is often an important aspect. A project thesis was written the previous semester as a preparation for this thesis, studying available theoretical and experimental research on slamming loads from the literature. In this chapter, the findings considered relevant for this thesis will be presented shortly. In the project thesis, the applicability limits of different analytical and numerical theories on slamming were studied. This is of importance when a comparison is made between theoretical predictions and measured impact loads in this thesis. Theories together with their applicability limits will therefore be presented. A summary of some previously performed slamming experiments studied in the project thesis will be given. The focus is the challenges met when the aim is to reflect theoretical assumptions in the experimental set-up.

2.1 ANALYTICAL AND NUMERICAL STUDIES ON SLAMMING

The first method presented to tackle the problem of slamming was the work of von Karman (1929). His method was intended for the impact of seaplane floats during landing on water. Wagner (1932) presented his method three years later, and this is probably the most well known paper on the subject of slamming. He used a flat plate approximation to estimate the slamming loads, meaning the body is modelled as a flat plate based on the assumed body boundary conditions. His asymptotic theory is applicable for blunt bodies, i.e. small local deadrise angles. Unlike von Karman, Wagner included the local rise up of water along the body during impact. Both methods give conservative estimates of the slamming pressure. Several methods have been developed after the pioneering work by von Karman and Wagner.

A method for determining the slamming loads for the two-dimensional vertical water entry of a symmetric body was developed by Dobrovol'skaya (1969) using a similarity solution. She considered two-dimensional irrotational similarity flows with dimensionless hydrodynamic characteristics and established an accurate gravityless solution. The method is valid for wedge shaped sections and can be used to verify other theories.

Zhao and Faltinsen (1993) solved the two-dimensional water entry problem using a boundary element method (BEM). When investigating small deadrise angles, it is difficult to handle the intersection between the body and the free surface numerically. This is because a small error in the estimation of the angle between the body and the free surface will result in large errors in the prediction of the intersection and therefore destroy the solution. Zhao and Faltinsen avoided this by introducing a control surface

normal to the body surface at the spray root. This method is applicable to a range of body shapes and varying impact velocity with time can be included.

Zhao et al. (1996) also used a BEM to make a two-dimensional generalized Wagner method that proved to be more robust for engineering applications than the classical Wagner theory (1932). The method is generalized to larger local deadrise angles than what Wagner's asymptotic solution allows. The main difference from Wagner's theory (1932) is that the exact body boundary condition is satisfied at each time instant. The wetted body surface is found by a time integration of the fluid particles vertical velocities on the free surface to find the particles intersection with the body surface. Wagner also did this, but analytically for the simplified geometry of a flat plate.

Three-dimensional methods are also developed, among these are the methods presented by Scolan and Korobkin (2001) and Faltinsen and Chezhian (2005), both based on the Wagner-theory. Faltinsen and Chezhian (2005) presented a theory that makes it possible to use the generalized Wagner method for an arbitrary three-dimensional body. Scolan and Korobkin (2001) studied the impact of a three-dimensional body with an elliptical contact line by using the Wagner approach.

2.1.1 Applicability of analytical and numerical methods

Theoretical and numerical methods are often verified by comparison with experimental results, and vice versa. For the comparison to be successful, it is important that the experiment reflects the theoretical assumptions. The theoretical assumptions will lead to a set of applicability limits. If the experiment does not meet these limits, the theoretical predictions cannot be expected to agree with measured data. The applicability limits of the theories presented in the previous section will be discussed in the following.

All the presented theoretical models are based on the assumptions of a rigid body and potential flow of an incompressible fluid. The assumption of incompressibility requires that the impact velocity cannot be too high. If it is, compressible effects can be of concern. In the initial stage of the water entry, compressible effects will matter. Due to the body acting on the water a wave will be generated with the speed of sound, propagating from the body surface due to this disturbance. This means the pressure reach a maximum value being the acoustic pressure. For the classical Wagner method (1932) the pressure goes to infinity as $Vt \to 0$ because the compressibility is neglected and the pressure will not be limited to the acoustic pressure as it is supposed to. This will mostly be a problem close to the centreline where the initial stage takes action. Further away from the centreline the effect of neglecting compressibility will not be as important.

When no air entrapment is assumed, this implicates that the deadrise angle cannot be too small. Takemoto (1984) and Yamamoto et al. (1984) presented experimental results for the pressure on wedges with common experimental errors accounted for. The results showed to be in good agreement with Wagner's (1932) theory for deadrise angles between $\approx 3°$ and $15°$. A reason for the disagreement when $\beta <\approx 3°$ is the air that can be entrapped between body and fluid for such small deadrise angles. When a volume of air is enclosed, this air can start oscillating due to air compressibility, which again will lead to pressure oscillations. It can also lead to a secondary impact as the cavity will collapse after some time, and the whole surface will become wet (Faltinsen 2010).

Gravity is neglected in most of the methods presented, because fluid accelerations are

much larger than the gravitational acceleration during initial impact. However, this only holds if the time scale involved is sufficiently small. After some time, gravitational effects can matter. Neglecting gravity leads to the surface condition $\phi = 0$. This means that the surface is flat. Neglecting gravity means we do not include any radiation damping, hydrostatic and non-linear Froude-Kriloff forces. This is fine as long as the considered time scale is small.

The assumption of no flow separation is also present in the theoretical models. Here it is not viscous flow separation that is considered, but non-viscous. This can happen for example at a sharp corner, and the assumption of no flow separation will therefore put limitations on the shape of the body. When the body is asymmetric, the flow will separate at the apex leading to the development of a vortex. This vortex will increase the velocities and hence lower the pressure. The non-viscous flow separation can also happen on a curved body surface, such as a horizontal circular cylinder. Wang (2014) concludes that the separation occurs in the jet because the particles in the jet tip moves in a curved tail. The centripetal acceleration will work normal to the jet flow into the body surface. To meet this pressure gradient, the pressure on the wetted surface near the jet tip must be lower than atmospheric pressure. This can lead to air entering the area, causing the pressure gradient to be too low and the jet tip will tangentially move away from the body.

The three-dimensional theories presented are important for many practical applications, but not many attempts have been made for dealing with arbitrary shaped three-dimensional bodies. The two-dimensional theories are therefore important for design and research of structures exposed to slamming loads. For the body to be considered two-dimensional in an experiment the body is restricted to a cross-section (or an infinite cylinder). The flow around the body should be as close to two-dimensional as possible. If these conditions are not properly met, three-dimensional effects can occur and produce results that deviate from the intended two-dimensional results.

In table 2.1 different theoretical models are compared with respect to their applicability limits. In this thesis, Wagner's theory (1932) will be used for comparison with experimental data. As gravity is neglected in his theory, it is important to be aware of the limited time duration where the theory can provide reliable results. It is also noted that Wagner (1932) assume a constant water entry velocity.

Table 2.1 – Comparison of the applicability limits of theoretical models. β = deadrise angle, Asym. = possible to apply theory to asymmetric body shape.

	Body Shape	β	2D/3D	Gravity incl.	Asym.
Wagner's solution	Arbitrary	$3° \leq \beta \leq 15°$	2D	No	No
Similarity solution	Wedge	$4° \leq \beta \leq 81°$	2D	No	No
BEM	Arbitrary	$2 - 3° \leq \beta \leq 81°$	2D	Yes	No
Generalized Wagner	Arbitrary	$\beta < 40°$	2D	Yes	Yes
Inversed Wagner	Elliptical plane	$3° \leq \beta \leq 15°$	3D	No	No
Generalized Wagner 3D	Arbitrary	$\beta < 40°$	3D	Yes	Yes

2.2 IMPLEMENTATION OF CLASSICAL WAGNER THEORY

During the project thesis, a Matlab code was developed to find the pressure distribution and generate pressure time series from classical Wagner theory (1932). The codes can be found in appendix A, and are used for comparison with experimental data in this thesis. The basis for the implementation was the composite solution presented by Armand and Cointe (1986) and Cointe (1991). The details of the implementation will not be presented here.

The implemented code provides valid results for small deadrise angle, and β is the only input needed to run the code. An example for $\beta = 4°$ is shown in figure 2.1, where the implemented code is verified by plotting it together with the plot found in the lecture notes by Faltinsen (1997). The comparison is satisfying. There are small deviations present near the peak. This might be due to the method used to digitalise the plotted graph of the results from paper, which will not be as exact as wanted.

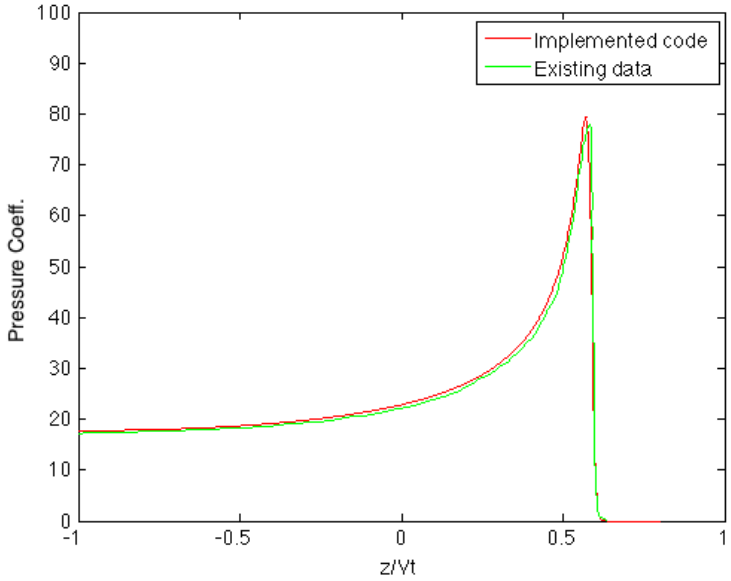

Figure 2.1 – Pressure distribution from implemented code compared with existing results for $\beta = 4°$.

The code to generate pressure time series can be used for wedge shaped sections. The input needed to run the code is the vertical position of pressure sensors and the drop height. This code uses the spatial pressure coefficient distribution shown in 2.1 to calculate the pressure over each sensor with time.

2.3 EXPERIMENTAL STUDIES ON SLAMMING

An experimental analysis is an important aspect of this thesis. To get a better understanding of the procedure and typical challenges met, three different slamming experiments are studied from the literature. Two of them are drop tests of two-dimensional wedges and one is a three-dimensional drop test of a wedge shaped body. The experiments together with their major findings will be shortly presented in the following.

Yettou et al. (2005) reported an experiment studying the pressure distribution on a wedge upon water entry. The influence of drop height, deadrise angle and wedge mass on the pressure distribution was examined. An important aspect of their experiment was the influence of the varying wedge velocity through impact. They found that the wedge mass did not affect the initial impact velocity, but during water entry an increased mass led to a smaller deceleration. The deceleration was found to be inversely proportional to the deadrise angle. For the pressure distribution, they reported that the pressure coefficient increased with decreasing deadrise angle, while the influence of varying drop height and wedge mass was negligible.

Tveitnes et al. (2008) developed a test rig to maintain constant water entry velocity for drop tests of two-dimensional wedges. They used their experimental results for comparison with CFD analyses and other theoretical estimates from the literature. Unfortunately, keeping the wedge velocity constant proved to be challenging. Significant dynamic noise caused by the wedge surface and rig drive system affected the measurements. It proved to be demanding to keep the velocity constant as a result of the rapid increase in wet chines entry force.

Chezhian (2003) performed a three-dimensional experiment aiming to maintain a nearly constant velocity during water entry by giving the body a very large structural mass. The experimental results were used to verify a numerical simulation for three-dimensional impact covered in the same publication. He found a good agreement between numerical estimates and experimental results. Many different error sources were considered. For the pressure time series, he found that the experimental results were in general on the lower side of the numerical prediction. This was most likely due to the sensor area being larger than the spatial extent of the pressure peak, which made the sensors measure an average value instead of the correct peak value. He also found that hydroelasticity might have reduced the measured pressure.

2.3.1 Comments on experimental challenges

From the experiments presented above, some general comments can be made regarding challenges met when investigating the water entry problem. They are all connected to a comparison between theory and experiments, due to the assumptions made in theoretical approximations. How these assumptions are met in practice is an important aspect to keep in mind when evaluating such comparisons.

The first comment concerns the impact velocity, which is assumed constant in many theories such as those of Wagner (1932), Dobrovol'skaya (1969) and Faltinsen and Chezhian (2005). Experiments like the one by Yettou et al. (2005) demonstrate that the velocity is often changing throughout the impact. Tveitnes et al. (2008) showed that keeping the velocity constant can be difficult, even when the test rig is designed for this purpose. Faltinsen (1990) states that the vertical force is dependent on the impact

velocity and Chezhian (2003) argues that using the initial impact velocity in theoretical methods can lead to an underestimation of the impact loads. This is if the velocity is decreasing during water entry. Yettou et al. (2005) argues that a variation of impact velocity can change the spatial pressure distribution from the theoretical prediction.

Another assumption in many theories is two-dimensionality. To ensure two-dimensionality the body is restricted to a cross section (or an infinite cylinder). Faltinsen and Zhao (1998) compared the maximum pressure coefficient for a wedge and a cone. A cone represents the extreme case of three-dimensional flow while a wedge cross section represents a two-dimensional case. From this comparison they found that three-dimensional effects can cause the pressure loading to decrease with up to 50 %. A cone is an extreme case so a smaller reduction is expected for other body shapes. Even so, this states the significance of defining two- or three-dimensionality when experiment and theory are compared.

Structural vibrations are a common problem for drop tests. Dynamic disturbances can in the worst case destroy the data, as it partly did for Tveitnes et al. (2008). Structural vibrations may also be connected with hydroelasticity. If hydroelasticity occur, the assumption of a rigid body is no longer valid. For Chezhian (2003), it reduced the recorded pressures. Hydroelastic behaviour will be discussed briefly in the following.

2.3.1.1 Hydroelasticity

Hydroelasticity will not be discussed in detail here, but should be mentioned, as it can be relevant for slamming experiments. Hydroelasticity is excited when the highest wet natural period of the structure is comparable to or higher than the loading time of the slamming. Other natural periods can also matter, but it is often the highest one that is excited. Hydroelasticity is a dynamic interaction between structure and fluid. The hydrodynamic loads from the impact can affect the structural vibrations, which again can start elastic vibrations. These vibrations will disturb the fluid and can generate pressure oscillations. Physical effects such as compressibility and air cushions may be relevant if hydroelasticity is excited.

Different physical effects related to slamming have different time scales. When the slamming problem is analysed from a structural point of view the time scale of the maximum stresses is the important scale and is given by the highest wet natural period of the structure. This implies that air cushions and compressibility have a small effect since the time scale for these are smaller than the structural one.

When the deadrise angle is small (typically $\beta < 5°$), hydroelasticity must be considered (Faltinsen 2010). The importance of hydroelasticity increases as the impact velocity and the highest natural period of the structure increase. When hydroelasticity is not excited, a quasi-static approach can be used. This means that the hydrodynamic loads are calculated for a rigid body and then used for the structural analysis. For the cases where hydroelasticity takes place, it is not possible to separate the hydrodynamic and structural problem as they interact. This coupling leads to impact pressure and dynamics that can vary highly from the quasi-static solution.

3

MEASUREMENT TECHNIQUES

In the previous chapter, factors that can affect the consistency between theoretical models and experimental data were discussed. Lack of this consistency is not the only possible reason for deviations between theoretical model and measurements. A drop test will set high standards for the instrumentation used. The instrumentation and experimental set-up can represent potential error sources, and will therefore be studied in this chapter.

A slamming experiment is not an easy experiment. The impact on a rigid body entering water is short, typically only milliseconds. The parameters of interest during this short time period undergo rapid changes. Quick variation of pressure in space and time has proved to be challenging to measure. In this chapter, the measurement techniques and data acquisition tools that can be applied to a slamming experiment will be presented. Advantages and challenges in terms of the accuracy and errors will be discussed in the context of a typical drop test of a two-dimensional body. Factors in the experimental performance and test set-up that can influence the measurements will also be examined. Most of the theory presented in this chapter is collected from Steen (2014), Das (2009) and Van Nuffel et al. (2013).

3.1 INSTRUMENTATION

For a typical slamming experiment, a variety of instrumentation is needed to examine the phenomenon properly. The choice of instrumentation depends on what features of the slamming phenomenon the experiment focuses on. In this section, a range of instruments will be presented. Potential challenges met when applying them to a slamming experiment will be discussed.

3.1.1 Transducer principles: displacement and strain

For strain and displacement transducers, three principles are governing and can be used to split the transducer into different groups. The transducer groups are resistive-, inductive- and capacitance transducers. These principles can also be used in force and pressure transducers, accelerometers and for velocity measurements.

Resistive transducers

Resistive transducers are based on a change in resistance due to some external physical signal. The most common type of resistive transducer is the potentiometer type. It is based on a direct correlation between the electrical and mechanical domain, where the mechanical movement changes a part of the total potentiometer resistance.

Another well-known resistive transducer is based on the change of resistance due to strain, by using strain gauges. The strain gauges measure strain as change in electrical resistance. The elongation of the strain gauge causes the change in resistance. The rate of change in resistance per change of length (elongation) depends on the material used. Hence, a more or less sensitive strain gauge can be formed by the choice of material. A Wheatstone bridge circuit (figure 3.1) can measure the change in resistance. The strain gauge occupies one of the resistances in the bridge circuit. In the other arms of the bridge the resistances are known, and balances so that the voltage difference between B and D is zero. When the strain gauge is elongated, it will cause a change in strain that changes the resistance. The resistance difference between B and D will be non-zero and proportional to the change in resistance and thereby proportional to the change in strain. This unbalance will lead to a voltage output. By measuring this change in voltage, the strain can be measured.

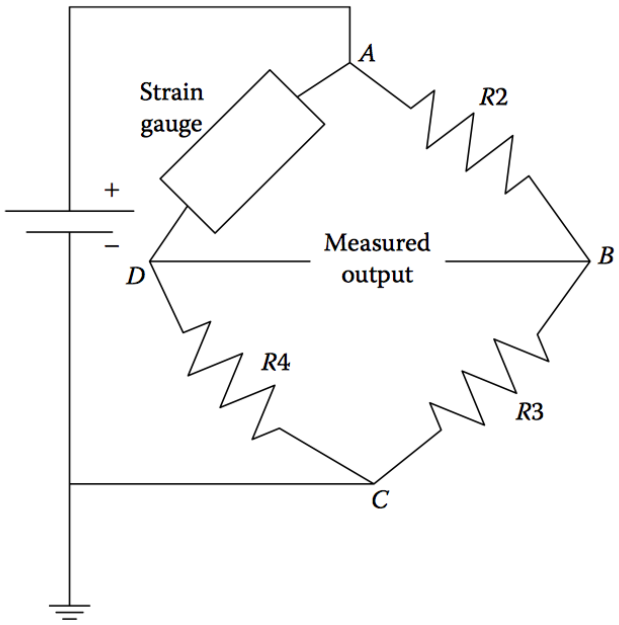

Figure 3.1 – Wheatstone bridge circuit. (Das 2009)

Inductive transducers

Inductive transducers work on the principle of magnetic induction of voltage. The transducer must consist of a conductor and a magnetic field. A relative movement between the two will induce a voltage in the conductor. As a movement causes this, they are limited to dynamic measurements, but can be used in pressure cells, force transducers, velocity measurements and accelerometers.

Capacitance transducers

A capacitance transducer is based on the change of capacitance between two parallel plates or a plate attached between a pair of outer plates (figure 3.2). As the plates are conductive, relative movement between them generates a change in capacitance. The relative movement is caused by an external disturbance, marked by F in the figure. These transducer types only require a small driving force, but can cause some noise. They are also very sensitive to liquids, which can increase the capacitance significantly (Das 2009).

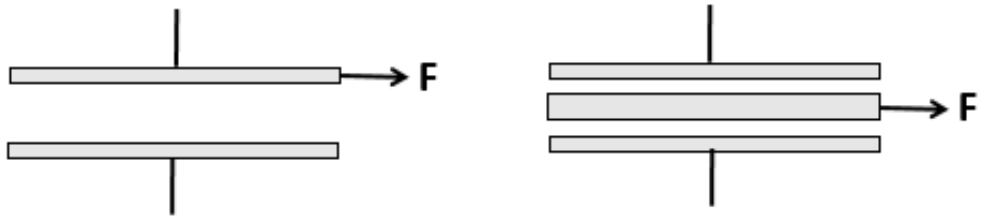

Figure 3.2 – Capacitance transducers for displacement measurements. (Steen 2014)

3.1.2 Pressure measurements

Pressure is an important parameter for a drop test. During impact, the pressure will go through rapid changes in both time and space. The choice of pressure transducer depends on the requirements associated with the phenomena under investigation. For dynamic response such as slamming, the transducers resonance frequency and rise time is important. This will be discussed in more detail. Pressure transducers can be classified according to the technology they are based on. The three most common types will be described shortly.

3.1.2.1 Pressure transducers

Piezoelectric pressure cells

Piezoelectric behaviour means that an electric charge can be induced in a material due to the impact of a force. An example of such a material is quartz crystal. Piezoelectric crystals will generate an electrical charge due to the deformation caused by an external applied pressure. The electrical charge can be converted into volts and will be proportional to the applied pressure. These pressure cells are only applicable for dynamic measurements as the charge will disappear after a while if a constant compressive force is applied. Piezoelectric pressure cells can be made very stiff and can therefore be characterized by high resonance frequencies. They also have a very short response time, which makes them capable of measuring high frequency pressure pulses. This sensor type is shown in figure 3.3.

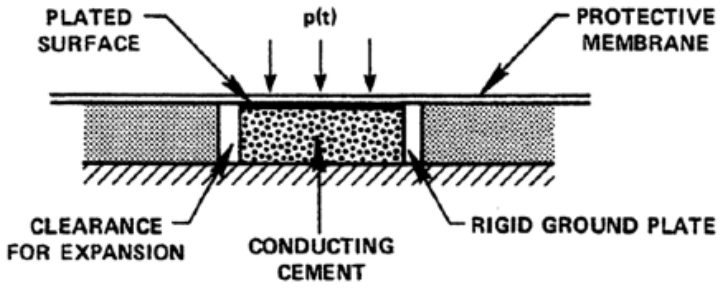

Figure 3.3 – Piezoelectric pressure cell. (Steen 2014)

Capacitance pressure cell

A variable capacitance transducer, such as the one shown in figure 3.4, works on the technology of a change in capacitance due to an external pressure. The capacitance will change due to a varying distance between a metal diaphragm and a fixed metal

plate. Capacitance pressure cells are generally quite stable and linear, but they can be sensitive to high temperatures and are more complicated to set up than other sensor types.

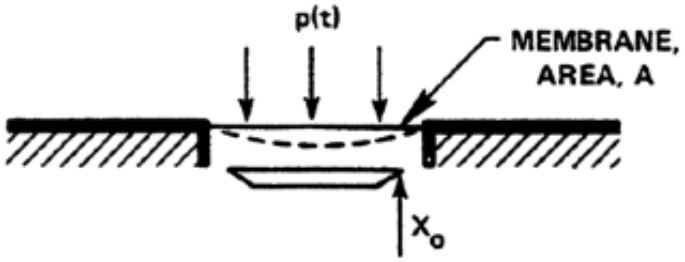

Figure 3.4 – Capacitance pressure cell. (Steen 2014)

Piezoresistive pressure cells
Strain based pressure cells may be the most frequently used type and depend on strain gauges to measure the pressure. This type of pressure cells can also be referred to as piezoresitive pressure sensors. The strain is measured in the same way as described in the section on resistive transducers by applying a Wheatstone bridge. As shown in figure 3.5 the strain gauge is placed on a diaphragm that is elastic and works as a seal. A deflection of the diaphragm will cause an elongation of the strain gauge that will be transformed to an output voltage by the Wheatstone bridge. These types of pressure sensors come in several different varieties dependent on the type of strain gauge used.

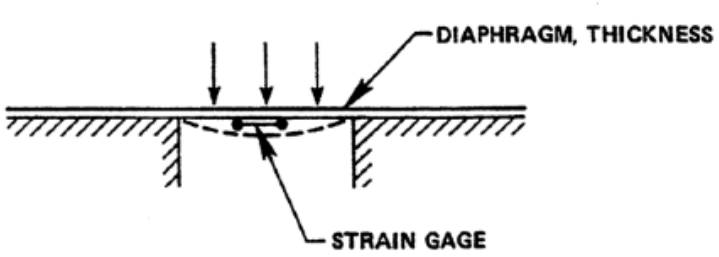

Figure 3.5 – Strain gauge pressure cell. (Steen 2014)

Pressure sensing tape
Pressure sensing films have been developed in the later years. The film is an elastic film that can be taped to the surface and is equipped with many small pressure sensors. It is based on the principle of change in conductivity by the applied external pressure using a semi-conductive material. By taping this type of film on the body, the pressure distribution can easily be obtained.

3.1.2.2 Pressure measurements: Potential challenges

Slamming is a dynamic impact and great variation of the pressure occurs both in time and space. A challenge is to correctly measure the peak pressure which duration is in the order of milliseconds or less. This leads to a requirement for the data sampling rate, as the measurements must be frequent enough to catch the real pressure peak. For a zero deviation between the real and measured value the pressure must be sampled at the exact time of the peak pressure's occurrence. When the sampling rate is too low, the measured maximum pressure may vary between two identical drops (with stochastic behaviour disregarded). This is because the pressure peak can be situated anywhere between two subsequent samples. The largest deviation will take place when the peak is placed exactly in the middle of two samples. A sufficiently high sampling rate should therefore be applied, although a large sampling rate will lead to large data files.

The pressure pulses travel quickly over the body surface during a slamming event. The spatial extent of the pressure peak is small, and the pressure sensor area should be designed according to this. If the sensor area is too large it will measure the average pressure value over its area instead of the exact pressure peak leading to a loss of local details.

Pressure transducers can be exposed to a temperature shock during water entry due to a temperature difference between air and water. Van Nuffel et al. (2013) investigated the effect of such a temperature shock on piezoelectric sensors. After the first pressure peak, the pressure was found to drift away in both positive and negative direction. An explanation was found in the thermal nature of the sensor materials where a preloaded piezoelectric crystal is situated in a steel housing. The thermal expansion coefficient of the crystal is 20 times smaller than for steel. This causes the steel to expand/contract more than the crystal during a sudden change in temperature. For a sudden cooling, the steel housing will contract more than the crystal causing an increased preloading of the crystal that will be interpreted as a positive pressure output signal. For a sudden heating, the steel will expand more, causing a negative pressure output signal. To avoid such effects one can either make the air/water temperature difference very small or adjust the sensors to the water temperature before the water impact. Piezoresistive pressure sensors can also experience a temperature shock as the sensor front gets heated from an electric current that is applied through the sensor front. This can cause a temperature shock even when water and air have the same temperature.

In general, pressure sensors should be used only for measurements with response frequencies well below the resonance frequency of the pressure sensor. As the rise time of the pressure is in the order of milliseconds, a very high resonance period for the sensor is required to avoid dynamic amplification.

The position of the pressure sensor surface relative to the body surface may have a significant effect on the pressure measurements if they are not exactly flushed. There are two cases of such a misalignment: either the sensor is sticking out of the body or it is slightly inside the body surface. In both cases, it can lead to air being trapped along the sensor edge or a change in the flow field around the sensor. Van Nuffel et al. (2013) found that the peak pressure was significantly decreased for both cases compared to the peak pressure when sensor and body were exactly flushed. There are also sensors where the sensor surface itself is not entirely flat which may also affect the pressure recordings.

3.1.3 Force measurements

For a slamming experiment, the investigation of forces can be of interest both alone and for comparison with integrated measured pressure. Force transducers are often placed on the body surface in panels to find the load over an area of the body during impact with water. In the same manner as for pressure transducers, force transducers can be classified according to the technology they are based upon. Two common types of force transducers are presented in the following based on the literature of Elbestawi (1998).

3.1.3.1 Force transducers

Strain based force sensors

These types of force transducers are based on a structure that will easily deform under the influence of an external load. Attached to this structure are a number of strain gauges that will produce an electrical signal when connected to a Wheatstone bridge. The force is determined by integrating the strain of each individual strain measurement. The elastic element can have many shapes depending on the wanted capacity, dimension and performance. Possible shapes are cantilever beam, S-beam or circular cylinders. A requirement for the elastic material is a linear relationship between applied force and strain. Strain load cells can have a load capacity ranging from 5 N to more than 500 MN.

The beam type is an example of an elastic element. It consists of a simple cantilever beam with strain gauges attached to it. The strain gauges are oriented along the axis of the beam and will elongate when the elastic beam is subject to an external load and bends. The sensitivity and force range depend on the shape of the beam cross section and the position of the loading across the beam length.

Piezo-electric force sensors

The properties of piezoelectric crystals are already explained. An electrical charge will develop when a force deforms the crystal. This sensor type can measure forces ranging from 1 to 200 kN. By using a pre-tensioned bolt on the sensor it is capable of measuring both compressive and tensile forces. The electrical charge will leak, and if the load is not subject to change it will fade. Therefore, piezoelectric force sensors are suited for dynamic measurements. They can also operate in a wide temperature range.

3.1.3.2 Force measurements: Potential challenges

In a typical slamming experiment, a drop test rig is used together with the impacting body. Combined, they form a complex dynamic system. Resonance frequencies of test rig, impacting body and force sensors can affect the force measurements and may cause noise or disturbances. If resonance occurs in the force sensor, the force output signal can be frequency dependent. If the vibrations are severe, they can destroy the measurements.

For strain based force sensors, the shape of the elastic element can affect the reliability of the results. Some element types will provide the best accuracy when the loading is perpendicular. For a drop test with a body that has an angle, the loads will not be perpendicular. Another possible challenge can be oscillations in many degrees of freedom. When many degrees of freedom are activated as response in the force panel, accuracy can be lost when converting the signal back to the actual loading (P. B. Berntsen 2015, pers. comm., 9 May).

3.1.4 Position, Velocity and Acceleration measurements

For position, velocity and acceleration measurements it is often sufficient to measure one of them and derive or integrate the two other quantities from the data obtained. Sometimes it is of interest to measure one or more quantities individually. Tracking the position of the body after it is dropped can be valuable as it describes in which phase of the water entry the body is at each time instant. When evaluating time series of measured pressure or force, the corresponding position gives a better understanding of what is happening at a certain time during impact.

Position can be measured directly by for example a potentiometer. Voltage is generated as a wiper slides against a resistive element. The wiper is connected to a mechanical shaft or wire that can either move linearly or rotate. In this way, a potentiometer can measure both displacement in a straight line or angular movement. A potentiometer is a quite inexpensive and common position transducer, but noise may occur due to vibrations during the relative movement. To eliminate this noise data should be filtered accordingly.

During impact with water, the body may experience a change in velocity. When the weight of the body is larger than the maximum slamming force, the body will decelerate after initial water entry. The velocity can influence the vertical force as well as the pressure distribution. Many numerical and analytical theories assume constant water entry velocity. Data of the velocity development can help interpret potential discrepancies between theory and experiment. Velocity can easily be derived from position measurements from instruments such as a potentiometer. Another method to measure a linear velocity is to measure the average velocity from distance travelled over a certain time interval. Today the availability of high-speed video cameras with up 12000 frames per second broadens the range of applicable velocities (Pinney and Baker 1998). The average speed can be found for a sequence of positions by knowing the length scale and flash rate of the camera. Using a video camera will also provide a practical visualisation of the water entry process.

The time change of the intersection point between free surface and body is considered an important parameter for slamming. Wave gauge tape can be used to find the intersection points and monitor the change in wetted surface with time. They work on the principle of their resistance changing with wetted length. The change in resistance can be measured by using a voltage source and a voltage driver circuit. The change in wetted surface is an important parameter present in many numerical estimates of slamming loads. A possible error source of using wave gauge tape to find the intersection point is the spray from the jet, which may cause the tape to react before it is affected by the water pileup. It can also be affected by small waves/disturbances of the free surface during initial impact.

Accelerometers can be used to monitor how the body is influenced by impact with water. Acceleration transducers use the relation between acceleration, mass and force $a(t)=F(t)/m$. Accelerometers can be based on the principle of strain gauges or piezoelectricity. For the *strain gauge based accelerometer*, a mass is connected to a beam that will deflect due to inertia forces when accelerated. The strain gauges are used to measure the deflection, which can be used to determine the acceleration. For a *piezo-electricity based accelerometer*, a piezoelectric material is used so a deflection of the material will lead to the generation of an electrical charge. The electric charge will be proportional to applied pressure. The pressure is applied by using a mass that

when accelerated will cause inertia forces which over an area produces a pressure that will deform the material. The charge is converted to a voltage output signal and the acceleration can be measured.

It is in general important to use an accelerometer with a natural frequency well above the oscillation frequency of the measured acceleration. If resonance occurs it may influence the mass which will lead to a frequency dependent output signal. It is also important to note that the accelerometers will add a mass to the structure under consideration, but the mass can be constructed to be very light.

Water velocity measurements
In some cases it can be of interest to investigate the fluid flow along the body during impact. For an asymmetric body there may be flow separation and for very small deadrise angles there is a possibility of air entrapment. Under such scenarios, fluid velocity measurements could be of interest to visualise the details.

Laser Doppler Velocimetry - LDV uses a shift in reflected light frequency to determine velocity and direction of a fluid flow. For this principle to work, light-reflecting particles must be dissolved in the water, but no other sensors are required in the area under investigation. LDV is capable of measuring quick changes in the flow field.

Particle Image Velocimetry - PIV is similar to LDV in the sense that particles must be dissolved to ensure light reflection. The main difference is that LDV measures velocity at one point while PIV measure the velocity in an area. Laser light is shredded by a spreading lens and reflected by the particles. By taking two stereo photographs with a short time interval, the movement of the fluid particles can be tracked. As PIV can map a velocity distribution instead of the velocity at one point, it is more frequently used in the later years than LDV.

3.2 DATA ACQUISITION

This section will provide the reader with insight in basic data acquisition used for slamming experiments. Measurements are needed to gain and verify knowledge and are obtained by the use of instruments. In most experiments a collection of instruments are needed to collect information about the phenomena investigated. Instruments can be both analog and digital. Nowadays, it is common to use digital instruments because of the advantages of computer storage and data handling. However, the transducer or sensor itself is often analog. An analog-to-digital converter is therefore used to convert the analog signals before they are further processed. A typical set up of a data acquisition system is shown in 3.6. There is a transducer or sensor stage, a signal-conditioning stage and an output stage. The analog transducer signals are often conditioned by analog electronics even though they are configured as digital instruments.

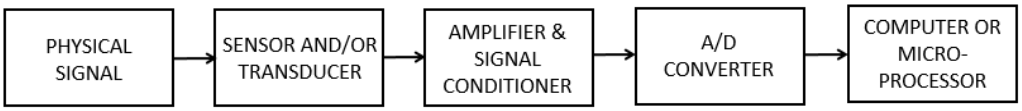

Figure 3.6 – Stages in a typical data acquisition system.

The response ('physical signal', figure 3.6) is affecting the sensor or transducer. A sensor is a device that responds to a changing response while a transducer transfers energy from

on form to another (Eren 2014). The sensor senses the change of the physical signal, while the transducer reacts to the magnitude or intensity of the physical signal that one wants to measure. A typical transducer will have a signal output in the order of microvolts. One of the functions of the signal conditioner is therefore to amplify (scale) this output up to $+/-$ 10 volt range. Other possible functions of a signal conditioner are sampling, filtering, phase shifting or noise elimination.

The process of digitalising an analog transducer signal is performed in the A/D-converter. The A/D-converter can process several signals simultaneously depending on the number of bridges it is equipped with. Thus, a larger sampling frequency implies that a larger number of bridges is required. Experiments that require very high sampling frequencies need special A/D-converters. The resolution of a sample is also an important feature of the converter, meaning how many bits it will use to represent each sample. If the A/D-converter uses 8-bit for representation of a sample it means it will choose the value nearest the $2^8 = 256$ values. This would be characterized as a low resolution A/D-converter. Expensive models use 20-bit, resulting in 1048576 possible values. If a low resolution A/D converter is applied, as much as possible of the range should be used. If this is not the case, there is a risk of ending up with a very low number of possible values, which will result in poor measurements and lost data details. To avoid this one should be aware of the range of values the analog signals from the transducer will have in order to choose the right resolution of the A/D-converter according to this value. When the signal from the transducer is digitalised it can be sent to a computer or microprocessor for storage and processing.

In the following, some important aspects of the data acquisition will be presented, focusing on data sampling and filtering of measured data.

3.2.1 Sampling

A time series is a sequence of observations measured through time, and can be either discrete or continuous. For a continuous time series there would be an infinite amount of observations between two points in time. In most practical cases (as for a slamming experiment) the time series will be discrete, meaning the observations are sampled at equal intervals of time. The size of this time interval must be adjusted to fit the variation in time of the process to be recorded.

If the time interval between each sample is denoted h_s, the sampling frequency can be defined as $f_s = \frac{1}{h_s}$. The higher the sampling frequency, the more data storage capacity is needed. Defining the bits used to store each sample as b_n and the total time of recording T, the data storage needed will be $b_n \cdot f_s \cdot T$. The choice of sampling frequency will therefore be a compromise between a sufficient frequency to catch all details of the process and data storage capacity.

Errors in the recorded signal will occur if the sampling frequency is too low. Figure 3.7 shows an example of a sinusoidal sampled at a frequency $\frac{1}{h_s}$. The resulting measured signal does not properly represent the original signal. The Nyquist theorem, or sampling theorem states that a continuous signal can only be properly sampled if it does not contain frequencies above one-half of the sampling rate. The limit is defined by the Nyquist frequency $f_N = \frac{1}{2h_s}$. This means that to theoretically represent a sine wave properly a sampling frequency of minimum two samples per cycle is needed.

For slamming experiments, a very high sampling frequency is needed. The rise time of

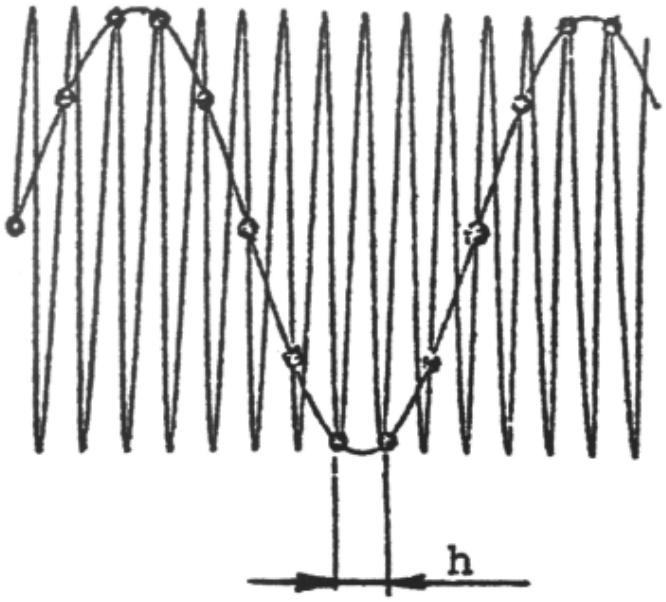

Figure 3.7 – Sinusoidal signal sampled at a frequency $1/h_s$. (Steen 2010)

the pressure is in the order of milliseconds, and the duration of the maximum pressure is in the same order before it starts to decrease. Especially when the deadrise angle is small, a high sampling frequency is required for reliable results. Van Nuffel et al. (2013) suggests a minimum sampling frequency of 300 kHz for small deadrise angles.

3.2.2 Filtering

Filters can be both analog and digital. Analog filters will be applied before the A/D-converter, while digital filters can be applied in computer programs during the post-processing of the time series. Roughly, one can say that there are three types of filters:

- Low pass filters
- High pass filters
- Band pass filters

Before the three types are described, some expressions used will be defined. The transfer function is defined as the ratio between the output and input signal and is denoted $H(f)$. The cut-off frequency is usually defined to be where the signal amplitude is reduced to 0.707 times its original value (Smith, 2002).

The low pass filter will allow low frequencies through and reject frequencies over a cut-off frequency f_c. It can be used to remove high-frequency noise from the time series.

The high pass filter will reject frequencies below a cut-off frequency f_c and allow all frequencies above to pass through. It can be used to remove constant or low frequency values.

The band pass filter will pass a certain range of frequencies between the cut-off frequencies f_{c1} and f_{c2} through and reject all other frequencies above or below this range. It can for instance be used to extract a certain frequency range from the time series.

The frequency values allowed to pass through the filter is often called the pass band, while the frequencies rejected is called the stop band. An illustration of the filter types is shown in figure 3.8.

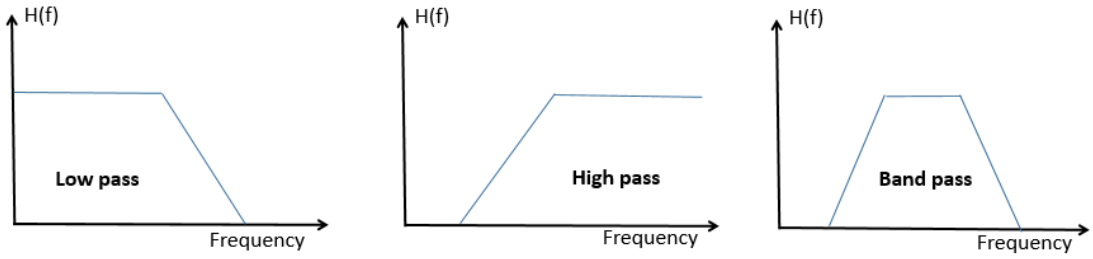

Figure 3.8 – Illustration of filter types.

For a slamming experiment, noise and disturbances from force panels or from the test rig can be present in the recorded signal. To remove noise, a low pass filter can be applied. When applying low pass filters to slamming experiments, care must be taken when setting the cut-off frequency. As the rise time of the force and pressure is in the order of milliseconds, the cut-off frequency must be sufficiently high to preserve it.

3.3 PERFORMANCE AND TEST SET-UP

Many slamming experiments are used for validation of analytical and numerical theories, which are all based upon a set of boundary conditions. It is therefore important to be aware of how the kinematic and dynamic conditions of an experiment match these theoretical assumptions. For validating a theoretical model, the assumptions must be integrated in the experimental set-up. In this section, some aspects that one should be aware of in the performance and test set-up of a slamming experiment will be discussed.

3.3.1 Free surface condition

An initially flat free surface is a common assumption in numerical theories, and it is important to meet this criterion when a comparison with experimental values is performed. Small disturbances/wrinkles on the free surface can cause large deviations in peak pressure. If a small wrinkle appears at the intersection between the body and the free surface during initial impact, it will change the local deadrise angle. A small change in deadrise angle will have a large effect on the pressure peak. This effect will impair the repeatability of the experiment and can occur only on some of the drops when the wrinkle is in the 'right' position. It is therefore important to make sure the surface is completely calm before starting a new measurement.

3.3.2 Body surface condition

During a drop test of a body, several subsequent drops are done, meaning the body is wetted after the first drop. Van Nuffel et al. (2013) compared ten subsequent drops for both a wet and a dry body surface. They found that for the wetted body the average pressure peak was significantly lower and a larger scatter appeared. Lower average pressure is explained by the presence of water droplets on the sensor surface. Coherent forces between the water molecules will cause the water on the sensor and in the tank to merge together right before impact. This will soften the impact loads on the body

surface. The scatter is introduced due to the variability of droplet position between each drop. To avoid these effects it is important to wipe the body and sensors dry between each drop.

3.3.3 Three-dimensional effects

A drop test programme can be either two- or three-dimensional. The two represents completely different scenarios, and distinguishing between them in both test set-up and choice of theoretical model to compare with is important. In practice, two-dimensionality means that the body is restricted to a cross-section (or an infinite cylinder). If the experiment is fully two-dimensional, the aim is to restrict the flow to these two dimensions only. Due to this, it is not only the shape of the body that is important. When the body is dropped into a tank, the ideal condition for a two-dimensional experiment would be no gap at all between the tank and the body. This is not possible as the friction between the tank wall and the body will affect the velocity, and it will not be a 'free fall'. Instead, the gap between the tank wall and the body should be as small as possible to restrict the flow.

4

EXPERIMENTAL INVESTIGATION

An experimental programme was carried out at MARINTEK to investigate the free-fall drop of a two-dimensional wedge into initially calm water. The aim of the test was a qualification of the force and pressure sensors. In this chapter, the experiment will be presented together with an analysis of the data obtained. Pressure and force on the wedge surface during water entry were measured, together with position. This chapter contains an investigation of the features of the impact loads for different water entry velocities.

Figure 4.1 illustrates the parameters characterising the slamming pressure during water entry of a blunt rigid body. Slamming pressure has a very short rise time followed by the peak pressure. The maximum pressure coefficient is denoted $C_{p_{\max}}$ in the figure. The decay time of the pressure after $C_{p_{\max}}$ is much larger than the rise time. As the body penetrates the free surface, the slamming pressure is very localised and changes position with time. The value of the pressure peak is of a stochastic nature. It may vary from cycle to cycle, even when the drop height and deadrise angle is constant (Faltinsen 2010). Another important parameter is the spatial duration of the slamming pressure, denoted ΔS_s. In this analysis, this part of the pressure will be defined as the slamming pressure, which is the pressure exceeding 50% of maximum pressure. A vertical force will work on the body during water entry. The force is measured in the experiment and will be compared to integrated pressure. The acceleration and velocity during impact are also important parameters that will be investigated.

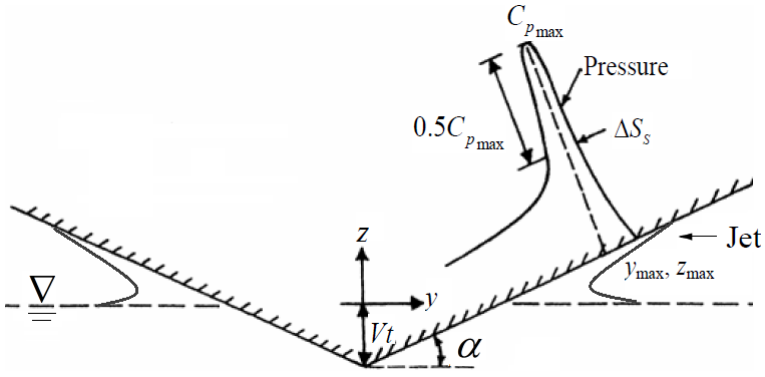

Figure 4.1 – Definition of parameters characterizing slamming pressure during water entry of a blunt two-dimensional body: α = deadrise angle; $C_{p_{\max}}$ = pressure coefficient at maximum pressure; $z_{\max}$ = z-coordinate of maximum pressure; ΔS_s = spatial extent of slamming pressure exceeding 50% of maximum pressure; t = time; V = water entry velocity. (Zhao and Faltinsen 1993)

4.1 EXPERIMENTAL SET-UP

4.1.1 Test rig

A test rig as pictured in figure 4.3 was used to drop a wedge shaped body into water. The wedge was dropped into a tank (height 4000 mm, width 283 mm) filled with water at approximately room temperature. In the tank there is a window that has been checked and concluded to be rigid enough to not affect any measurements. The wedge itself has dimensions as illustrated in figure 4.2, with a deadrise angle of 10°. The body is therefore considered blunt. It is built of compact aluminium, which should ensure that the assumption of a rigid body is applicable. MARINTEK has informed that the test rig itself is not a concern regarding natural frequencies that may be excited during the experiment. The gap between the tank wall and the wedge is less than 2 mm on each side of the width, W. This is expected to be sufficiently small to restrict the flow to two dimensions. On the transverse sides of the breadth B, the gap is 1665 mm. The weight of the wedge assembly is 170 kg. Force and pressure panel is mounted on the right hand side of the wedge.

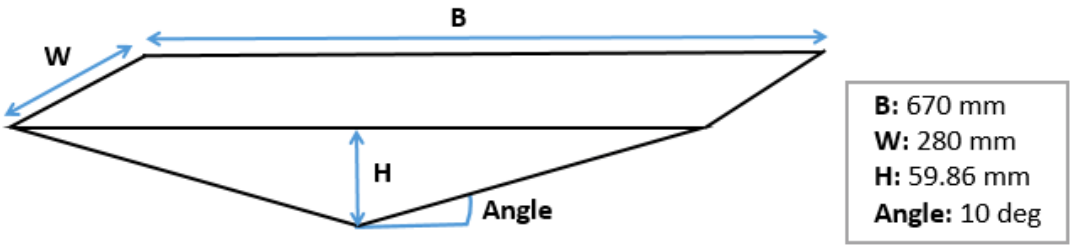

Figure 4.2 – Measured wedge dimensions.

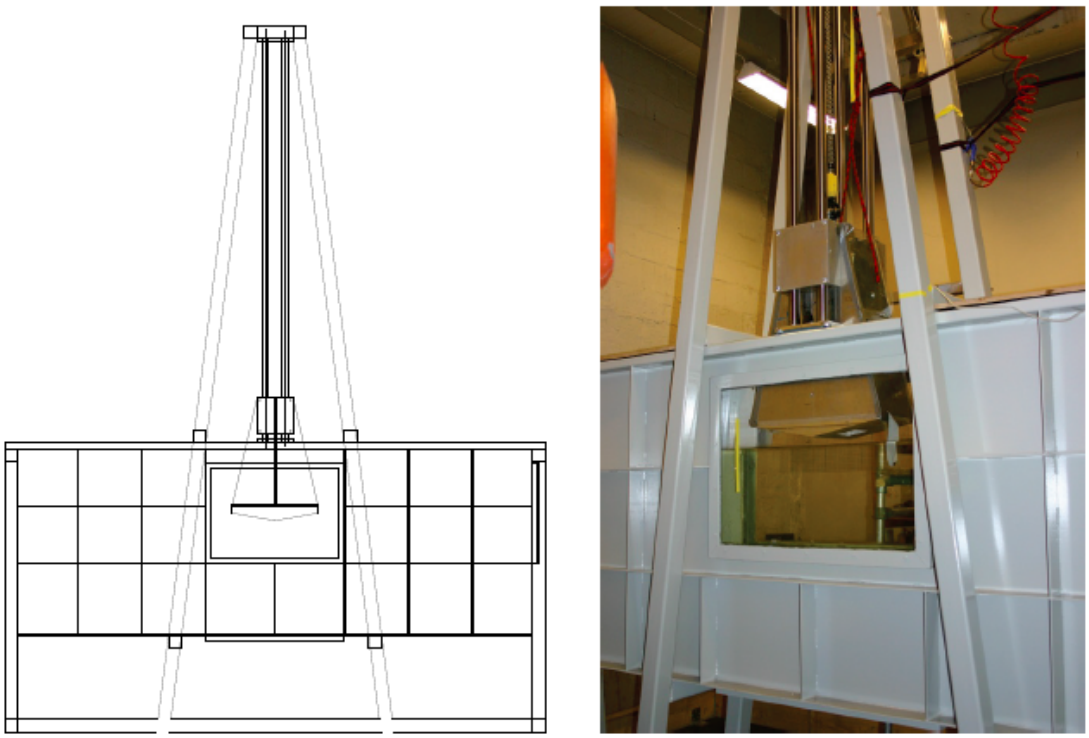

Figure 4.3 – Sketch and picture of test rig. (MARINTEK)

4.1.2 Sensors

Three different configurations of combined force and pressure panels are used in the experiment. The force and pressure sensor types are equal for the three panel configurations, but the number and position of pressure sensors differ. In figure 4.4 the position of the pressure sensors on the force panels as well as their numbering is illustrated. The indicated distance between pressure sensors are centre-to-centre. Force panel starts 75 mm from apex. All data was sampled at 50 kHz.

To set a limit for the size of this experimental investigation, only the 5x3 panel in figure 4.4a will be analysed. For the presented results in this chapter, potential differences in the behaviour of the three panel types will be disregarded.

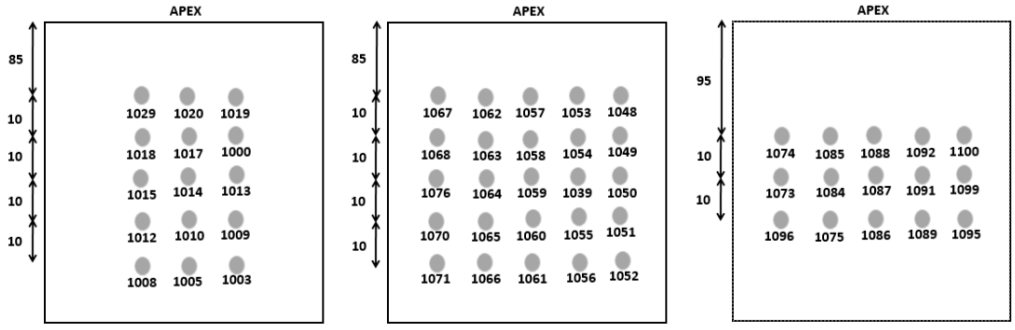

Figure 4.4 – Lay-out of the three different combined force and pressure panels with sensor numbering and position from wedge apex (mm) for the (a) 5x3 (b) 5x5 and (c) 3x5 panel configuration.

4.1.2.1 Pressure sensors

The piezoresistive pressure sensors are from Kulite (CT-190). They have a square sensing area of 2x2 mm and the diameter of the sensor front is 2.6 mm. Before the final drop tests that will be analysed in this chapter, initial drop tests were performed to check the pressure sensors. These tests were completed without the presence of a force panel. MARINTEK compared measured maximum pressures from the inital tests to predicted values by classical Wagner theory (1932) and a numerical BEM code SLAM-2D based on Zhao et al. (1993, 1996). Sensors showing values clearly differing from the predictions were removed before the final drop tests. It is noted that after the final drop tests, some sensors were again replaced. In the 5x3 panel that will be considered in this analysis the removed sensors were number 1000 and 1005. In the following analysis these sensors will be avoided when possible.

4.1.2.2 Force sensor panels

For the combined force and pressure panel, a 'beam' type of force sensor was applied. The force panel is of size 60x60 mm, and is mounted on the wedge using a hard type of plastic. The force senor panel is of the type HLCB2, manufactured by HBM. All force transducers were statically calibrated. Hammer tests were performed on the force panels in dry condition on the test rig with input frequencies up to 2 kHz. In these tests resonance frequencies and gain between input and response of the panel configurations were checked. The gain for all combined panels was found to be in the range 1.0 -

1.05, which is satisfactory. The combined panel type under investigation in this chapter showed resonance frequencies around 400 Hz.

4.2 EXPERIMENTAL PROCEDURE

Two rounds of experiments were carried out:

- **Initial drop tests:** of pressure sensors without force panel present, with drop heights of 0.1, 0.16 and 0.25 m
- **Final drop tests:** of combined force and pressure panel, with drop heights 0.1, 0.25 and 0.5 m

This analysis will be performed on the results from the 5x3 combined panel from the final drop tests. Results from the initial drop tests will be used for comparison in some analyses, but no further details from this round of experiments will be discussed. The same experimental procedure (disregarding drop height) was carried out for all tests, both final and initial.

No fixed start time was set for the measurements, but they started before the wedge was released for all tests. The wedge was released and ran through the free surface in the tank. Shortly after the force panel was submerged, oil dampers stopped the wedge. Between each drop, water on the wedge from the previous drop was wiped off. MARINTEK (K. Berget 2015, pers. comm., 18 March) informs that the waiting time between each drop was not set, but should be at least five minutes where they prepared for the next drop. For the 5x3 panel, 11 tests were executed and the numbering of these tests are listed in table 4.1.

During each drop, the pressure and force over the panel was measured, as well as the position of the wedge. It was intended to measure the acceleration, but during this analysis it became clear that the accelerometers were not attached to the wedge. The available acceleration measurements from the tests were only recording vibrations from where they were left.

Table 4.1 – Overview of tests performed for the 5x3 panel.

Test number	Drop Height [m]
9801	0.25
9802	0.25
9803	0.25
9804	0.25
9806	0.5
9807	0.5
9808	0.5
9809	0.5
9810	0.1
9811	0.1
9812	0.1

4.3 DATA ANALYSIS METHOD

The experimental data from the drop tests was received as binary Matlab files (.mat). To perform the analysis presented in this chapter several Matlab codes have been developed. The codes used in this chapter together with descriptions are found in appendix A and B. To connect the different codes to the presented results, the Matlab codes used in each part of the analysis are cited with footnotes where they are applied. All measurements were received in full scale and are scaled to model scale with a scaling factor $\lambda = 50$.[1]

4.4 IMPACT VELOCITY

Impact velocity is an important parameter that will affect both slamming force and pressure values. Faltinsen (2010) states that for deadrise angles larger than 5°, the maximum slamming pressure will be proportional to V^2. The hydrodynamic vertical force on a body penetrating the free surface with a velocity V(t) is defined by Faltinsen (1990) as

$$F_3 = \frac{d}{dt}\left(A_{33}\left(t\right)V\left(t\right)\right) + \rho g \Omega \tag{4.1}$$

where Ω is the volume of the submerged body and A_{33} is the high frequency added mass in heave. From these two statements it can be concluded that a change in velocity will affect the results and should be investigated. Chezhian (2003) investigated the velocity variation and found that it is dependent on the ratio between the body weight and the maximum slamming force. If the weight is larger, the body will keep accelerating after water entry. When the submergence increases, the added mass and hydrostatic load will increase and eventually lead to a deceleration of the body.

When the impacting body is dropped from a given height h, the initial impact velocity can be found by using the equality of potential and kinetic energy:

$$V = \sqrt{2gh}. \tag{4.2}$$

The velocity of each drop is found by numerical derivation of the position measurements.[2] The position measurements are low pass filtered to remove noise from the signal. It is noted that there is an uncertainty in the presented velocity connected with the derivation process and the filtering of the position measurements. As the position measurements cannot give the position of the spray root, a direct synchronization of pressure peaks and position measurements cannot be performed. Instead, the synchronization is checked by evaluating the derived velocity at the time where apex initially hits water against the value from eq. (4.2). This will also give an indication of the possible error in the derived velocity. Values of the initial velocity from eq. (4.2), experimental values (mean for each drop height) and an error estimate between the two are presented in table 4.2.

[1] Appendix B.1 - analyse.m
[2] Appendix B.2 - dispvelc.m

Table 4.2 – Theoretical velocity compared to experimental velocity. $V_{0_{calc}}$ = velocity by eq. (4.2), $V_{0_{exp}}$ = measured velocity from experiments, Error = $V_{0_{calc}}$ - $V_{0_{exp}}$. Positive directon downwards.

Drop Height [m]	$V_{0_{calc}}$ [m/s]	$V_{0_{exp}}$ [m/s]	Error [m/s]
0.1	1.400	1.402	0.002
0.25	2.215	2.214	-0.001
0.5	3.132	3.092	-0.040

A velocity time history for a 0.5 m drop is showed in figure 4.5. Gravity causes the wedge to accelerate towards the free surface with increasing velocity. One can observe that the velocity decreases again after impact until it reaches zero. The initial reduction of velocity is caused by water resistance and vertical forces working on the wedge during impact. The wedge is forced to a full stop by oil dampers.

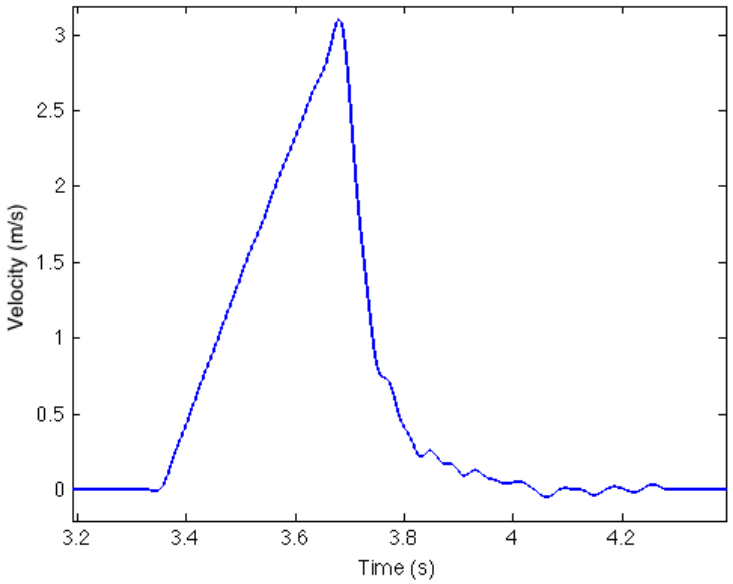

Figure 4.5 – Wedge velocity vs. time for 0.5 m drop height (Test 9807).

Plots of the velocities for 0.5 and 0.1 m drop height including the time instances of pressure peaks at first and last sensor row (red circles) and the time where apex hits water (black star) are presented in figure 4.6. Two values quantifying the velocity change for each drop height are presented in table 4.3. The mean velocity change for each drop height between initial impact and first pressure peak is presented to see if the assumption of constant velocity is applicable for the pressure. The change in velocity between the pressure peaks at the first and last sensor row is also presented.

It is observed that two different scenarios occur for the three drop heights. For 0.1 m drop height the velocity reaches its maximum value after the last pressure peak. For 0.25 m and 0.5 m the maximum velocity occur right before the first pressure peak. The velocity changes found in table 4.3 are small. As an attempt to correct for the error made by the derivation process, the velocity change can be considered with the error estimate from table 4.2. The values of ΔV_1 and ΔV_2 for 0.5 m drop height are inside this estimated error range, and it is possible to assume that the velocity is constant for

this drop height. For the other two drop heights the values of ΔV_1 and ΔV_2 are outside the suggested error range. A constant velocity can therefore not be assumed for 0.1 and 0.25 m drop height.

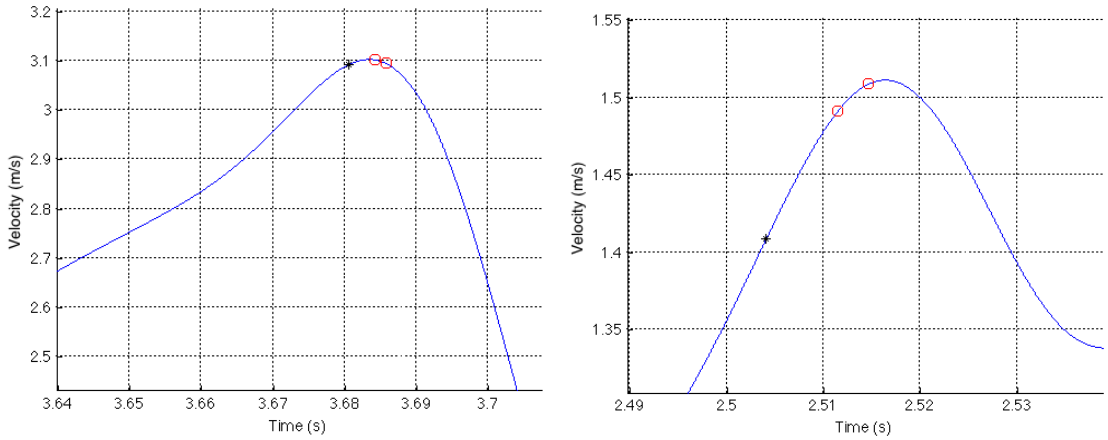

(a) **(b)**

Figure 4.6 – Velocity of wedge with red circles indicating first and last pressure peak and black star indicating initial impact for a) 0.5 m (Test 9807) and b) 0.1 m (Test 9810) drop height.

Table 4.3 – Mean variation in velocity for each drop height. ΔV_1 = velocity change between initial impact and peak pressure over first sensor row, ΔV_2 = velocity change between peak pressure over first and last sensor row. Positive value = velocity increase.

Drop Height [m]	ΔV_1 [m/s]	ΔV_2 [m/s]
0.1	0.063	0.0112
0.25	0.020	-0.0013
0.5	0.0069	-0.0085

4.4.1 Comment on velocity change

It is concluded that the velocity for 0.5 m drop height is constant during the slamming pressure measurements. For 0.1 and 0.25 m drop height, a small velocity increase is found between the time the wedge initially hit water and the first measured pressure peak (ΔV_1 from table 4.3). To evaluate this velocity change a possible error source is considered. That is the presence of a small wave trough under apex when the initial impact position is measured. If the vertical position of the wedge is denoted z, initial impact corresponds to the time t_0 where z=0, i.e. when apex hits the free surface. If a small disturbance in the free surface causes a small wave trough to be present underneath apex at time t_0, the wedge will hit the free surface at a time $t = t_0 + \Delta t$. If the wedge actually started to decelerate at the time where contact with water started, this means maximum velocity would occur at the time $t = t_0 + \Delta t$. Δt would therefore be the time from the position measurements show z=0 to the time where maximum velocity occur. Δt can therefore be found from the position and velocity data. From the equations of motion the depth of the trough Δz can be calculated as

$$\Delta z = g\frac{(\Delta t)^2}{2} \tag{4.3}$$

where g is the gravitational acceleration and Δt is the time passed from z=0 to maximum velocity. Inserting values for 0.1 and 0.25 m drop height, eq. (4.3) show that the necessary depths of the troughs to cause the increase in velocity are 0.75 and 0.23 mm for the two drop heights respectively. This means that the waves needed to cause the observed velocity change is very small. It is not concluded that this is happening, but it demonstrates how sensitive the measured velocity is to small disturbances in the free surface. This finding argues that the change in velocity found should not be emphasised too much.

4.5 ACCELERATION

A change in the acceleration of the wedge can change the pressure. If the wedge decelerates it will result in a decreasing pressure. The pressure corrected for non-constant velocity is expressed by Faltinsen (2010) as

$$p(t) = p(t)_{asymptotic} - \frac{dV}{dt}\sqrt{c^2 - x^2} \tag{4.4}$$

where 2c is the distanc between each spray root and x is the position along the wedge surface. Eq. (4.4) expresses how the pressure will decrease with a deceleration $\frac{dV}{dt}$ (positive direction downwards).

It became clear during this analysis of data from the experiment that the acceleration measurements were not usable. The accelerometers were not attached to the wedge and therefore no acceleration measurements were made. An attempt of analysing the acceleration as the second derivative of the position measurements was made. This numerical approach proved to cause large drifts in the resulting acceleration, so the time history was not satisfying. It is therefore decided to not investigate the accelerations further and only use the derived velocity as an indicator of what is happening during water entry.

4.6 PRESSURE RESULT ANALYSIS

4.6.1 Filtering

Different filters were considered for the pressure time series to eliminate noise from the signal. As the rise time for the pressure is very short, it proved to be demanding to filter away any noise without affecting the peak pressure. Figure 4.7 shows the attempt of applying 4th order Butterworth low pass filters with cut-off frequencies of 8000, 5000 and 2500 Hz to the pressure signal for drop height 0.5 m. The largest drop height is used to evaluate the filtering as the lowest rise time is expected here. A quick rise in pressure makes filtering demanding as high frequencies must be allowed to pass in order to maintain the full pressure peak. There is not much noise present in the signal and the filters lead to a loss in peak pressure, even for high cut-off frequencies. Due to this, it is decided to not filter the pressure time series. All pressure values represented in this chapter is therefore unfiltered.

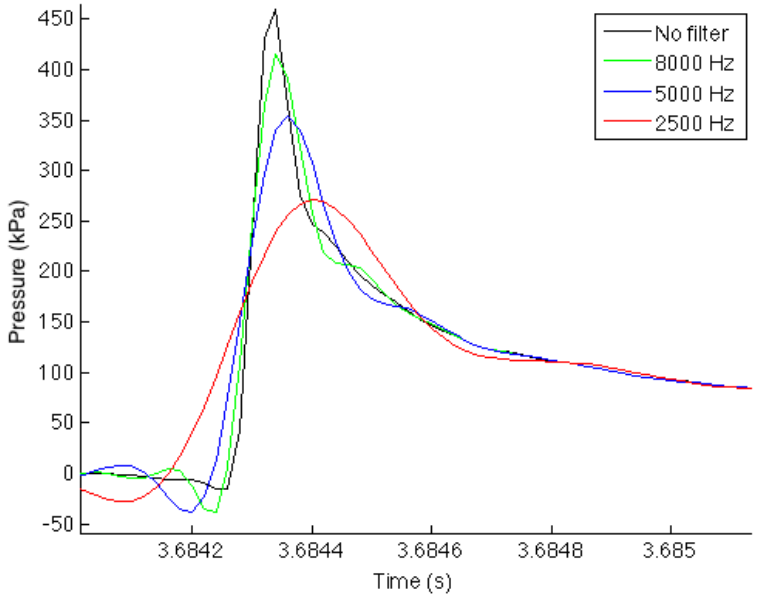

Figure 4.7 – Comparison of LP-filters for pressure time series. Drop height 0.5 m.

4.6.2 Time series

Time series of the pressures from drop heights of 0.5 m, 0.25 m and 0.1 m is shown in figure 4.10 - 4.12. They represent typical pressure measurements from a drop test. For each subfigure, the pressure from one row of sensors (i.e. same distance from apex) is plotted. It is important to notice that during the first peak the other sensor rows have not yet hit water. Figure 4.8 shows a sketch of the wedge upon water entry. In this sketch, only sensor rows 1-3 are in contact with water, the above rows will at this time not measure any impact pressure. The initial free surface is marked and the rise-up along the body is included. The water will after rising along the body form a jet. It can be assumed that the pressure in this jet is close to atmospheric pressure. In the jet root however, the maximum pressure will occur. In the sketched stage of impact, the peak pressure would occur at the third row of sensors which are situated in the jet root marked by c(t). This can be observed in the measurements in figure 4.10 - 4.12 as well. The first row shows peak pressures first, and then the other rows follow. It is

noted that the time axes in the plots does not represent the time after the wedge was dropped, as the start time of measurements varies from drop to drop. The pressure sensor numbering and location on the 5x3 panel is illustrated in figure 4.9 for reference.

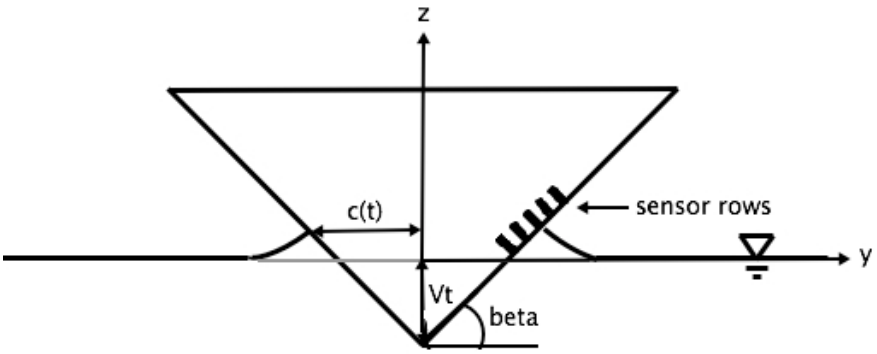

Figure 4.8 – Sketch of wedge with pressure sensors upon water entry.

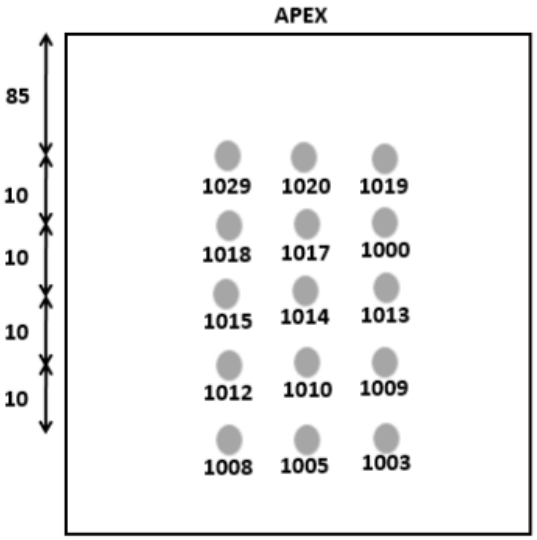

Figure 4.9 – Position and numbering of sensors at the 5x3 panel.

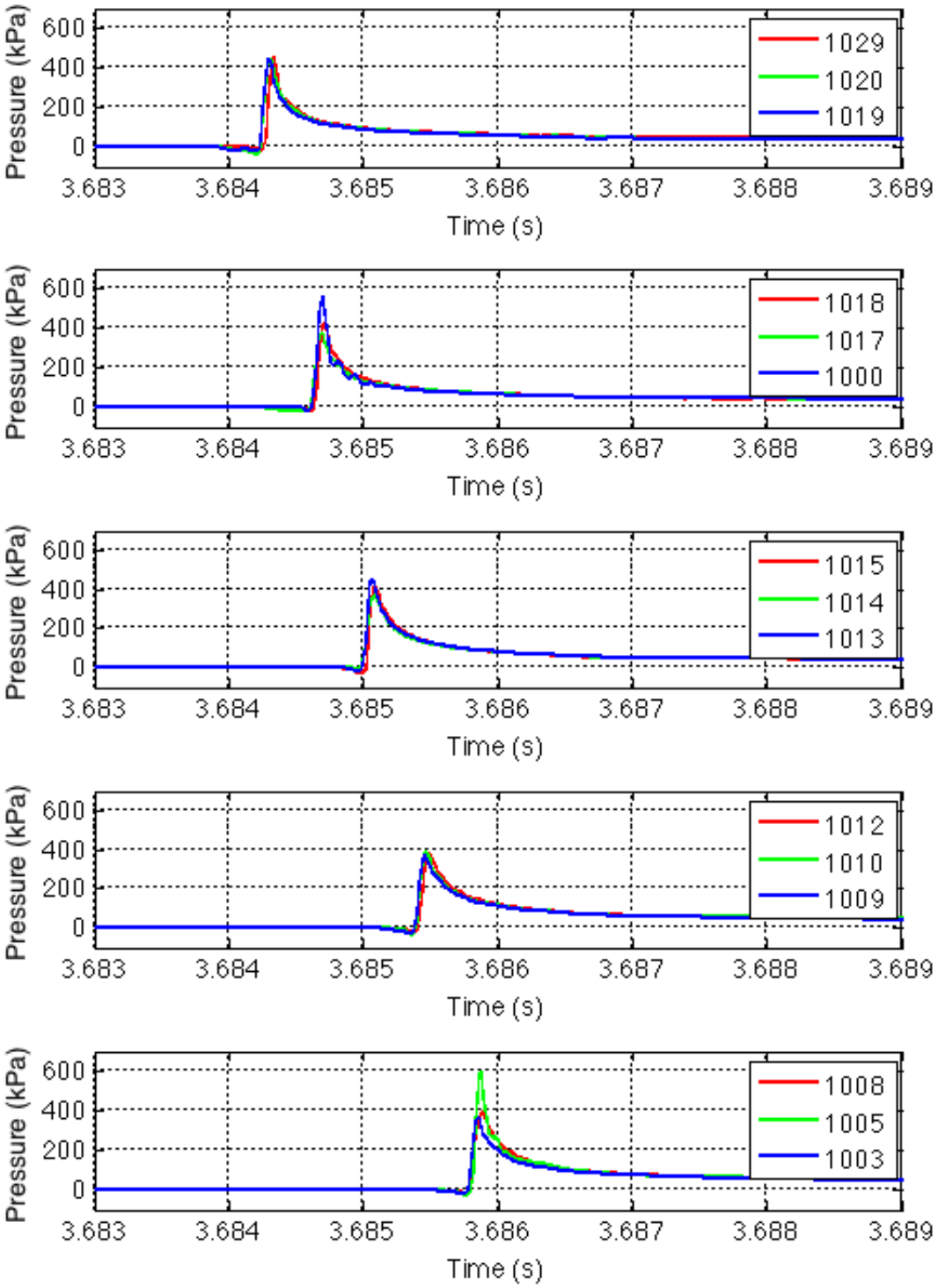

Figure 4.10 – Pressure records for a 0.5 m drop(test 9807). From the top: Row 1-5.

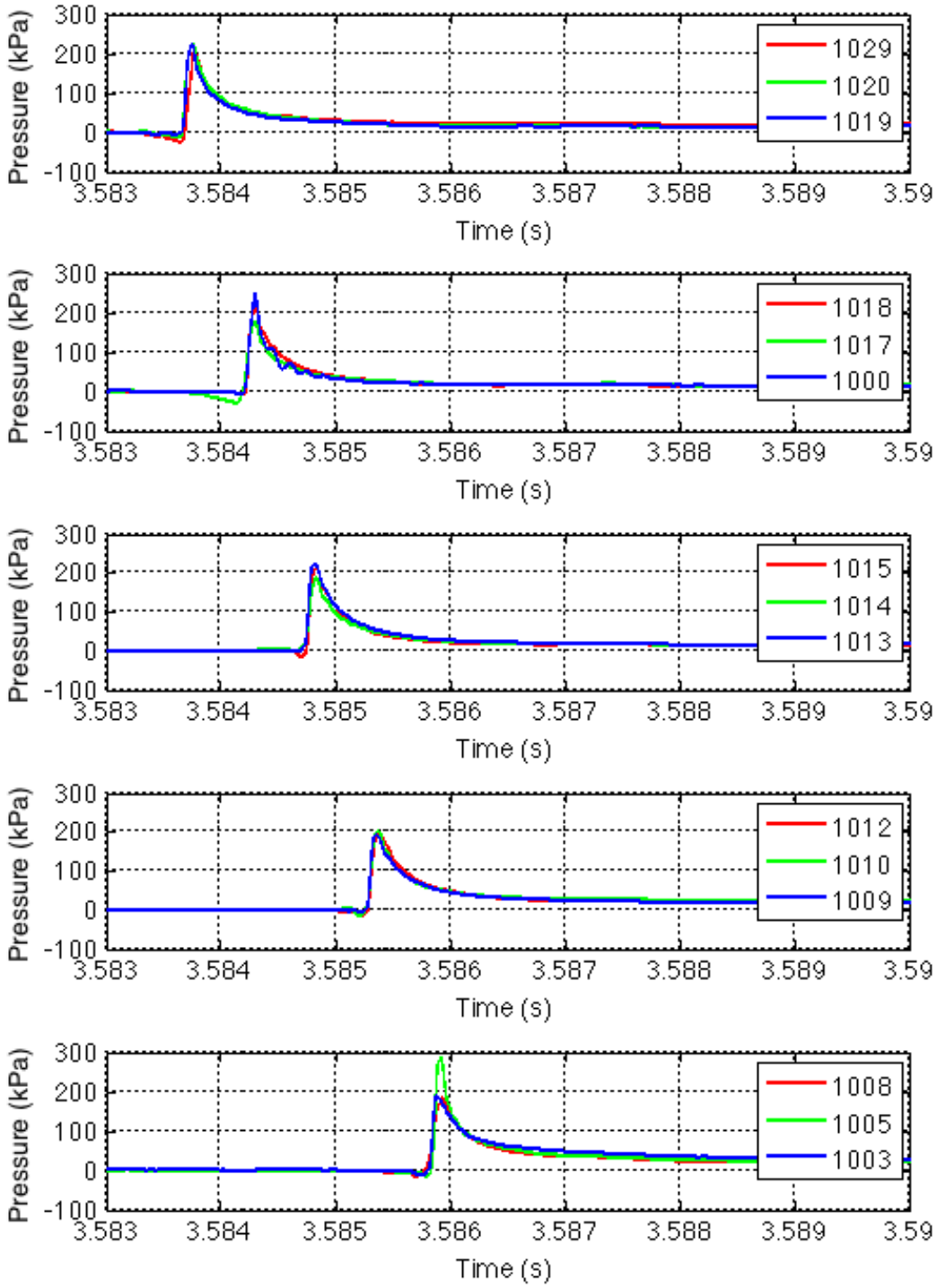

Figure 4.11 – Pressure records for a 0.25 m drop(test 9801). From the top: Row 1-5.

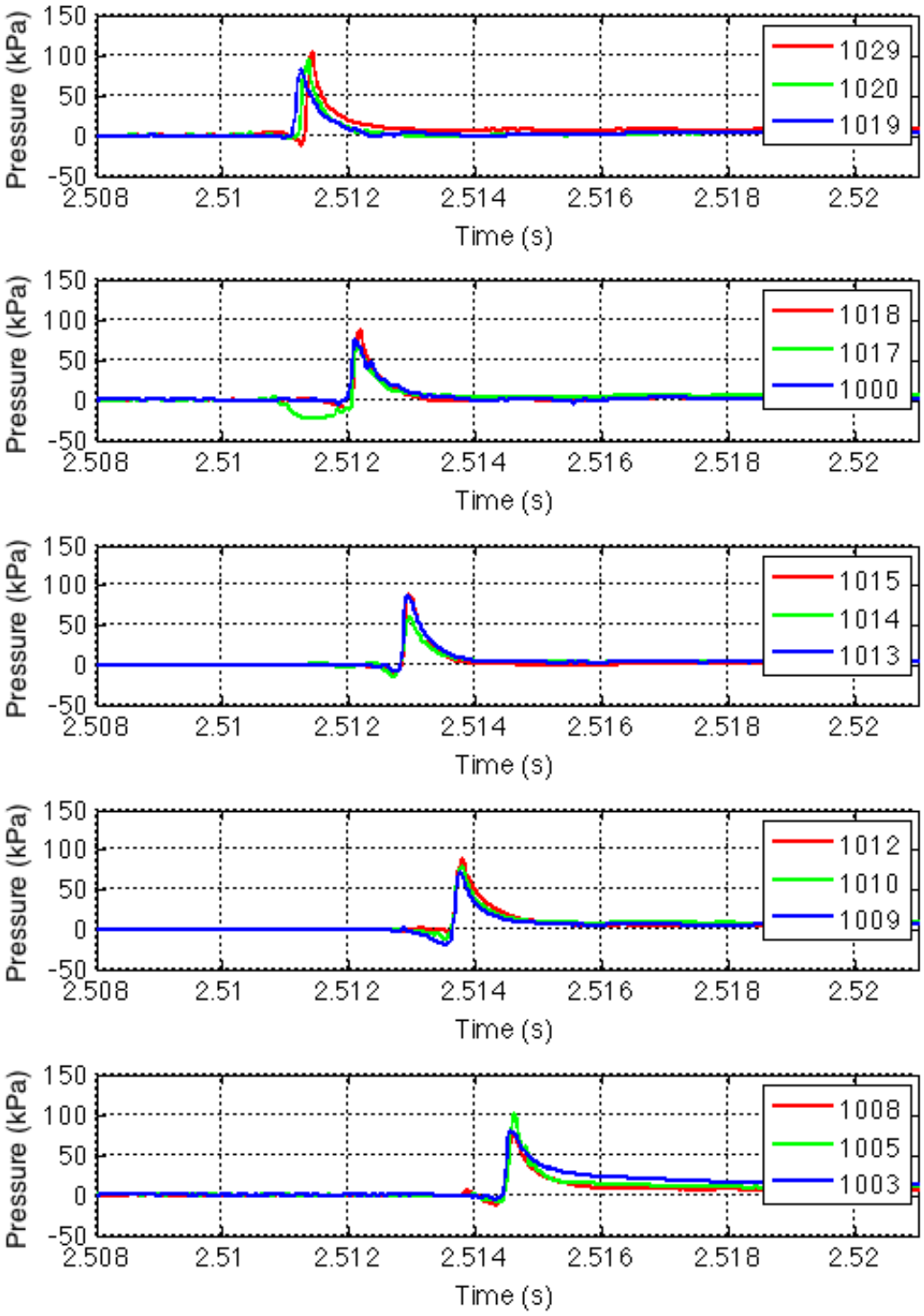

Figure 4.12 – Pressure records for a 0.1 m drop(test 9810). From the top: Row 1-5.

4.6.3 Pressure peaks

As seen in the time series the pressure will have a maximum value over each sensor. The peak pressure will typically occur when the sensor row is located at the spray root. Using Wagner's theory (1932) the value of the maximum pressure can be estimated as

$$p_{\max} = \frac{1}{2}\rho V^2 C_{p_{\max}} \tag{4.5}$$

where ρ is the density of water, V is the impact velocity and $C_{p_{\max}}$ is the maximum pressure coefficient given as

$$C_{p_{\max}} = \frac{\pi^2}{4}\cot^2\beta. \tag{4.6}$$

β is the deadrise angle of the wedge. Using these formulations and equation (4.2) for the velocity the expected maximum pressures are

$$\begin{aligned} h &= 0.1m & p_{\max} &= 80kPa \\ h &= 0.25m & p_{\max} &= 200kPa \\ h &= 0.5m & p_{\max} &= 390kPa \end{aligned}$$

Slamming is a phenomenon of a stochastic nature, so it is not expected that the pressure peaks will be exactly equal to these estimates for all peak pressure measurements. The mean of the maximum pressure over all sensors is found for all tests.[3] All tests at a given drop height is considered together and an average value is found for each drop height. The relative standard deviation of the maximum pressure between all sensors for all tests at equal drop height is also found. The results are presented in table 4.4.

Table 4.4 – Mean maximum pressure for each drop height together with the corresponding relative standard deviation.

Drop Height [m]	$p_{\max}$ [kPa]	Relative STD [%]
0.1	83.3	13.5
0.25	215.9	13.5
0.5	402.6	20.0

The results agree well with the estimates made, being on the upper side of the predicted values. As Wagner's theory is expected to overestimate the pressure due to the flat plate approximation, it is somewhat unexpected that the experimental values exceeds these estimates. For 0.1 m drop height it could be explained by the velocity increase that is occurring after apex initially hits water. Yettou et al. (2005) proposed estimating the peak pressure using the instantaneous velocity:

$$p_{\max} = \frac{1}{2}\rho C_{p_{\max}} (V(t))^2. \tag{4.7}$$

In eq. (4.7), Yettou et al. (2005) used a $C_{p_{\max}}$ corrected for non-constant velocity. Here the coefficient from Wagner is used. In section 4.4 the velocity for 0.5 m drop height was considered constant during the pressure peaks. For 0.1 m drop height the

[3] Appendix B.3 - maxp.m

velocity was found to increase slightly. Assuming this velocity change to be true, the mean velocity across the sensor rows is 1.47 m/s. This will lead to an estimated peak pressure of 85 kPa. For 0.25 m drop height the change in velocity could explain an increase of 3 kPa for the peak pressure. This does not cover the observed gap between theoretical estimate and experimental result. As the experimental peak pressures are above the Wagner estimates for all drop heights, a velocity change is not a reasonable explanation.

Peak pressures in a slamming experiment on a blunt body are expected to have a stochastic nature (Faltinsen 2010). The standard deviations presented in table 4.4 may therefore be considered normal. A larger relative standard deviation for the 0.5 m case could be caused by the pressure behaviour becoming more stochastic as the impact velocity increase.

4.6.4 Spatial pressure distribution

It is described in previous reports like Dobrovol'skaya (1969) that when the impact velocity is constant, the magnitude of the spatial pressure distribution will be constant. Yettou et al. (2005, 2006) reported from their drop tests with a two-dimensional wedge, that a variation in velocity can change the spatial pressure distribution. To find out if this could be the case in this experiments the spatial pressure distribution is found for different time instants. One column of sensors is used to represent the spatial distribution across the rows. For best accuracy, the column which does not contain any later replaced sensors is used (sensor 1029 - 1008). The mean and standard deviation of the pressure are found for all considered time instants over all tests at the same drop height.

Plots of the spatial distribution at each time instant a sensor reaches its maximum pressure value is shown for all drop heights in figure 4.13 to 4.15.[4] Error bars are included and the length of each error bar is two times the standard deviation. The numbering of the time instants (t1 - t5) in the plot corresponds to the time where row number n senses its maximum pressure. This means t1 corresponds to the time when row 1 (closest to apex) is in the spray root. It is noted that the first peak (t1) is alone because at this time instant only the first sensor row is in contact with water. The thicker black line represents the peak pressures.

[4] Appendix B.4 - spatial2.m

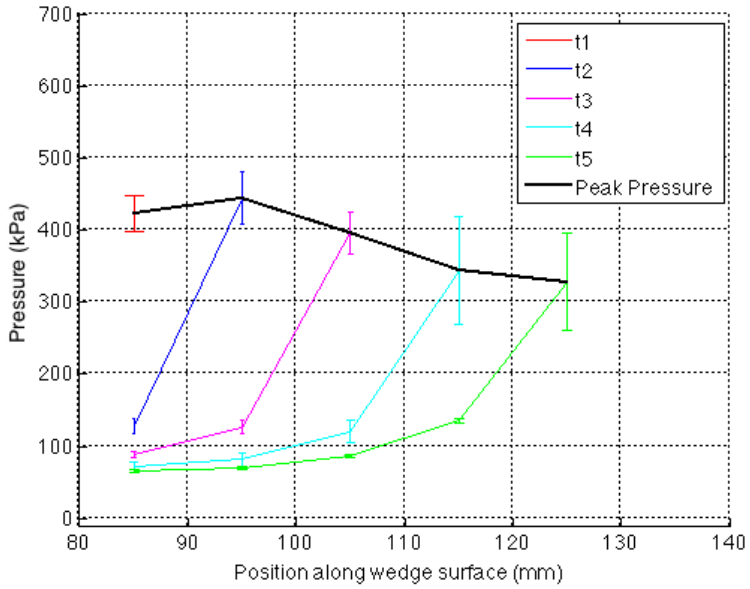

Figure 4.13 – Spatial pressure distribution along wedge surface at different times through impact for 0.5 m drop height.

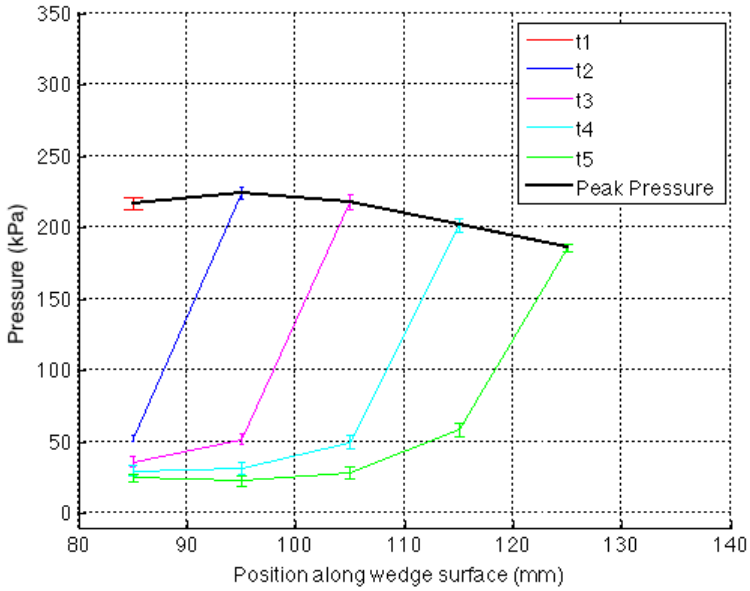

Figure 4.14 – Spatial pressure distribution along wedge surface at different times through impact for 0.25 m drop height.

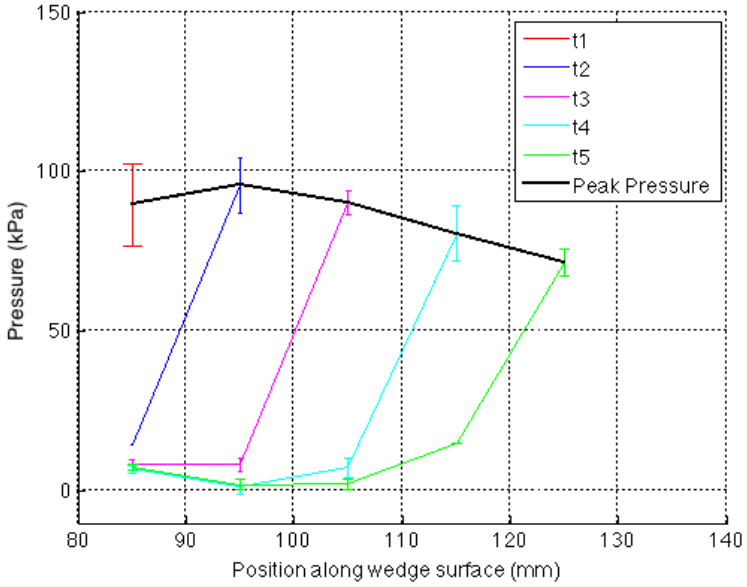

Figure 4.15 – Spatial pressure distribution along wedge surface at different times through impact for 0.1 m drop height.

Yettou et al. (2005) found that a reduced speed during impact led to a less steep and more rounded curve with a lower peak pressure. As there are only five sensor rows, the spatial distribution will not be smooth, which makes it harder to evaluate how the spatial distribution changes with time. Even so, it is observed that the slope from the measured point before peak pressure and peak pressure is quite constant for all time instances. This indicates that a velocity change is not affecting the pressure measurements. In section 4.4, the velocity was found to be constant for 0.5 m drop height from t1 to t5. This agrees well with the slopes of the curves t1-t5 in figure 4.13, that appear constant. For 0.1 m drop height, the velocity is increasing with 0.0112 m/s from t1 to t5. Studying the pressures distribution in figure 4.15, one can observe that the distance between the curves t1 to t5 is smaller than for the other drop heights. This is consisitent with a velocity increase.

The black lines in figure 4.13 to 4.15 represent the peak pressure across the rows. It is observed that the first row of sensors show a lower maximum pressure than row two for all drop heights. For the very short time interval between t1 and t2 it is not possible that a velocity change is the cause. It is assumed that this is some kind of sensor error. After the second sensor row the pressure decreases for all drop heights. A velocity change is again ruled out as an explanation. For 0.1 m drop height, the velocity increases slightly across the rows which implies an increase in pressure. The opposite behaviour is observed. Some other effect must be the reason for this decay across the rows. This will be discussed in section 4.7.

4.6.5 Pressure coefficient

The pressure coefficient is a non-dimensional measure of the slamming pressure and can be expressed as

$$C_p = \frac{p}{\frac{1}{2}\rho(V(t))^2} \tag{4.8}$$

where p is the slamming pressure, ρ is the density of water, V(t) is the impact velocity and t is time. Dobrovol'skaya (1969) and Zhao et al. (1993) both show that for a given deadrise angle, the spatial shape of the pressure coefficient distribution is constant. This holds when the assumptions of constant impact velocity and gravity neglected compared to fluid accelerations are applicable. For the data analysed in this chapter, it means that when the pressure is made non-dimensional it is expected that when plotting the pressure coefficients for all drop heights they will fall into one curve. For the impact on a 10° wedge, which is considered blunt, a steep curve is expected with a $C_{p_{\max}} = 80$. The spatial pressure distribution by Wagner's theory (1932) is presented in figure 4.16[5].

In the literature, the pressure coefficient is normally plotted against the non-dimensional water entry depth $\frac{z}{Vt}$ as in figure 4.16. As the time is not synchronized between the drops in this experiment it is chosen to plot the pressure coefficient against the position along the wedge. Values of C_p are found by taking the average of the measured pressure at all repeated test for each drop height.[6] To show the variation over the sensor rows only one column (sensor 1029 - 1008) is used to avoid data from later replaced sensors. Figure 4.17 shows the distribution of C_p at the time instant when the peak pressure occurs at the fifth row of sensors. $C_{p_{\max}}$ is found to be 73, 76 and 67 for 0.1, 0.25 and 0.5 m drop height respectively. This is lower than the estimate of $C_{p_{\max}} = 80$ by Wagner (1932). In section 4.6.3, the peak pressures were found to exceed the Wagner estimate. This was the mean over all sensors, while in figure 4.17 the peak pressure is from the fifth sensor row. It is therefore noted that the peak pressure decrease with increased distance from apex. It is also observed that the pressure coefficient in the tail reach values well below the ones presented in figure 4.16 for all drop heights. This discrepancy increases with decreasing drop height.

The curve for 0.1 m drop height shows a behaviour differing from the other two curves. At the considered time instant, the first row of sensors show a higher pressure than the second and third row. If the tails of the pressure peaks approach zero at the same speed the pressure over sensor row three would clearly be expected to last longer than the pressure from the first sensor row. Investigating the time series, it appears as if the second and third row has a much quicker decay than the other rows. This is shown in figure 4.18 and the same behaviour is found along this sensor column for all repeated tests at 0.1 m drop height. For 0.25 and 0.5 m drop height this is not the occurring. Unfortunately, the tests for 0.1 m drop height are performed after the tests on the other two heights. Therefore, one cannot conclude that this is a sensor error occurring in this round of experiments (0.1 m), or if it is something else happening for this exact drop height. Possible explanations will be discussed in section 4.7.

[5] Appendix A.1 - findtau.m
[6] Appendix B.5 - pressurecoeff.m

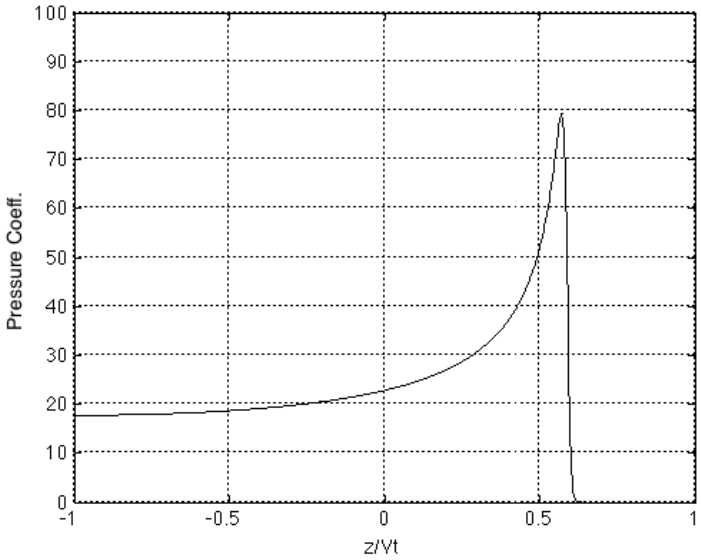

Figure 4.16 – Spatial pressure distribution from Wagner's theory as a function of non-dimensional water entry depth.

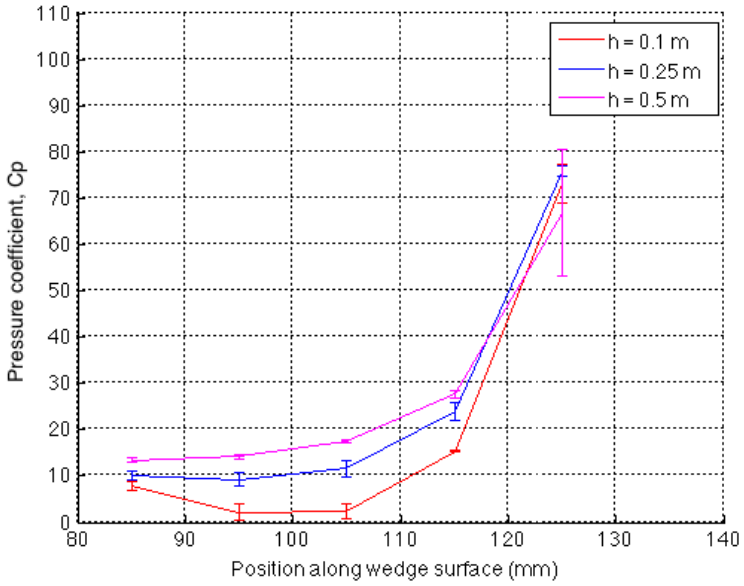

Figure 4.17 – Pressure coefficient as a function of the distance along the wedge compared for all drop heights when peak pressure is at the fifth sensor row.

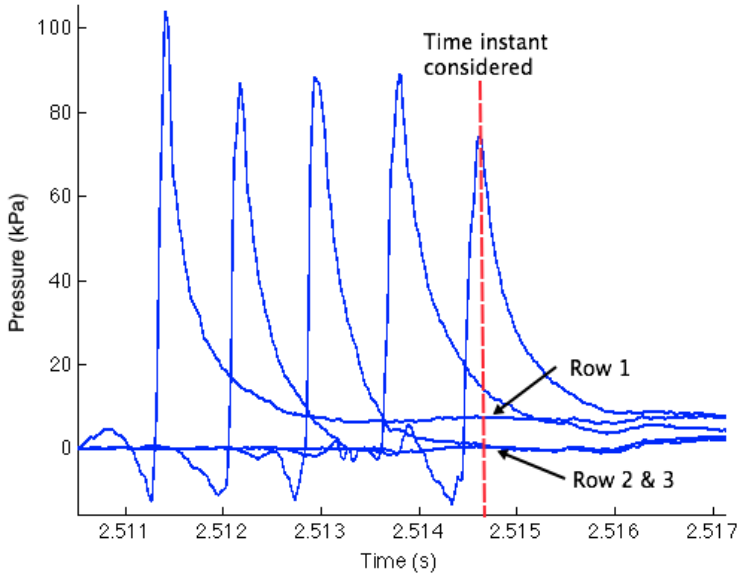

Figure 4.18 – Pressure time series for sensors 1029 - 1008 along the wedge for 0.1 m drop height. The time instant investigated is marked with corresponding pressure values for sensor rows 1, 2 and 3.

4.6.6 Slamming pressure duration

Parameters characterising slamming on a blunt rigid body from a hydrodynamic point of view were illustrated in figure 4.1. The pressure distribution and maxima on the wedge have already been investigated. Another important feature is the time duration and spatial extent of the slamming pressure. The initial high pressure peaks are directly connected with the sudden impact with water, but as the previously illustrated time series show the pressure has a long tail after the maximum pressure. After some time the pressure is no longer defined by the slamming phenomenon itself, but is a result of other factors such as gravity. In figure 4.1 the spatial extent of the slamming pressure is denoted ΔS_s and include the pressure exceeding 50% of maximum pressure.

In this analysis, a choice is made to look at the time duration of the slamming pressure (rather than the spatial extent). The time associated with the slamming is important when considering possible excited natural frequencies of sensors and test rig. It will also give a better representation of the decay of pressure observed for different drop heights. The slamming pressure duration is found as the mean time duration for all involved sensors where the pressure is above 50% of peak pressure.[7] In table 4.5 the mean duration for each drop height is presented together with the standard deviation. The duration of the slamming pressure at a fixed point on the body is expected to be in the order of milliseconds or less (Faltinsen 1990), and that is the case for these experimental results as well.

The observed trend for these tests indicates that the time duration increases with decreasing drop height. As discussed in section 4.6.5, a longer tail is found for sensor 1029 at 0.1 m drop height. Removing this sensor from the calculation of the mean duration only leads to a reduction of approximately 3 %. The conclusion that the

[7] Appendix B.6 - decay.m

longest duration is found for the 0.1 m case can therefore be drawn regardless of the behaviour of sensor 1029.

Table 4.5 – Duration of slamming pressure over each row for all tests and heights.

Drop Height [m]	Mean duration [ms]	Standard deviation [ms]
0.1	0.248	0.082
0.25	0.198	0.048
0.5	0.180	0.072

4.6.7 Re-evaluation of velocity

In section 4.4, the velocity change between the first and last pressure peak over the sensor rows were found. The change proved to be small or zero for all drop heights. The time it takes for the peak pressure to travel from the first sensor row to the last varies from 3.2 ms for 0.1 m drop height, to 0.9 ms for 0.5 m drop height. From the results in table 4.5, it is observed that the duration of the slamming pressure is much smaller than this time range. From this observation it can be concluded that a velocity change will not affect the decay of the pressure during the slamming pressure duration. The time scale is too small for the velocity to change and affect the pressure in the early part of the pressure tail.

4.6.8 Negative pressures

In the time series presented in section 4.6.2, negative pressures are reoccurring right before the rise of the pressure peaks. It is especially evident for the lowest drop height. MARINTEK (K. Berget 2015, pers. comm., 18 March) informs that from experience with previous drop tests, this negative pressure is a recurring problem for the Kulite pressure sensors. Berget also informs that the negative pressure is a local phenomenon and not dependent on the value of the measured pressure itself. For this reason he expects that the smallest drop height will experience the largest relative negative pressure. MARINTEK assumes that the reason for the negative pressures is a temperature shock in the sensor. When the sensors are switched on, an electric current travels through the sensor front and heats it up slightly. Even though the water and air are at equal temperature, the sensors will be warmer than the water due to this electrical heating when initially penetrating the water surface. They assume that this effect can last throughout the time series and even lower the results in the tail of the pressure measurements.

The results of an investigation of the mean negative pressure experienced over all sensors for each drop height are presented in table 4.6.[8] The relative minimum to the maximum pressure for each drop height is also given as well as standard deviation and relative standard deviation. As predicted, 0.1 m drop height shows a larger relative negative pressure, almost twice of the two other heights. If the negative pressure was completely unaffected by the drop height the minimum pressure should be the same for all drop heights, with a changing relative value. It can be seen in the table (4.6) that for 0.5 m drop height the mean negative pressure is twice as large as the other two. This could be due to the increased impact velocity, which may lead to a larger shock in the sensor due to a quicker temperature change. Kulite will not respond to any of these observations.

[8] Appendix B.7 - minp.m

Table 4.6 – Data for negative pressures: $p_{\min}$ = Mean minimum pressure, σ = Standard Deviation for minimum values, $p_{\min_{rel}}$ = Mean minimum pressure relative to mean maximum pressure, σ_{rel} = Relative standard deviation as percentage of mean minimum pressure.

Drop Height [m]	$p_{\min}$ [kPa]	σ [kPa]	$p_{\min_{rel}}$ [%]	σ_{rel} [%]
0.1	-12.15	4.85	-14.6	4.0
0.25	-16.6	5.60	-7.7	3.4
0.5	-28.6	6.86	-7.11	2.4

To check the assumption of a temperature shock causing the negative pressures the initial drop tests are investigated. If a temperature shock is the cause, the same values will be expected for the initial drop tests as for the final. It is chosen to analyse the 0.1 m drop height case as it shows the largest relative negative pressure. The same procedure is carried out, finding the mean negative pressure over all sensors. Taking the mean over the three tests performed for 0.1 m drop height the negative pressure is -7.74 kPa. This is only 64 % of the value from the final drop tests. From this result one may suspect that there is something about the final drop tests causing larger negative pressure values.

A final remark on a temperature shock causing the negative pressures is made looking at an arbitrary pressure time series in figure 4.19. If the negative pressure was affecting the whole pressure time series one would expect a lower peak pressure for the sensors with corresponding low negative pressures. This is not what is observed. The first peak is the highest, even though the negative pressure before this peak is one of the lowest. For the fourth peak there is no negative pressure, but the peak has the same value as the previous peak which experiences a negative drop. These observations do not support the assumption of a lasting effect of the negative pressures. A lasting thermal zero shift in the sensors is not present as the measured pressure after the wedge is stopped corresponds to the hydrostatic pressure.

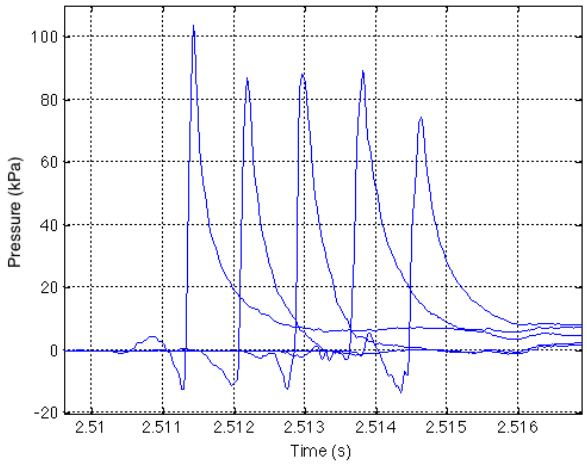

Figure 4.19 – Pressure time series for 0.1 m drop height for visualization of negative pressures. (test 9810, sensor 1029-1008) .

The time scale observed for the negative pressures is short and comparable to the rise of the pressure peaks. A thermal shock is not expected to be so quick, but to be drifting

through the time series. A last explanation for the negative pressure will be presented. The negative pressures can be linked to the curvature of the Kulite sensors front (C. Lugni 2015, pers. comm., 19 May). The sensor front is not completely flat, but has a curvature inwards. Inside this curvature, air can be trapped during impact. When impact occurs this air will be compressed. A compression of air would cause a positive pressure that can be observed before the negative drops. When the air cavity expands again during a collapse this will cause a negative pressure. This explanation is more likely considering both the small increase in pressure before the negative drop and the involved time scale of the negative pressures.

4.7 DISCUSSION OF RESULTS FROM PRESSURE ANALYSIS

From the analysis of the measurements from the pressure sensors there are results that deviates from the expected behaviour. The small changes found in the velocity during impact from section 4.4 is not a suited explanation for these unexpected features. From the analysis carried out in section 4.6 the following phenomena need further investigation:

1. The spatial distribution of maximum slamming pressure show a decay as the distance of the sensor position from apex increase. The decay occurs for all drop heights, so a velocity change can not explain it as the velocity is constant for 0.5 m drop height.
2. The spatial distribution of the pressure coefficient is below the Wagner (1932) estimate. This is for both maximum pressure coefficient and in the tail of the curve. The deviation from Wagner increase with decreasing drop height.
3. A much quicker decay towards zero is experienced by some sensors in the panel during the tests with 0.1 m drop height.
4. Negative pressures are reoccurring before the rise to peak pressure for all drop heights. The amount of the negative pressure relative to peak pressure is larger for 0.1 m drop height than for the other heights.

For the negative pressure mentioned in item four, the explanation is expected to be air that is trapped over the sensor front during impact. This conclusion is made based on the involved time scale of the negative pressures as well as the small positive value observed before the pressure drop. It is stressed that this is a best guess. Video recordings or flow visualization from the experiment would be necessary to verify it. As this is not available, this phenomenon needs further experimental investigation to be entirely understood.

For the other three items listed above, three physical effects will be investigated in the search for an explanation. That is three-dimensional effects, hydroelasticity and sensor errors. The effects will be discussed in the following.

4.7.1 Three-dimensional effects

The pressure coefficients are lower than predicted by Wagner (1932). A lowering of the pressure can be caused by three-dimensional effects. As the column of sensors analysed in section 4.6.5 is on the side of the panel and not from the middle column it would be more vulnerable to such effects. The pressure can 'leak' out on the sides. If the sensor columns closer to the edge of the panel was affected they may show a different pressure time history than the middle column. A comparison of the time history of all sensors in the first row is shown in 4.20 for a) 0.1 m and b) 0.5 m drop height. The test for 0.1 m height shows scatter in peak pressure, time instance of peak pressure and in the pressure tail. None of this can be observed for 0.5 m drop height. If three-dimensional effects were present, the pressure would be lower for the outer sensor columns represented by sensor 1029 and 1019. It seems like sensor 1029 is responding to 0.1 m drop height in a different way than the others. For 0.25 m drop height, the plot corresponds to the one for 0.5 m, but with sensor 1029 showing slightly higher values in the tail. This is most likely a sensor error rather than three-dimensional effects.

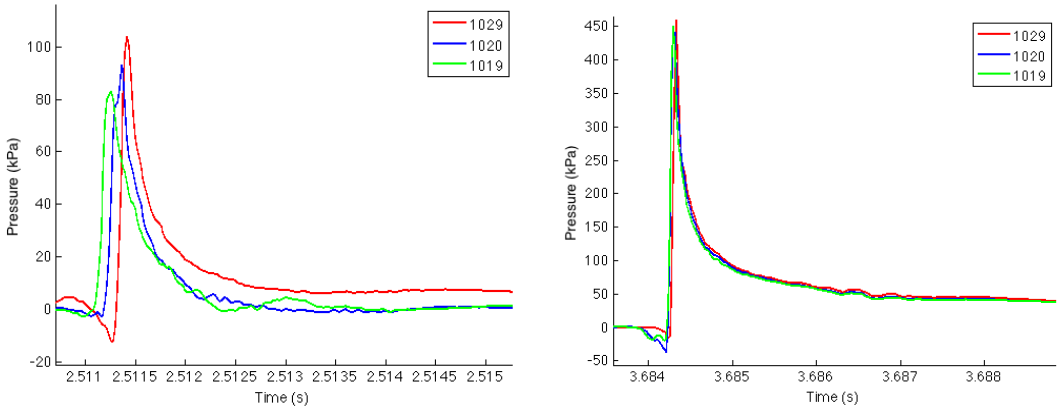

Figure 4.20 – Pressure history of row 1 for a) 0.1 m and b) 0.5 m drop height.

To check the possibility of three-dimensional effects in all tests, mean peak pressure for each sensor column is calculated.[9] If three-dimensional effects are affecting the measurements, a higher mean pressure will be expected in the middle column (sensor 1020-1005). The result of this check is presented in table 4.7. The middle sensor column is denoted *Column 2* while the two on each side are denoted *Column 1* (sensor 1029-1008) and *Column 3* (sensor 1019-1003). The results imply that three-dimensional effects are not affecting the mean pressure peaks as the middle column shows no trend of higher peak pressures.

It is noted that the distance between the columns investigated here is small as the pressure sensors are located on the force panel, which is only covering a small area of the wedge surface width. Due to this, possible three-dimensional effects may not show using this approach of analysing the pressure for each column as the difference in distance to the edge is relatively small. Three-dimensional effects can lead to other phenomena than lower peak pressure. The flow regime is changed as well as the added mass changing from the two-dimensional estimate. A further check for three-dimensional effects will be carried out in the following.

[9] Appendix B.8 - threedim.m

Table 4.7 – Mean peak pressure in kPa over each sensor column. Middle column: *Column 2* (sensor 1020-1005). Side columns: *Column 1* (sensor 1029-1008) and *Column 3* (sensor 1019-1003).

Drop Height [m]	Column 1 [kPa]	Column 2 [kPa]	Column 3 [kPa]
0.1	86	82	82
0.25	209	220	218
0.5	387	411	424

4.7.1.1 Analytical model for three-dimensional effects

Yettou et al. (2006) developed an analytical model for the impact of rigid wedges with varying velocity. This model also includes three-dimensional effects, using a correction factor from the theory of Zhao et al. (1996). The correction factor is defined as

$$f_{3D} = \frac{F_3}{F_3^{2D}}, \tag{4.9}$$

where F_3 is the vertical force per unit length of the wedge section and is defined as

$$F_3 = \frac{d}{dt}\left(0.5\rho\pi B^2(t)Vf\left(\frac{B}{L}\right)\right). \tag{4.10}$$

The ratio (B/L) is the breadth/length ratio of the intersection between the instantaneous free surface and the body surface. F_3^{2D} is the two-dimensional vertical force on the body which is valid when (B/L) approaches zero. Meyerhoff (1970) calculated the added mass of rectangular flat plates with a generalisation of Wagner's theory to three-dimensional flow. From these results different values of the factor f_{3D} can be found as a function of the ratio (B/L). The following values are presented by Zhao et al. (1996): $f_{3D}(0.25) = 0.95$, $f_{3D}(0.4) = 0.87$ and $f_{3D}(0.5) = 0.80$. $f_{3D}(0.5) = 0.80$ means a 20% reduction of the vertical force caused by three-dimensional effects.

For the analysed experiment, the length of the wedge is 280 mm. The factor f_{3D} is evaluated at the time instances where the instantaneous free surface (spray root) is intersecting with the sensor positions. For the first row of sensor placed at a breadth B=84 mm, (B/L)=0.3. For the last sensor row B=123 mm, (B/L)=0.44. From the above estimates of the correction factor one can assume a reduction of 10% for the first sensor row and 15% for the last. This implies that three-dimensional effects should be considered for this two-dimensional experiment. A small reduction is found from the correction factor, but it is sufficient to assume that three-dimensional effects cannot be disregarded.

From the values of the correction factor at the upper and lower sensor postions it can be assumed that the pressure will reduce as the distance from apex increase. In section 4.6.3 the maximum pressure was plotted as a function of sensor position. It was observed that the maximum pressure decreased across the sensor rows. This is found to be the behaviour across the rows for all tests at all drop heights. Three-dimensional effects are therefore considered a possible explanation for this behaviour. Although, with the experimental set-up used, it is not likely that the effects will be strong.

4.7.2 Hydroelasticity

Faltinsen (2000) states that when the deadrise angle is small, hydroelasticity should be considered. Hydroelasticity is a dynamic interaction between structure and fluid. It is excited when the highest wet natural period of the structure is comparable to or higher than the loading time of the slamming. Other natural periods can also matter, but it is often the highest one that is excited. For this experiment, vibrations of the force panel that the pressure sensors are mounted on would be the source of structural vibrations. Such vibrations can affect the pressure over the panel. Bereznitski (2001) describes a reduction of pressure to be a possible effect of hydroelastic behaviour. The possibility of hydroelasticity causing the quicker decay of some sensors towards zero and a reduction in peak pressure across the rows is considered.

4.7.2.1 Comparison with pressure from initial drop tests

As an attempt to see if hydroelastic behaviour is influencing the measurements, the pressure from the initial drop tests are compared to the final drop tests[10]. Since the initial drop tests are performed without the force panel, no vibrations are expected to occur during these tests. The initial drop test pressure panel consists of 6x6 sensors starting 62 mm from apex. They are not placed at the same positions as the sensors in the final drop tests, and the two tests can therefore not be compared directly. This is solved by generating pressure time series for each panel using the Matlab code of Wagner theory (1932) to compare against[11]. If the tests with and without the force panel show different behaviour compared to Wagner time series, hydroelastic behaviour in the final drop tests may be suspected. The results of this comparison is shown in figure 4.21.

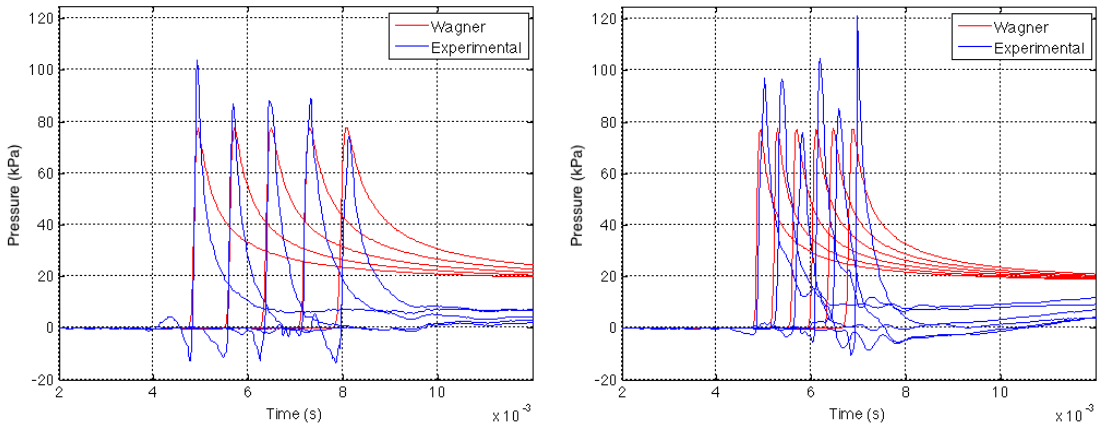

Figure 4.21 – Pressure time series from drop test compared to time series generated by Wagner (1932) Matlab code for 0.1 m drop height for the two cases: (a) final test with force panel present (Test 9810) and (b) initial test without force panel.

From figure 4.21 it can be observed that the pressure peaks are in general larger for the initial drop test without a force panel present. For the initial test, the average maximum

[10] Appendix B.9 - hydroelasticity.m
[11] Appendix A.2 - maketimehistory.m

pressure over all sensors is 90.3 kPa with a standard deviation of 15 kPa. For the final test with the force panel present the average maximum pressure is 82.5 kPa with a standard deviation of 12 kPa. The experimental pressure peaks are underestimated by Wagner's theory, which is not expected. And the deviation from Wagner's estimate of 80 kPa is larger for the initial tests. It was found in section 4.4 that the velocity for the final test presented here was 1.463 m/s during the first pressure peak. For the initial test, the velocity at the first pressure peak is actually lower, being 1.450 m/s. This means a higher velocity for the inital test is not the reason for the higher peak pressures.

The pressure peaks have a noticeable different distribution along the rows. For the final drop test (a), the maxima are larger closer to apex and then they decrease and get closer to the Wagner prediction. For the initial drop test (b), the experimental maxima show an oscillatory nature. The frequency of this oscillation is roughly estimated to be 1300 Hz. This same oscillating peak behaviour at 1300 Hz is found across all rows for all sensors for this specific panel and drop height in the initial tests. A possible explanation could be small disturbances in the free surface. If the free surface is not completely flat, small wrinkles can change the local deadrise angle between water and body. This will change the pressure peaks correspondingly. Nevertheless, a frequency of 1300 Hz is considered too high to support this explanation. No further comments are made on these oscillations.

It is also noted that the pressure measurements for the initial drop tests show more oscillations than the final drop test. If hydroelasticity affected the measurements it would be expected that the final drop test with the vibrating force panel showed this behaviour, not the other way around. The time duration of the slamming pressure (being 50 % of maximum pressure) appears to correspond quite well for the two cases. In general there are no differences between the two recorded pressure time series that indicates hydroelasticity to be affecting the pressure data of the final drop tests.

4.7.3 Error analysis of pressure measurments

Two of the listed items in this discussion of the results can possibly be explained by being inside a pressure measurement error range. That is the spatial distribution of the pressure coefficient and the spatial distribution of maximum pressure. These results have been presented as mean values together with standard deviations. The standard deviation will quantify the precision error, which is the error that can be found from repetition of an experiment. The other type of error is the bias error. Bias errors cannot be measured from repetition of experiments, but can be estimated based on experience and educated guesses (Steen 2014). In this section the error propagation wil be investigated, that is the combined effect of all independent error sources on the measurements. The error propagation can be defined by the root sum square method (Steen 2014) as

$$e = \sqrt{e_P^2 + e_B^2} \tag{4.11}$$

where e_P is the total precision error and e_B is the total bias error. To estimate the total error, all possible error sources must be identified. It is not easy to identify all sources. As an error analysis is not a fundamental part of this thesis only some error sources will

be investigated, and the procedure is simplified. For the precision error the standard deviations will be used. For the bias error two sources will be considered:

1. An error in the measured velocity
2. The presence of small disturbances on the free surface

4.7.3.1 Estimation of bias error

For a measurement X the reduction equation can be defined as

$$X = f_r(Y_1, Y_2..., Y_N) \tag{4.12}$$

where f_r is a function of N parameters $Y_1...Y_N$ denoted elemental error sources (Steen 2014). It is assumed that a small change in a parameter Y_i will result in a small change in the measured value X. By using Taylor expansion the error e_i from an elemental error source Y_i can be defined as

$$e_i = \frac{\partial X}{\partial Y_i}\Delta Y_i. \tag{4.13}$$

The value of ΔY_i is unknown, but some small deviations from the predicted value will be evaluated. This can also be considered a sensitivity analysis. To estimate the effect of the change of Y_i on the measurement X classical Wagner theory (1932) will be applied. $\frac{\partial X}{\partial Y_i}$ is denoted the influence coefficient, κ_i.

First a small variation in velocity will be considered. From section 4.4 an estimate of the velocity error was made comparing the experimental initial velocity to the theoretical value from energy conservation. From Wagner the maximum pressure is defined as

$$p_{\max} = C_{p_{\max}}\frac{1}{2}\rho V^2 = \frac{\pi^2}{4}\cot^2\beta\frac{1}{2}\rho V^2 \tag{4.14}$$

where $C_{p_{\max}}$ is the maximum pressure coefficient, β is the deadrise angle and V is the impact velocity. Deriving this expression with respect to velocity and insert for $\beta = 10°$ and $\rho = 1000\frac{kg}{m^3}$ the sensitivity to variation in velocity on $p_{\max}$ in kPa is:

$$\kappa_{vel} = 80V. \tag{4.15}$$

In eq. (4.15) the velocity V is the theoretical value of the initial velocity. The velocity error estimates from section 4.4 are used. The corresponding error estimates from the velocity variation for the peak pressure is presented in table 4.8 using eq. 4.13.

Table 4.8 – Error estimate for maximum pressure due to a variation in velocity. The velocity error is found in section 4.4. Here the absolute value is used.

Drop Height [m]	Error [m/s]	Error [kPa]
0.1	0.002	±0.224
0.25	0.001	±0.177
0.5	0.040	±10.02

If small wrinkles or waves are present on the free surface this can change the local deadrise angle. This can change the maximum pressure coefficient and thereby the maximum pressure. Using the maximum pressure coefficient from Wagner (1932) the influence coefficient is found by numerical derivation of the maximum pressure coefficient around $\beta = 10°$. A linear approximation at this point show a influence coefficient $\kappa_{\beta 2} = 16.2$.

In the above influence coefficient $\beta = 10°$. From the experimental set up there is a difference in the deadrise angle on each side of the wedge of $\pm 0.004°$. Considering the possibility of small disturbances in the free surface the variation in deadrise angle is set to $\pm 0.5°$. Error estimates for the maximum pressure and maximum pressure coefficient due to this variation are shown in table 4.9.

Table 4.9 – Error estimate for max. pressure $p_{\max}$ and pressure coefficient $C_{P_{\max}}$ due to a variation in deadrise angle of $\pm 0.5°$.

Drop Height [m]	Error on $p_{\max}$ [kPa]	Error on $C_{P_{\max}}$ [-]
0.1	± 7.94	± 8.10
0.25	± 19.87	± 8.10
0.5	± 39.73	± 8.10

4.7.3.2 Total error evaluation

Together with the estimated error from a variation in velocity and local deadrise angle, the sensor error given by the manufacturer will also be included. For the Kulite CT-190 (M) pressure sensors it is specified that the combined non-linearity, hysteresis and repeatability error is 0.5% of full scale measurements. The sensors used are designed for a pressure input range of 350 kPa. This means the sensor error on the maximum pressure can be set to 1.75 kPa.

The total error on the maximum pressure is presented in table 4.10 by using eq. (4.11). Including the sensor error may be counting some error sources twice as the standard deviation is also included. For simplicity, the standard deviation is taken as the mean standard deviation of all pressure peaks for each drop height.

Table 4.10 – Total error estimate for $p_{\max}$. $e_{\Delta V}$ = error due to a variation in velocity, $e_{\Delta \beta}$ = error due to a variation in deadrise angle, e_{sens} = error from sensor specification, e_P = precision error from standard deviation, e_{tot} = total error.

Drop Height [m]	$e_{\Delta V}$ [kPa]	$e_{\Delta \beta}$ [kPa]	e_{sens} [kPa]	e_P [kPa]	e_{tot} [kPa]
0.1	± 0.224	± 7.94	± 1.75	± 11.25	± 19.33
0.25	± 0.177	± 19.87	± 1.75	± 27.68	± 47.61
0.5	± 10.02	± 39.73	± 1.75	± 80.67	± 121.66

Considering the total error relative to the mean maximum pressure for each drop height a percentage ratio of 23.2, 22.0 and 30.2 % is found for 0.1, 0.25 and 0.5 m drop height respectively. The observed decay in maximum pressure with increasing distance from apex found in section 4.6.4 will now be evaluated with the total error estimate. The decrease in maximim pressure from the first sensor row to the last is 16, 35 and 93 kPa for 0.1, 0.25 and 0.5 m drop height respectively. These changes in pressure is within

the total error range presented in table 4.10. It is therefore concluded that the decay observed should not be overemphasized as it can be an effect of errors in the pressure measurements.

For the maximum pressure coefficient the total error is presented in table 4.11. The standard deviation is included, taken as the mean value of the standard deviations at each drop height. The error given by the sensor manufacturer is also included as a possible variation in maximum pressure. For the maximum pressure coefficient this gives a influence coefficient:

$$\kappa_{sens} = \frac{2}{V^2} \tag{4.16}$$

Table 4.11 – Total error estimate for $C_{P_{\max}}$. $e_{\Delta\beta}$ = error due to a variation in deadrise angle, e_{sens} = error from sensor specification, e_P = precision error from standard deviation, e_{tot} = total error.

Drop Height [m]	$e_{\Delta\beta}$ [-]	e_{sens} [-]	e_P [-]	e_{tot} [-]
0.1	±8.10	±1.79	±4.25	±12.71
0.25	±8.10	±0.71	±0.17	±8.83
0.5	±8.10	±0.36	±13.78	±21.88

In section 4.6.5 the maximum pressure coefficients were found to deviate from the prediction by Wagner (1932) of $C_{P_{\max}} = 80$. The experimental values for $C_{P_{\max}}$ were 73, 76 and 67 for 0.1, 0.25 and 0.5 m drop height respectively. The deviation from the Wagner value is therefore 7, 4 and 13, which is inside the total error range from table 4.11. It is therefore possible that the lower results for pressure coefficients relative to the expected values are due to experimental errors.

4.7.4 Final remarks on the pressure analysis

Before the analysis of the pressure measurements was carried out in section 4.6, the velocity was investigated. The fact that there are no available acceleration recordings from this experiment makes the velocity an important parameter. From the analysis in section 4.4, the velocity was found to be constant for 0.5 m drop height. The change in velocity increased with decreasing drop height. Even so, the velocity change is uncertain due to the derivation and filtering used in the process of obtaining the velocity. It is therefore decided that a change in velocity is not an explanation for any observed features in the pressure analysis.

Mean peak pressures from the experiment are above the predicted value by Wagner (1932). This is not expected. In a slamming experiment, a static and a dynamic calibration of the pressure sensors are standard procedure. Wagner's theory is often used as the real value of the peak pressure during the dynamic calibration. It is a possibility that the high pressure peaks are due to an error in the calibration factor. The factor is unknown, so this suggestion cannot be investigated further in this thesis.

For the spatial distribution of the pressure, the peak pressure was found to decrease with increasing distance from apex. Three-dimensional effects are considered, and it is possible that there is some small effect for the upper sensor rows. Regardless, the small gap between tank wall and wedge argues that three-dimensional effects are not

severe for this experimental set-up. It is therefore concluded that measurement errors investigated in section 4.7.3 is the most likely reason for the decrease in peak pressure. The same conclusion is drawn for the spatial distribution of the pressure coefficient, which is lower than predicted by the asymptotic solution.

Several explanations for the negative pressures that occur before the pressure peaks have been established through conversations with researchers familiar with the Kulite sensors. A temperature shock was the preliminary conclusion. Based on the short time duration of the negative pressures and no visible effect of it in the peak or the tail of the pressure time series, this explanation is precluded. The believed reason for the negative pressures is air being trapped in the curvature of the Kulite sensor surface. This conclusion is supported by the positive pressures occurring before the negative drop, which agrees with air being compressed during initial impact with water.

The above explanations for the observed behaviour of the pressure cannot be verified. There are no video recordings or flow visualizations made in the experiment. Without this, the explanations presented here are the best educated guesses that can be made considering the information available.

4.8 FORCE ANALYSIS

4.8.1 Filtering

The measured signal from the force panel is strongly affected by noise and dynamical disturbances from the panel sensor mass. From the hammer tests performed at MARINTEK, the natural frequency of the force sensors used in the combined force and pressure panel was found to be around 400 Hz. Looking at the unfiltered force signal in figure 4.22, the dynamical disturbance can be seen clearly in the tail after maximum force. The force measurements are oscillating at a frequency of 400 Hz approximately, which is also seen in the FFT's. To remove the dynamic disturbance a fourth order band stop filter is applied with cut-offs at 350 Hz and 450 Hz. Noise is also visible in the signal and is removed by applying a fourth order low pass filter at 600 Hz.[12]

4.8.2 Time series

Figure 4.22, 4.23 and 4.24 show the development of the force on the force panel during impact. Both the filtered and original signal is included in the plots to display the effect of the filtering. It appears that the filtering causes a change in the rise time, which should be noted during further investigation of this part of the force development.

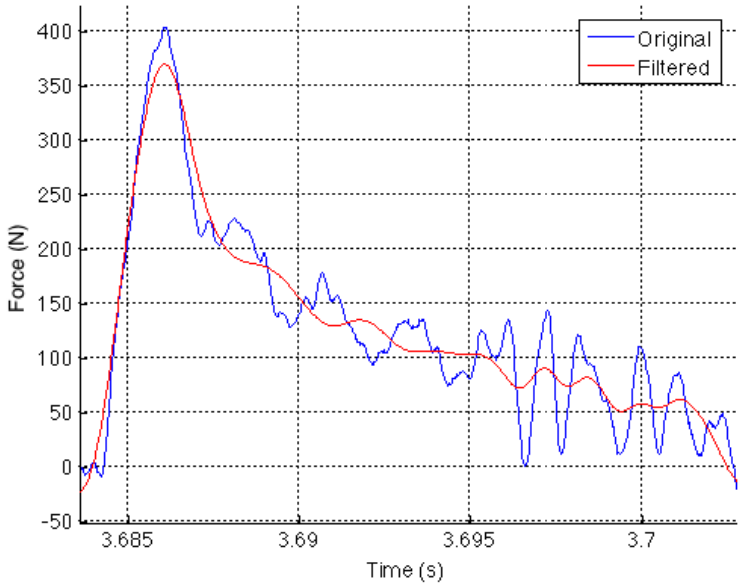

Figure 4.22 – Force panel signal vs. time for 0.5 m drop height (Test 9807). Original and filtered signal presented.

[12] Appendix B.1 - analyse.m

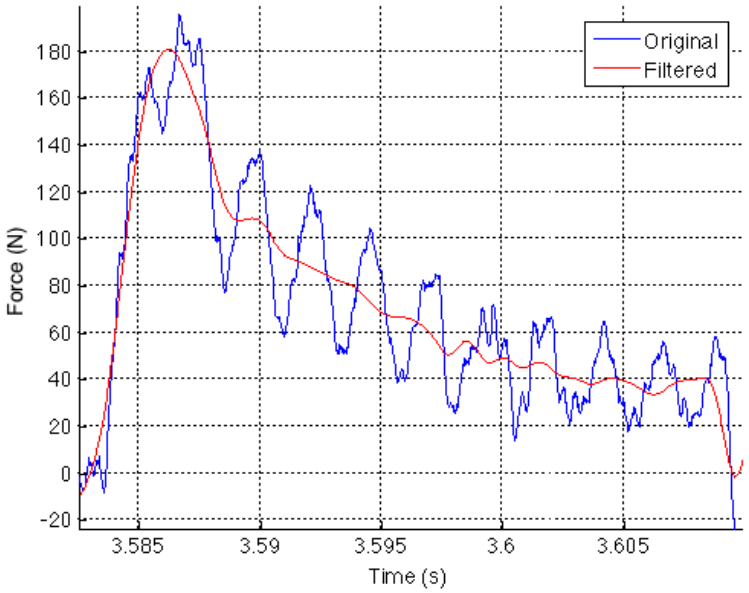

Figure 4.23 – Force panel signal vs. time for 0.25 m drop height (Test 9801). Original and filtered signal presented.

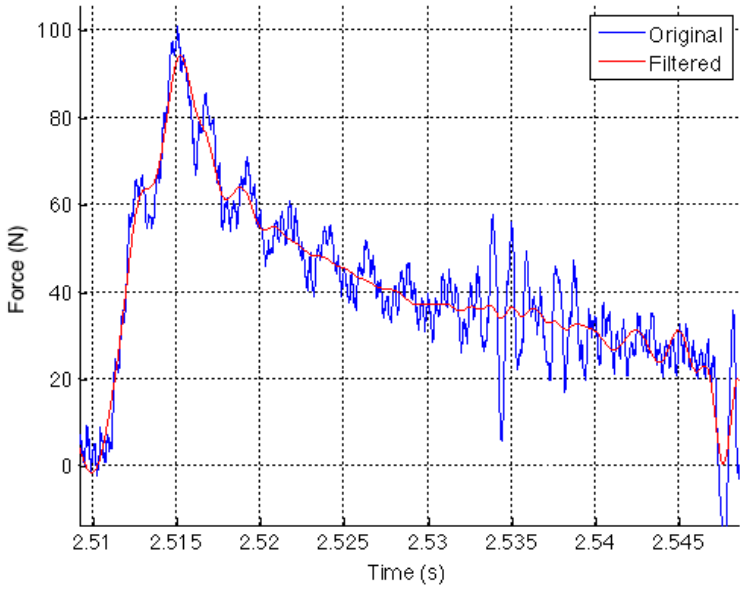

Figure 4.24 – Force panel signal vs. time for 0.1 m drop height (Test 9810). Original and filtered signal presented.

4.8.3 Comparison with integrated pressure

Integrated average pressure measured by the pressure sensors are compared to the force signal.[13] The unfiltered force measurements are used to include the correct rise time lost with the filtering. In figure 4.25 - 4.27 the results of this comparison are presented. By using the average pressure over all sensor rows at all sampled time instances, the force is found by multiplying this with the force panel area. The integrated pressure appears very jagged during the rise phase of the force, which is due to the finite spacing between the pressure sensors.

For 0.5 m drop height (figure 4.22) the agreement between force signal and integrated pressure is satisfying. As the drop height decreases, a larger discrepancy is found, especially in the tail after maximum force. For 0.25 m drop height (figure 4.23) the agreement is good during the rise up to maximum force, but in the tail the integrated pressure has a quicker decay than the force signal. For 0.1 m drop height (figure 4.24) this discrepancy in the tail becomes much more evident. The integrated pressure during the rise of the force is also clearly below the force signal.

For 0.1 m drop height, the force signal displays a deviation from zero before the force rise to its maximum. This deviation starts about 0.15 seconds before the rise and has an average value of approximately 5 N. Evaluating the position measurements, it appears that this deviation starts at the exact time instant where the wedge is released. As this deviation is seen in the end of the measurements as well, a correction is made, subtracting 5 N from the force measurements. It is not sufficient to make the comparison satisfying. This deviation is assumed to be caused by missing zero measurements, but this is not confirmed. Part of the explanation for the large discrepancy observed for the lowest drop height especially might be a loss of local details caused by the use of average pressure over the panel to estimate the force.

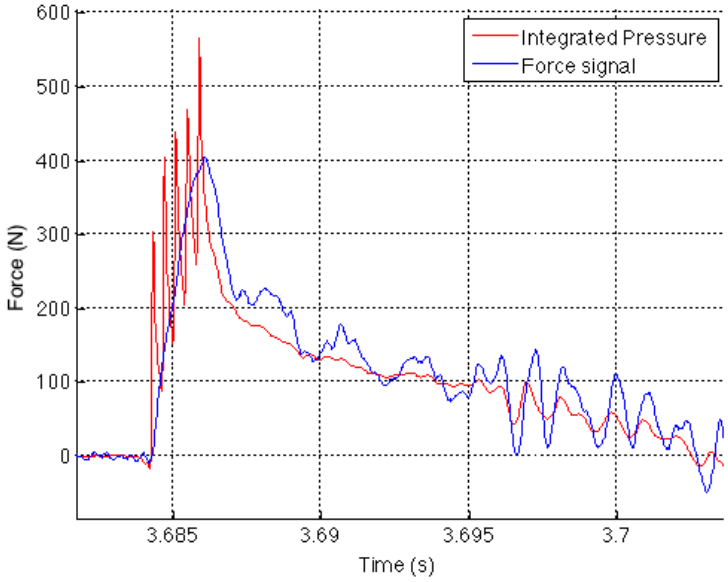

Figure 4.25 – Force panel signal compared to force from averaged pressure for 0.5 m drop height (Test 9807).

[13] Appendix B.10 - integral.m

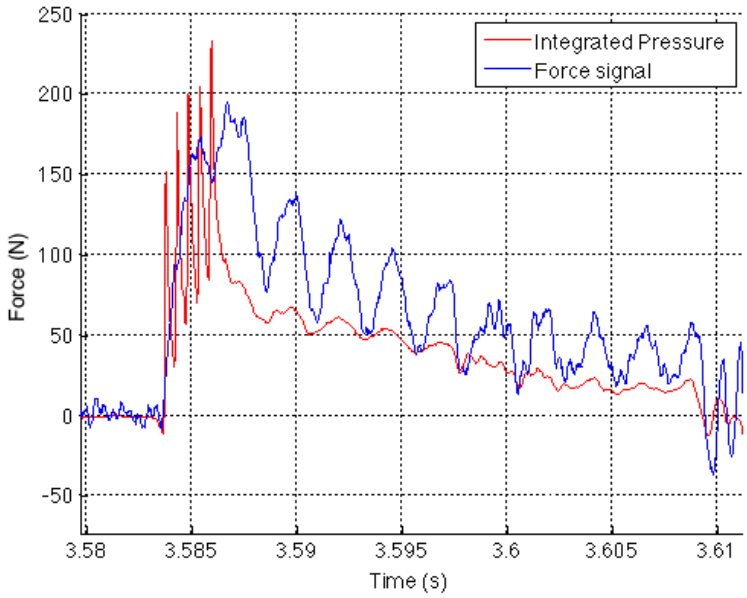

Figure 4.26 – Force panel signal compared to force from averaged pressure for 0.25 m drop height (Test 9801).

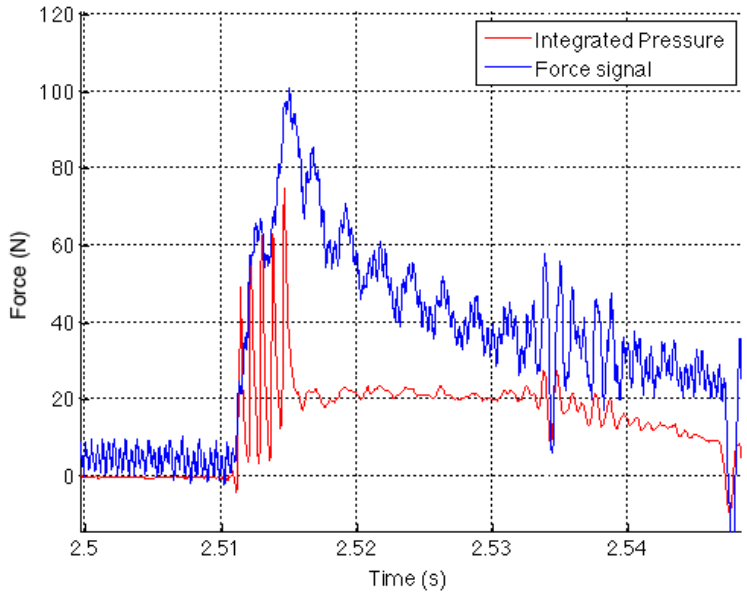

Figure 4.27 – Force panel signal compared to force from averaged pressure for 0.1 m drop height (Test 9810).

4.8.3.1 Uncertainty of pressure integration

The method used to integrate the pressure time series may not be optimal. An average value at each time instant is used, which will cause a loss of local details and a possible reduction of the actual pressure over the panel. For the first row of sensors, the calculated average pressure should be quite correct. The problem occurs in the later rows where the average pressure will be affected by the quickly decreasing pressure of the previous rows. This can lead to an underestimation of the pressure that will be enhanced with time. This effect would be present at all drop heights. Therefore, it is considered a source of uncertaintly, rather than an explanation for the increasing discrepancy with decreasing drop height.

4.8.4 Comparison with classical Wagner theory

The large discrepancy between the integrated pressure and the measured force for 0.1 m drop height is further investigated by comparison with classical Wagner theory (1932)[14]. Wagner used a flat plate approximation to solve the boundary value problem as a blunt rigid body penetrates the free surface with a constant water entry velocity. In the project thesis a Matlab code was developed to generate pressure time series based on Wagner's theory[15]. Pressure time series are now generated using Wagner's theory at the actual sensor positions along the wedge. Assuming the pressure distribution in time and space from Wagner to be applicable for this experiment, the generated pressure time series can be integrated and compared with the force measurements. The results from this comparison are presented in figure 4.28 and 4.29 for 0.5 and 0.1 m drop height respectively.

As it is previously found that the experimental maximum pressure corresponds well with the Wagner maximum, the theory is considered somewhat applicable. Even so, one should be aware of the weaknesses of using Wagner's theory for this experiment. As the theory is valid for blunt bodies (small deadrise angles), this experiment is already in a more uncertain zone, evaluating a 10° deadrise angle. It is also noted that even though the Wagner theory is considered quite reliable for estimating maximum pressures, it will give poorer results for force estimates. Another important aspect is the neglected gravity assumed in this theoretical model, which is only valid when the fluid accelerations are large. The estimates of pressures and forces from Wagner will only be valid until gravity becomes important. This means that after some time the results from Wagner will overestimate the force and pressure.

Some observations can be made for both drop heights. In figure 4.28 for 0.5 m drop height the Wagner integrated pressure is in good accordance with the measured integrated pressure during the rise of the force. The force from Wagner grows larger than the measured values towards the peak and throughout the tail it preserves a larger value. This behaviour is expected due to the neglected gravity.

For 0.1 m drop height, it has been established that the experimental integrated pressure does not compare well with the force measurements. In figure 4.29 a very good agreement is observed between the measured force signal and the Wagner integrated pressure. Such a good comparison is not expected. The expected behaviour is in accordance with what is observed for 0.5 m drop height, with the Wagner integrated pressure overestimating the measured values after some time. During the jagged part of

[14] Appendix B.10 - integral.m
[15] Appendix A.2 - maketimehistory.m

the experimental integrated pressure (caused by the pressure peaks), the large deviation from the integrated pressure by Wagner is surprising. From section 4.6.3, the pressure peaks for 0.1 m drop height are found to be close to the Wagner estimates. This could indicate that the measured force show values higher than the real ones. Explanations for the discrepancy will be discussed further in section 4.9.

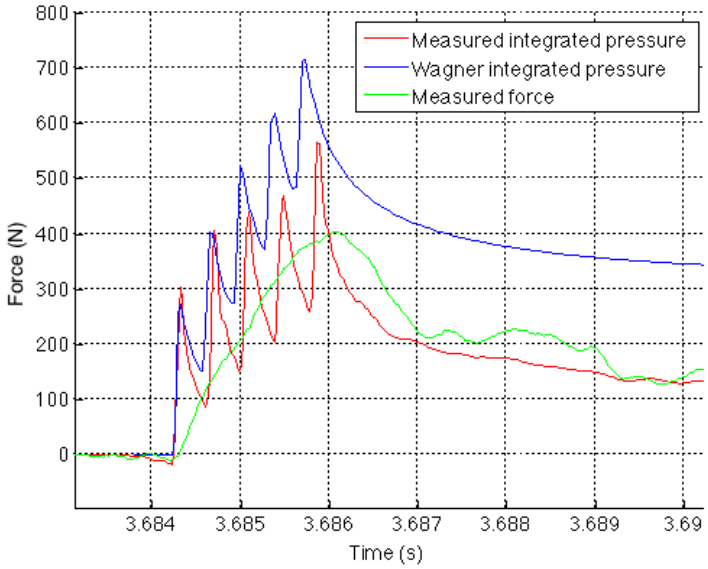

Figure 4.28 – Force panel signal compared to force from averaged experimental pressure and averaged pressure from Wagner (1932) for 0.5 m drop height (Test 9807).

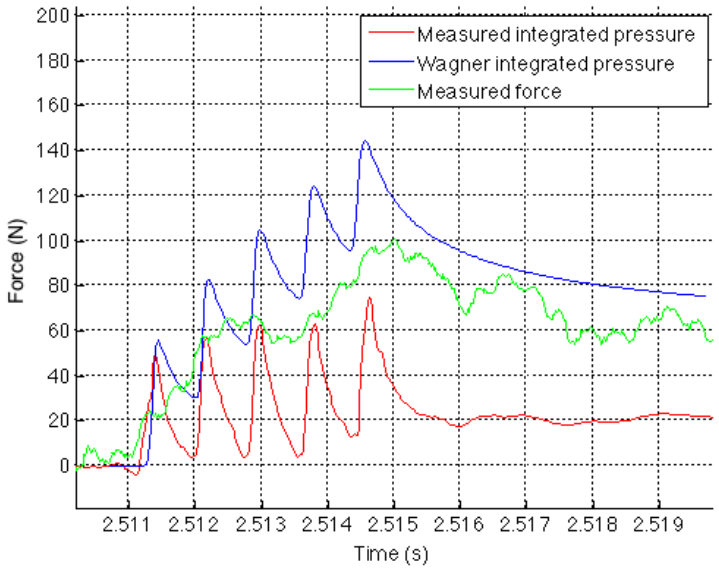

Figure 4.29 – Force panel signal compared to force from averaged experimental pressure and averaged pressure from Wagner (1932) for 0.1 m drop height (Test 9810).

Another comparison with Wagner's theory is made using an expression for the force over the force panel by mathematically integrating the pressure[16]. By Greco (2012) we have the two-dimensional vertical force along a wedge expressed as:

$$F_3 = \int_{x_a}^{c(t)} p(t)dx = \frac{\rho V^2 c\pi}{2\tan\beta}\left(\frac{\pi}{2} - \arcsin\left(\frac{x_a}{|c|}\right)\right) \tag{4.17}$$

where x_a and $c(t)$ are the horizontal coordinates of the start of the force panel and the spray root respectively, β is the deadrise angle, V is the impact velocity and p(t) is the pressure from Wagner (1932). The maximum force on the force panel will take place at the time instant when the spray root is at the upper edge of the force panel, i.e. when the panel is fully submerged. Defining the upper horizontal coordinate of the force panel as x_b the maximum vertical force on the panel can be defined as

$$F_{3\max} = \frac{\rho V^2 x_b \pi}{2\tan\beta}\left(\frac{\pi}{2} - \arcsin\left(\frac{x_a}{|x_b|}\right)\right). \tag{4.18}$$

To make the force three-dimensional it is multiplied by the width of the panel, which in this experiment is 60 mm. The results are presented in table 4.12 together with the corresponding experimental averaged maximum force for each drop height. Percentage values are also given for the ratio between the experimental and theoretical force. It is expected that the theoretical value will overestimate the force. It is observed that for 0.5 and 0.25 m drop height the force ratio is equal while for 0.1 m drop height the experimental force show a higher value compared to the theoretical estimate. This can be interpreted as an indication of the force measurements for 0.1 m drop height showing values that are higher than the actual value.

Table 4.12 – Maximum force on force panel based on Wagner's theory (1932) compared to experimental values.

Drop Height [m]	Wagner $F_{3\,\max}$ [N]	Experimental $F_{3\,\max}$ [N]	Force ratio [%]
0.1	136.9	94.1	68.7
0.25	342.2	184.0	53.8
0.5	684.4	369.6	54.0

4.8.5 Duration of slamming force

The duration of the slamming force is defined as the time period where the force measurements are above 50 % of the maximum force. To find the duration the filtered force measurements are used. From the time axes in figure 4.22 - 4.24 the duration of the slamming force appears to increase with decreasing drop height. Investigating this further shows that the duration is 9, 5 and 3 ms for 0.1, 0.25 and 0.5 m drop height respectively[17]. This behaviour is expected. Wagner (1932) also predicted that the wetted surface will increase linearly with the impact velocity. The loading time

[16] Appendix B.11 - Forcean.m
[17] Appendix B.6 - decay.m

depends on the change of wetted area. A slower increase in wetted surface (lower velocity) will therefore lead to a longer duration of the vertical force on the body.

For the slamming pressure, the longest duration occurs for 0.1 m drop height as well. Even so, figure 4.24 shows that the integrated pressure decreases a lot quicker than the force measurements for this drop height.

4.8.6 Rise time

The rise time of the force from zero to maximum is investigated. As mentioned, the filtering appears to cause a longer rise time. To avoid this, the start time of the rise is taken from the unfiltered time series while the time of maximum force is taken from the filtered time series to avoid dynamic amplification. The results are presented in table 4.13 with all values in milliseconds. For a comparison the rise time predicted from Wagner's theory (1932) is included. The estimates from Wagner agree well with the experimental values.

Table 4.13 – Results for force rise time. t_{exp} = mean rise time for each drop height, σ = standard deviation between tests, t_{Wag} = predicted rise time from Wagner's theory (1932).

Drop Height [m]	t_{exp} [ms]	σ [ms]	t_{Wag} [ms]
0.1	4.97	0.13	4.74
0.25	2.64	0.12	2.99
0.5	1.86	0.08	2.12

If the rise time of the force is close to the natural period of the panel the measurements will be more exposed to dynamic amplification. The natural period of the panel is 2.5 ms. This is closest to the rise time for 0.25 m drop height. The drops from 0.1 m drop height should be the least affected by dynamic amplification. This indicates that the higher maximum force compared to Wagner's estimate found in section 4.8.4 for the lowest drop height is not caused by dynamic amplification.

4.9 DISCUSSION OF RESULTS FROM FORCE ANALYSIS

In section 4.8, a large discrepancy was found between the integrated pressure and force measurements for 0.1 m drop height. As the comparison is better for the other two drop heights, this discrepancy implies that there is some error or physical effect that is occurring for the lowest drop height. As for the pressure measurements, it is investigated if three-dimensional effects or hydroelasticity could be the reason for this discrepancy.

4.9.1 Three-dimensional effects

Three-dimensional effects were evaluated in section 4.7.1 for the pressure measurements. Correction factors from Zhao et al. (1996) were found for the time instances of peak pressure measurements over the panel. This correction factor is now considered for the force measurements. Maximum force occurs when the spray root is at the upper end of the panel. At the end of the force panel the breadth is 133 mm which gives (B/L)=0.47. The correction factor for this ratio implies a 20% reduction of the vertical force caused by three-dimensional effects.

Considering the discrepancy between integrated pressure and force measurements for 0.1 m drop height, the correction factor disagrees with the experimental results. The force measurements are above the integrated pressure. If three-dimensional effects were lowering the force on the panel, a smaller discrepancy would be expected for this comparison. The pressure was found to decrease in accordance with the correction factor as the distance from apex increase. If this pressure behaviour is caused by three-dimensional effects, they are for some unknown reason not affecting the force measurements. This finding supports the assumption of a decreased maximum pressure with increased distance from apex to be caused by measurement errors rather than three-dimensional effects.

4.9.2 Hydroelasticity

For hydrodynamic calculations it is common to assume a rigid body. Using this assumption one can find the pressure on the body and use this to determine the structural response without considering any coupling between the two. As it has already been declared that there are vibrations in the force panel excited by the impact loads it is suspected that hydroelasticity is occurring. From the analysis of hydroelasticity for the pressure measurements in section 4.7.2 any indication of hydroelastic behaviour was not found. This evaluation of hydroelasticity was focused on the time interval around the pressure peaks. For the force measurements a longer time duration is relevant. A continued analysis of hydroelasticity will therefore be carried out. The initial drop tests are used for comparison again as they are measuring pressure without possible disturbances from the vibrating force panel.

4.9.2.1 Comparison with initial drop tests

A comparison is made between the integrated pressure time series from an initial drop test and integrated pressure generated on the basis of Wagner's theory (1932) for 0.1 m drop height.[18]. It is displayed in figure 4.30 together with the same comparison for a final drop test (test 9810). For the initial drop test (4.30b) it can be observed that the integrated pressure from the experiment is closer to the Wagner estimate for a longer

[18] Appendix B.9 - hydroelasticity.m

part of the force rise than the final test (4.30a). The integrated pressure from the initial drop test reaches a higher value quicker than the final test.

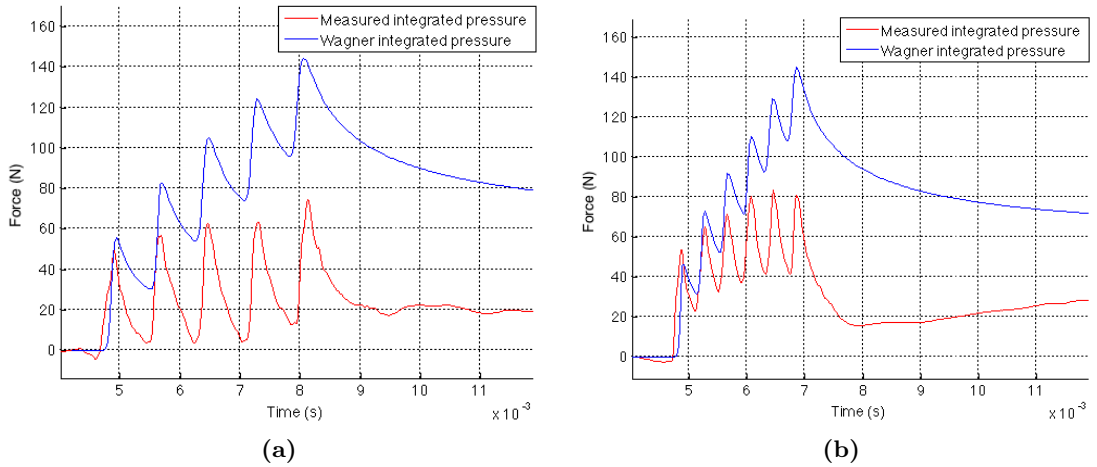

Figure 4.30 – Integrated pressure time series from drop test compared to integrated pressure generated by Wagner (1932) Matlab code for 0.1 m drop height for the two cases: (a) with force panel present (Test 9810) and (b) without force panel.

It is observed in figure 4.27 that the integrated pressure for 0.1 m drop height show oscillations in the pressure tail. These oscillations are also present for 0.25 m drop height, but less distinct. From this, one could expect that hydroelasticity is lowering the pressure in the tail. It is observed that the integrated pressure for the initial and final drop tests fall down to the same pressure level of 20 kPa. Hydroelasticity will not occur for the inital tests. This indicates that hydroelasticity cannot be the explanation for the low integrated pressure compared to the force.

4.9.2.2 The quasi-steady approach

The assumption of a rigid body makes it possible to use the impact pressure on the body to calculate the structural response. This quasi-steady approach is only valid if hydroelasticity is not excited. As stated by Bereznitski (2001) and Faltinsen (2010), the validity of this approach depends on the ratio between the duration of the loading relative to the natural period of the dry structure. Results from Faltinsen (1999) show that a when the ratio is larger than 2, a quasi-steady approach is applicable. For the case to be fully quasi-steady the ratio should be larger than 5 (M. Greco 2015, pers. comm., 17 April).

The natural period of the force panel is found in the hammer test as 2.5 ms. Load time is found to increase with decreasing drop height, from 3 ms for 0.5 m to 9 ms for 0.1 m. This implies that the higher drop heights are more sensitive to hydroelasticity. Calculating the ratios for the three drop heights it is found to be 1.2, 2 and 3.6 for 0.5, 0.25 and 0.1 m drop height respectively. These ratios show that for 0.5 m drop height hydroelasticity should definitely be considered. For 0.25 and 0.1 m drop height hydroelasticity can still affect the results, but in a smaller scale. It is the lowest drop height that show the largest discrepancy between force and integrated pressure. As this case is least sensitive to hydroelasticity, it is supposedly not the reason for the large discrepancy found between integrated pressure and force measurements.

4.9.2.3 Preliminary conclusion on hydroelasticity

The aim of this investigation of hydroelastic behaviour was a possible explanation for the discrepancy between force measurements and integrated pressure for the lowest drop height. Comparing the initial drop tests without a vibrating force panel to the final drop tests did not give any indication of hydroelasticity. One would expect a oscillating pressure for the tests with a force panel present. The comparison shows the opposite, with a more oscillating pressure behaviour for the initial drop tests. The fact that the higher drop heights are more sensitive to hydroelasticity breaks down the hypothesis of hydroelasticity causing the discrepancy between force and integrated pressure. It is therefore for now concluded that hydroelasticity is not an explanation for the discrepancy. Even so, hydroelastic effects are not fully disregarded. In the tail of the pressure recordings one can observe oscillations.

The oscillations can be explained by the case studied by Faltinsen (2000). He describes how it takes time to build up elastic deformations during water impact of a flat plate. There will be a phase that he defines as the structural inertia phase. During this phase, the force impulse works on the body, but the vibrations will not start until the plate is fully wetted. After the structural inertia phase, Faltinsen (2000) describes a free vibration phase where the maximum strains occur. As the deadrise angle is 10° in this case one would expect a somewhat different behaviour than for a flat plate. A larger deadrise angle means a longer force impulse. This means it will take more time before a free vibration phase will start. It should also be noted here that the wedge is stopped right after the force panel is fully submerged. Therefore, there is a possibility that what can be seen in the pressure recordings is not a free vibration phase. It could be that the measurements only show a coupling between the hydrodynamic and structural loads and this may result in the oscillatory behaviour in the pressure tail.

4.9.3 Performance of force sensors

It cannot be ruled out that the discrepancy between integrated pressure and force measurements are due to a force sensor error. The tests for 0.1 m drop height were executed as a last round of experiments. It is not possible to conclude on whether or not a sensor error occurred, as there is no later reference.

For the 'beam' type of force sensor used in these tests, there are possible error sources. The force sensors used are designed to measure perpendicular loading. With a 10° deadrise angle the force working on the panel will not be perpendicular. This will lead to a poorer quality of the force measurements. When the force works on a part of the panel only the quality will also fall. This uncertainty will be present until the whole panel is covered, i. e. until maximum force occur. In the decay of the force measurements the largest discrepancy is found, but this source of error is no longer valid at this time. Many degrees of freedom can be activated as response in the panel. Returning the force measurements back to the actual loading can be difficult, and this process may lead to an uncertainty.

It is not possible to tell how much these sources of uncertainty are affecting the force measurements. Regardless, they demonstrate that there are reasons to not rely fully on the force measurements when comparing against integrated pressure.

4.9.4 Pressure behaviour during force measurements

In figure 4.22 - 4.24 a difference in the overall shape of the integrated pressure can be observed. For 0.5 and 0.25 m drop height the integrated pressure displays a triangular shape as it increases quickly and then reduces more slowly. For 0.1 m drop height, the integrated pressure peaks and then it falls straight down to a lower value. The gradual decrease that is showing for the other drop heights is not observed for 0.1 m.

Plots of the time series during the time intervals corresponding to the time of the presented integrated pressure in figure 4.22 and 4.23 is illustrated in figure 4.31. For 0.5 m drop height in figure 4.31b the pressure time series for all sensors show an equal slope and thereafter blend into one curve. For 0.1 m drop height some measurements go quickly towards zero after peak pressure while others show a longer tail as observed for the other drop heights. It is considered that the sensors that approach zero fast will lower the average pressure used in the integrated pressure.

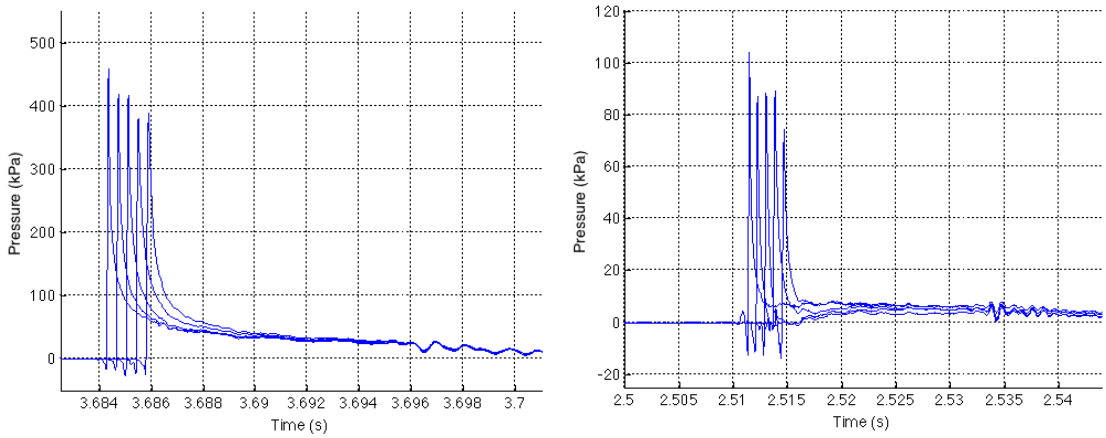

Figure 4.31 – Pressure time series at the same time interval as the presented comparison between force and integrated pressure for a) 0.5 m drop height and b) 0.1 m drop height.

To check this assumption a pressure time series that does not show this quick decay towards zero is used for the pressure integration. By 'copying' this time series to the other sensors, the average pressure is found in the same way as in section 4.8.3. The time series for the fourth sensor (fourth peak from the left) in figure 4.31b is used for all sensors. The result is shown in figure 4.32. It is observed that the comparison is more satisfying in the rise up to maximum force than it is for the original time series. In the force tail, the comparison is still poor.

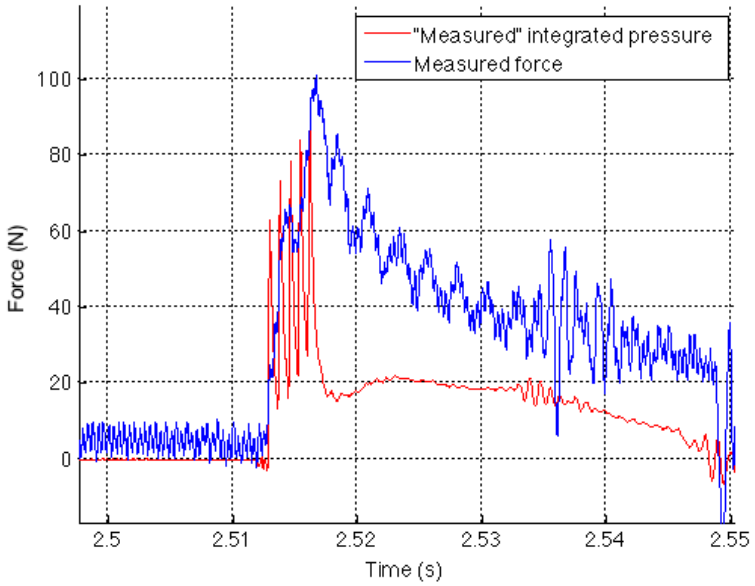

Figure 4.32 – Force panel signal compared to integrated pressure with pressure over all sensors as pressure from sensor 1012 for 0.1 m drop height (test 9810).

4.9.5 Final remark on force analysis

The force measurements have been compared to the integrated pressure from the force sensors. The main question left from the force analysis is why a large discrepancy is found for 0.1 m drop height. For 0.5 m drop height the comparison is very good and it is slightly poorer for 0.25 m drop height.

Comparing force measurements to integrated pressure generated from classical Wagner theory (1932), the behaviour for 0.1 m drop height is again deviating from the others. It is expected that the Wagner integrated pressure will overestimate the force measurements after some time, but for the lowest drop height the comparison is very good through the decay of the force. This implies that the force measurements are too high, as it is expected to decrease much faster than Wagner predicts. For the measured maximum force, the value for 0.1 m drop height is again showing a higher value relative to maximum force predicted by Wagner. The other two height show a force ratio of 54 % compared to Wagner, while the lowest drop height show a ratio of almost 70 %.

Three-dimensional effects are considered for the force measurements, but it is concluded that they are not affecting the measurements. Three-dimensional effects are not likely to occur for the applied test set-up. It is also an argument that these effects would lower the force. For 0.1 m drop height the comparison with Wagner implies that the force measurements are above the expected values.

Hydroelasticity is also considered as it can diminish the pressure over the body. Comparison of integrated pressure from an initial drop test with force measurements from a final drop test show the same large discrepancy for 0.1 m drop height. A force panel is not present in the initial drop tests and it is the vibrations from this panel that would initiate the hydroelastic behaviour. It is therefore concluded that the discrepancy cannot be explained by hydroelasticity.

The only explanation left is measurement errors. It has already been concluded in the

pressure analysis that error sources can explain deviations of the pressure measurements from theoretical predictions. As mentioned in section 4.9.3 there are also uncertainties present in the force measurements. The lowest drop height will be more sensitive to errors due to its lower measurement values. It is suspected that the force measurements for 0.1 m drop height are showing values higher than the real ones. It is also observed that the pressure measurements for this drop height show a different decay in pressure than for the other heights. The best guess for an explanation of the discrepancy is a combination of these two measurement errors.

5

PARAMETER STUDY

In this chapter a parameter study will be carried out in two parts. First, the repeatability of the pressure and force measurements will be investigated. Repeatability is an important aspect of an experiment. Even though the maximum pressures are expected to have a stochastic nature (Faltinsen 2010), it is expected that the pressure sensors will preserve an amount of repeatability. An error estimate was made for the maximum pressures in chapter 4. This measurement error was found to be the most likely explanation for differences between measurements and theoretical predictions. In this chapter, the error estimate can be checked by comparison with the repeatability.

The second part consists of an investigation of how different features of the slamming phenomenon depend on a varying drop height. Linear or non-linear behaviour of different involved quantities are discussed. Two Matlab codes are used in this chapter. The code used to investigate the repeatability can be found in Appendix C.1, while the code for investigation of drop height dependency is found in Appendix C.2.

5.1 REPEATABILITY

When an error analysis is carried out, two types of errors are distinguished: bias and precision errors. Bias errors are systematic errors that cannot be revealed from repetition of an experiment. Precision errors on the other hand are random errors that appear as a scatter in the measurements when they are repeated.

Repeatability can be defined as the variation in measurements from a single instrument for a given item under the same test conditions when repeated measurements are compared. The drop tests were performed four times for 0.5 and 0.25 m drop height and three times for 0.1 m. The repeatability of the experimental measurements can therefore be investigated.

To evaluate the repeatability it is necessary to compare the measurements at the exact same stage of impact through time. As the start time of each drop test is at some arbitrary time before the wedge was released it requires some reference point to synchronize the recordings between drops. A first attempt was made using the time instant where the position measurements are zero (when apex initially hits the free surface). It turned out these measurements were not accurate enough to synchronize the quick pressure peaks. The reference point for the synchronization between drops will therefore be taken in the data under consideration, such as a pressure peak over a given sensor for pressure measurements. There will probably be an error connected to this synchronization method as well, but it is considered the best alternative.

The results of the repeatability analysis consist of the mean and standard deviation found over N repeated tests. The mean of a measurement A is calculated as:

$$\mu = \frac{1}{N}\sum_{i=1}^{N} A_i \tag{5.1}$$

and the standard deviation is found as:

$$S = \sqrt{\frac{1}{N-1}\sum_{i=1}^{N} |A_i - \mu|^2} \tag{5.2}$$

5.1.1 Repeatability of pressure measurements

To synchronize the pressure recordings from N repeated tests, the time instance of maximum pressure over the first sensor row is used. One column of sensors is analysed (sensor 1029 - 1008) for two drop heights, 0.1 m and 0.5 m. The mean pressure for each sensor at each sample point is found together with the standard deviation. In figure 5.1 and 5.2 the mean is presented as a solid line while the magnitude of standard deviation is represented by a shaded area about the mean line. It is observed that the largest standard deviations occur around the peak pressures, which complies with the findings of Lewis et al. (2010).

The repeatability of the pressure peaks are investigated in more detail. Faltinsen (2010) describes that in the initial phase of the pressure development, large pressures appear that are very sensitive to small changes in the local flow details. This results in a strongly stochastic behaviour of the maximum pressure. In the current experimental data, the standard deviation of the maximum pressure relative to the peak pressure value appears to increase with increasing drop height. The conclusion that the maximum pressure becomes more stochastic in nature as the water entry velocity increase is also suggested in Faltinsen (2010).

Lewis et al. (2010) estimated the error on the maximum pressure based on sensor error given by the manufacturer as well as errors from amplifier and data acquisition systems. Their total error was estimated to be 1.1 %. The repeatability of the maximum pressure proved to be inside this error range. For the data analysed here the maximum variation in peak pressure is found to be 15 and 20 % for 0.1 and 0.5 m drop height respectively. These values are far above the values from Lewis et al. (2010). It is noted that Lewis et al. (2010) performed their drop test with a 25° deadrise angle. This would imply a less stochastic behaviour of the pressure peaks. Regardless, the large difference suggests that there are other error sources present in the MARINTEK experiment.

In the previous chapter an error analysis was made for the maximum pressure, trying to estimate the total error. Standard deviation, sensor error from sensor specification sheet, error from velocity measurements and the effect of small wrinkles on the free surface were included. The total error was estimated to be 23.2 and 30.2 % of maximum pressure for 0.1 and 0.5 m drop height respectively. These results agree quite well with the repeatability error established in this section. The error estimates are above the experimental values, which implies that the error estimates made are conservative. This could be explained by an overestimation of the variation in deadrise angle caused by disturbances in the free surface.

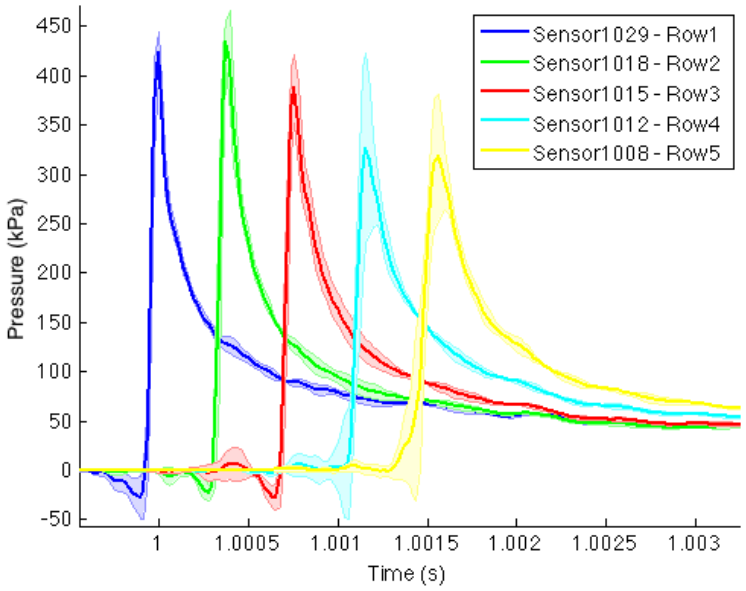

Figure 5.1 – Mean pressure time history of sensors 1029 - 1008 with shaded area representing the magnitude of the standard deviation for 0.5 m drop height.

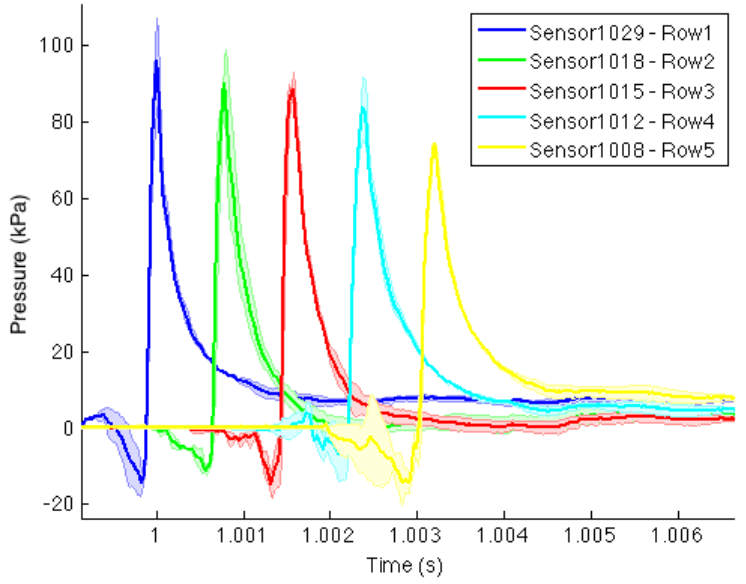

Figure 5.2 – Mean pressure time history of sensors 1029 - 1008 with shaded area representing the magnitude of the standard deviation for 0.1 m drop height.

5.1.2 Repeatability of force measurements

Force time series are synchronized over N repeated tests by using the time instant of the maximum force as reference. Figure 5.3 and 5.4 show the mean force together with the magnitude of the standard deviation represented as a shaded area about the mean line. In general, the repeatability is found to be satisfying, at least during the duration of the slamming force. Further along the tail of the force measurements, a larger standard deviation is found. For 0.5 m drop height the standard deviation starts to grow in magnitude when the force stabilizes around zero and will therefore not be of much importance for the experimental results. For 0.1 m drop height there is more noise present during the decay of the force measurements. Noise is considered disturbances of random nature and a larger standard deviation would be expected when noise affects the measurements. The noise seems to be connected with an abrupt decrease of the measured force. It is considered that as the duration of the force is longer for 0.1 m drop height, the noise may be caused by the wedge being stopped. In this experiment, the wedge was stopped right after the force panel was fully submerged. Evaluating the position measurements and derived velocity at the time of the abrupt force decrease, it does not coincide with the time the wedge is stopped. Because the wedge is stopped by oil dampers it is a possibility that a deceleration from them have started, which causes the noise although it is not entirely stopped. This could explain the sudden force loss and noise.

For the maximum force value, a relative standard deviation to the maximum force is found to be 1.2 % for 0.5 m drop height. Compared to results from Tveitnes et al. (2008), this value is satisfying as they found the standard deviation of their force measurements to vary between 1 and 3 %. For 0.1 m drop height the result is not very satisfying, showing a relative standard deviation of 15 %. To check if the relative standard deviation increases with decreasing drop height, the 0.25 m drop height case is checked. It shows a standard deviation close to the one found for 0.5 m drop height. The lack of repeatability is only showing for 0.1 m drop height. This suggests that the force measurements for the lowest drop height is more sensitive and less certain.

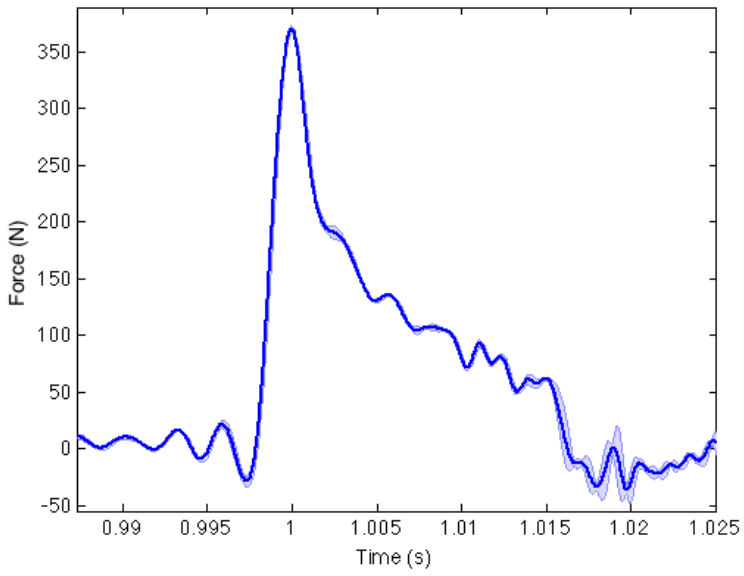

Figure 5.3 – Mean filtered force time history from force panel with shaded area representing the magnitude of the standard deviation for 0.5 m drop height.

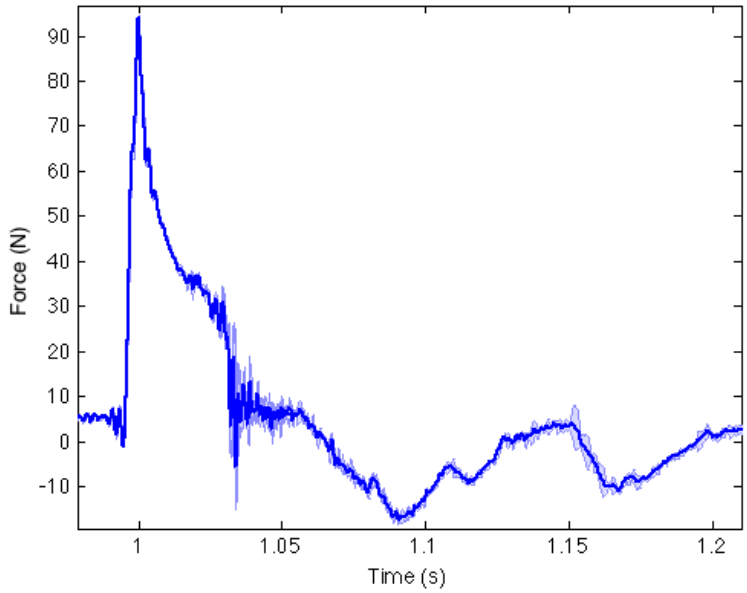

Figure 5.4 – Mean filtered force time history from force panel with shaded area representing the magnitude of the standard deviation for 0.1 m drop height.

5.1.3 Final remark on repeatability

For the pressure peaks, the repeatability is poor. This is expected, as the pressure peaks are very sensitive to small variations in physical conditions (Faltinsen 2010). Considering the error estimates made in the chapter 4, the poor repeatability of the peak pressures can be explained by error sources such as disturbances of the free surface. Pressure peaks during slamming are of a stochastic nature (Faltinsen 2010). The error estimates used to explain the features of the recorded pressure in chapter 4 is above the maximum standard deviation found in this repeatability analysis. If the error is overestimated, or if some errors does not show in this repeatability analysis is unknown.

Force measurements are expected to show better repeatability as the force itself is less responsive to small variations in physical conditions. For 0.5 m and 0.25 m drop height, the repeatability is very satisfying, and in accordance with the expected repeatability. For 0.1 m drop height, the standard deviation is 15 times larger than for the other heights for the maximum force. In chapter 4, it was suggested that an error is occurring for the force measurements at the lowest drop height. The poor repeatability for 0.1 m supports this hypothesis.

5.2 LINEAR AND NON-LINEAR VARIATION OF LOCAL QUANTITIES

An analysis is carried out to find how the features of the slamming phenomenon vary with drop height (and impact velocity). The investigation is done to see if the quantities have a linear or non-linear behaviour. The variation along the rows is also evaluated. A comparison is made with the experiment carried out by Yang et al. (2007) who performed a drop test with a 10° wedge with drop heights ranging from 0.05 to 0.5 m. The weight of their wedge was 60 kg, that is 110 kg lighter than the wedge in the MARINTEK experiment.

5.2.1 Peak pressure

An investigation of the variation of peak pressure with drop height is carried out. The peak pressure is found for each sensor for all final drop tests and the mean is taken over each row. This mean row peak pressure is presented in figure 5.5 as a function of drop height. As the drop height increases the maximum pressure increases, and the variation appears to be linear. Faltinsen (2010) states that when the deadrise angle is larger than 5°, the maximum slamming pressure is proportional to the square of the impact velocity. As the impact velocity can be defined as $\sqrt{2gh}$ we have the following relation between maximum pressure and drop height:

$$p_{\max} \propto V^2 \propto h. \tag{5.3}$$

This corresponds well with the behaviour seen in figure 5.5. As the maximum pressure depends on the impact velocity, it is expected that the rows closer to apex will experience the highest pressure peaks if the wedge is decelerated. This is the case for the data presented by Yang et al. (2007). As the velocity is close to constant for MARINTEK's data, the measurement error found in chapter 4 is assumed to be the reason for the scatter here.

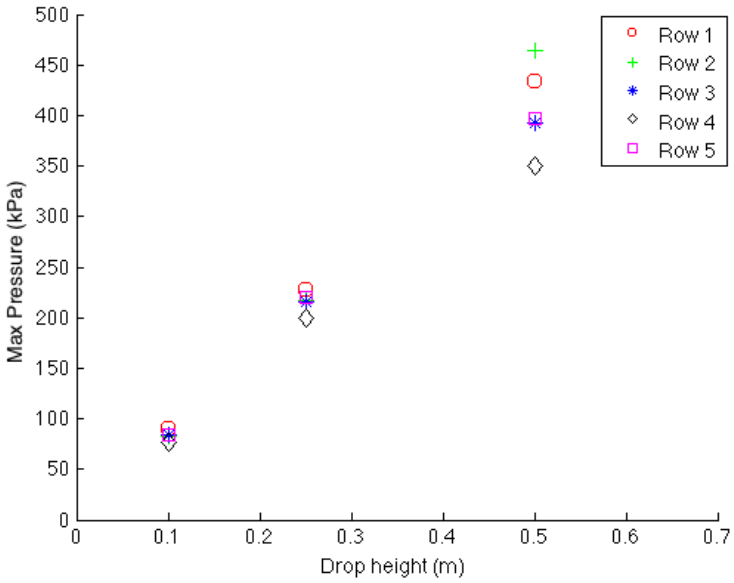

Figure 5.5 – Variation of mean peak pressure with drop height over each sensor row.

5.2.2 Pressure coefficient

The pressure coefficient is defined as

$$C_p = \frac{p}{\frac{1}{2}\rho V^2} \tag{5.4}$$

where p is the pressure, ρ is the density of water and V is the impact velocity. In this analysis, the variation of the maximum pressure coefficient with drop height is considered. The mean maximum pressure over each sensor row is made non-dimensional using equation (5.4). The result is shown in figure 5.6. As the maximum pressure is expected to be proportional to V^2, the non-dimensional expression (5.4) should be unaffected by the drop height and only depend on the deadrise angle. This seems to agree well with the behaviour observed in figure 5.6. The scatter across the rows is largest for 0.5 m drop height, while it is smallest for 0.25 m. Yang et al. (2007) showed that the scatter did not change with drop height for their data. They used the actual velocity at the time instance of the maximum pressure. The velocity change is small or zero for the MARINTEK experiment. It is therefore expected that the scatter is mostly related to measurement errors, as discussed in chapter 4.

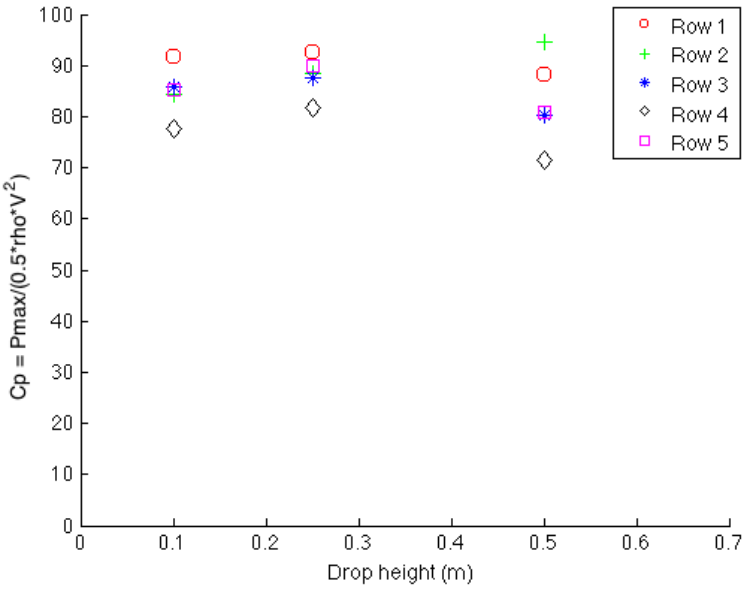

Figure 5.6 – Variation of maximum pressure coefficient with drop height over each sensor row.

5.2.3 Duration of slamming pressure

The duration of the slamming pressure is defined as the time range where the pressure on the wedge exceeds 50% of maximum pressure. The average duration over each sensor row is found for all drop tests. The results over each row for each drop height is shown in figure 5.7. A trend towards an inversely proportional relationship between drop height and duration of the slamming pressure is seen. This could be expected as a lower impact velocity will give a softer impact. However, for 0.25 and 0.5 m drop height the duration appears to be very similar. If the duration was actually inversely proportional to the drop height, one would expect a longer duration for 0.25 m than for 0.5 m.

From the similarity solution (Dobrovol'skaya 1969), the spatial extent of the slamming pressure is proportional to the horizontal distance to the spray root, c. As the sensors are positioned equally for all drop heights, one would expect the spatial duration of the slamming pressure to remain constant for all heights. The time duration would then depend on the velocity, which will be proportional to the square of the drop height, $\sqrt{h}$. From this argumentation one could assume the slamming pressure duration to be inversely proportional to $\sqrt{h}$. Across the rows, the duration seems to increase with increasing distance from apex.

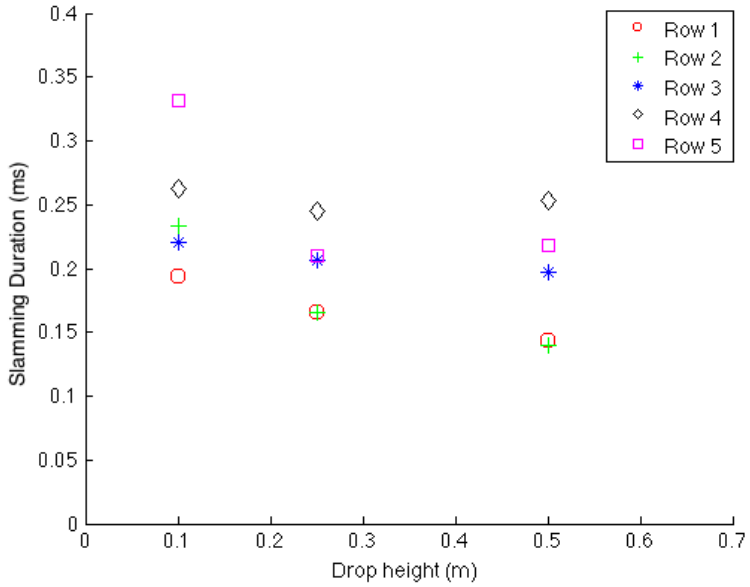

Figure 5.7 – Variation of slamming pressure duration (50% of maximum pressure) with drop height over each sensor row.

5.2.4 Pressure rise time

Pressure rise time is here defined as the time it takes for the pressure to increase up to its peak. The start time is taken as the time of maximum negative pressure before the rise start, or at zero pressure before the peak for those measurements that do not show negative pressures. Variation of pressure rise time with drop height is presented in figure 5.8. The relation between rise time and drop height appears to be non-linear. For 0.25 and 0.5 m drop height the rise time is approximately 0.15 ms. For 0.1 m drop height the rise time almost doubles. A contributory cause for this increased rise time could be the larger negative pressures seen for the lowest drop height. It is not considered the whole explanation, as the negative pressure is small relative to the whole rise up to maximum pressure.

Two other observations are made. Across the rows, a tendency towards increased rise time with increased distance from apex is seen. The second observation is the scatter of the results for each drop height, which is remarkably lower for 0.25 m drop height.

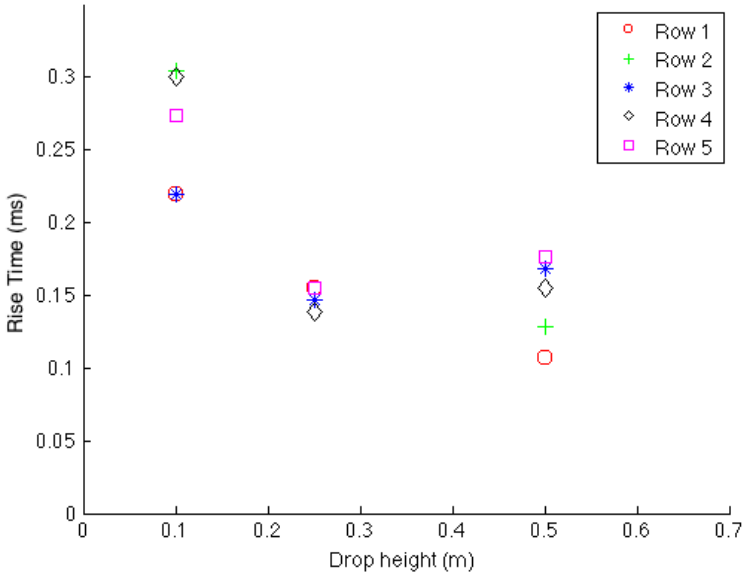

Figure 5.8 – Variation of pressure rise time with drop height over each sensor row.

5.2.5 Slamming force

The variation of the slamming force on the force panel with drop height is also evaluated. For each drop height, the maximum force for all tests at this height is found and presented in figure 5.9. In the previous chapter, the following expression was derived for the maximum force on the panel (Greco 2012):

$$F_{3\max} = \frac{\rho V^2 x_b \pi}{2 \tan \beta} \left(\frac{\pi}{2} - \arcsin \left(\frac{x_a}{|x_b|} \right) \right). \tag{5.5}$$

From this equation one can assume that the maximum force will be proportional to V^2, and therefore proportional to the drop height h. From figure 5.9 a tendency towards a linear dependency can be seen. The maximum force for 0.1 m drop height deviaties from the linear behaviour. It was suggested in chapter 4 that the force measurements for this drop height show values higher than the real ones. This hypothesis is supported by the value for 0.1 m drop height in figure 5.9.

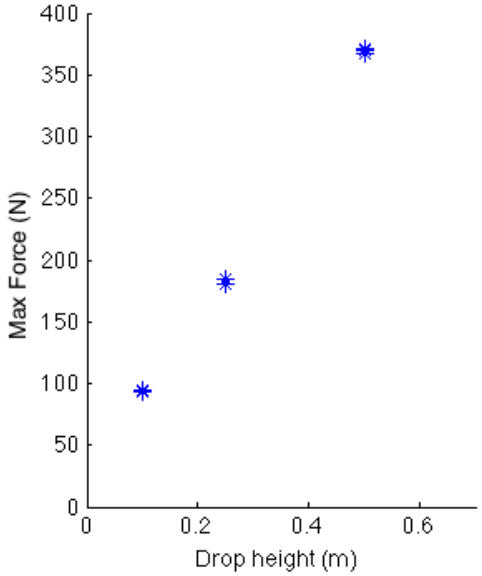

Figure 5.9 – Variation of maximum slamming force with drop height.

5.2.6 Duration of slamming force

The duration of the slamming force is defined as the time interval where the force is above 50% of maximum force. In figure 5.10 the duration for each test at each drop height is presented. The duration of the slamming force can be assumed to be proportional to the change in wetted surface (Wagner 1932). A higher impact velocity will therefore lead to a quicker change in wetted surface and a corresponding shorter duration of the slamming force. From figure 5.10, the duration of the slamming force appears to be inversely proportional to the drop height. It is noted that there is a larger scatter between the tests at 0.25 m drop height.

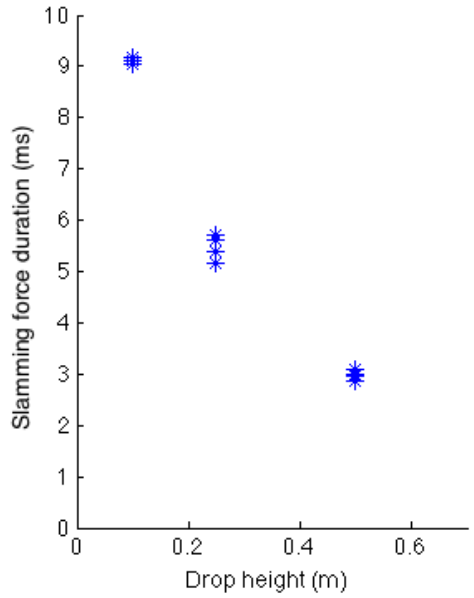

Figure 5.10 – Variation of slamming force duration with drop height.

5.2.7 Final remark on drop height dependency

From the above analysis, the variables that resemble a linear variation with drop height is the pressure peaks, the maximum force and the slamming force duration. A non-linear variation with drop height is observed for the pressure coefficient, slamming pressure duration and pressure rise time. The observed variation of the maximum slamming force with drop height supports the hypothesis of a measurement error for the force at 0.1 m drop height, as it deviates from the linear behaviour.

The scatter across the rows varies for the different quantities. For the pressure peaks and pressure coefficient, the scatter increases with increasing drop height. This is similar to what is found in Faltinsen (2010), and indicate that the nature of the pressure peaks become more stochastic as the impact velocity increase. For pressure duration and rise time, the scatter is remarkably lower for 0.25 m drop height than for the other two heights. It seems like the pressure sensors behave more stably for 0.25 m.

6

EXPERIMENTAL COMPARISON

In this chapter, a second drop test of a 10° wedge in similar conditions will be studied. The hope is to better understand the observed discrepancies from theoretical predictions in the MARINTEK experiment. By evaluating and comparing to a second drop test, increased insight in expected results for a drop test of a 10° wedge can be obtained. The goal is not to find equal results, but to explain the outcome of the comparison from the available literature on slamming.

Not many drop tests of wedges with 10° deadrise angle are available, and only two possible experiments were found. One was performed by Sayeed et al. (2010), with the aim of investigating the slamming loads on a wedge formed section. The other was performed by Yang et al. (2007) to study the water entry of symmetric wedges and a stern section for a modern containership. Due to lack of experimental data from the experiment by Sayeed et al. (2010), the experiment by Yang et al. (2007) will be used.

The experiment by Yang et al. (2007) will be presented shortly, and pressure measurements and impact velocity will be compared to those found in this thesis from MARINTEK's experiment.

6.1 EXPERIMENTAL SET-UP

6.1.1 Model and rail system

A two-dimensional symmetric wedge model with dimensions as illustrated in figure 6.1 is used. It is dropped into a tank with width 2.5 m and length 5.4 m. The depth is varied in the experiment, but for the results considered here a water depth of 1.5 m is applied. The wedge is attached to a guide rail system to lead it vertically through the free surface. Bush bearings are installed between the wedge model and the rail to reduce friction. To eliminate disturbances when the model is initially dropped, an electro-magnetic system is used to release it. The model is made of wood to ensure rigidity. The weight is varied between 50 and 60 kg. In the results presented in the following, the weight is 60 kg.

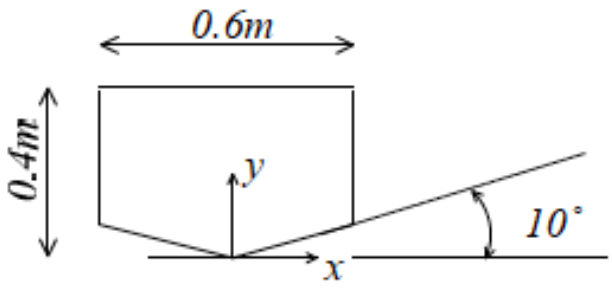

Figure 6.1 – Schematic view of 10° wedge used in the experiment. (Yang et al. 2007)

6.1.2 Measurement systems

To measure the pressure along the wedge surface, five pressure sensors are applied. The sensor type is not specified in their report, and attempts of establishing contact with the writers have not been successful. Pressure sensors are located 100 mm from the middle of the model. They are placed 50, 100, 150, 200 and 250 mm from apex. Four accelerometers are also attached on the inner bottom of the model corners. A sampling frequency of 5 kHz is used for all measurements together with a 10 kHz low pass filter.

6.2 RESULTS

The results that will be used for comparison in this chapter are shown in figure 6.2. These results are from a drop height of 0.5 m, and a comparison will only be made for this drop height. The acceleration is measured by the four accelerometers, while the velocity is integrated from the acceleration measurements. Pressure time histories for all five pressure sensors are also shown. All tests were conducted twice to ensure a satisfying repeatability. The data in figure 6.2 will be digitalized for further comparison. This process may lead to a small loss of accuracy, but this is not considered a problem.

6.3 COMPARISON

For simplicity, the two experiments compared in this chapter will be referred to as:

- *Experiment 1*: the experiment by MARINTEK analysed in this thesis
- *Experiment 2*: the experiment by Yang et al. (2007) used for comparison in this chapter

6.3.1 Velocity

The velocity plot from figure 6.2 is digitalized and compared to the velocity from a final drop test in *Experiment 1* (Test 9807). There is a slight difference in maximum velocity. Where *Experiment 1* have an initial impact velocity of 3.1 m/s, *Experiment 2* only reach 3.0 m/s. The lower velocity in the latter case is expected by the authors of the report to be caused by friction in the rail system. Velocities for drops with 0.5 m drop height is presented in figure 6.3 for both *Experiment 1* (6.3a) and *Experiment 2* (6.3b). The marked circles on the velocity plots represent pressure peaks. For *Experiment 1* (fig. 6.3 a), the first circle represents peak pressure at the first sensor row (85 mm from apex) and the second circle peak pressure at the fifth row (125 mm from apex).

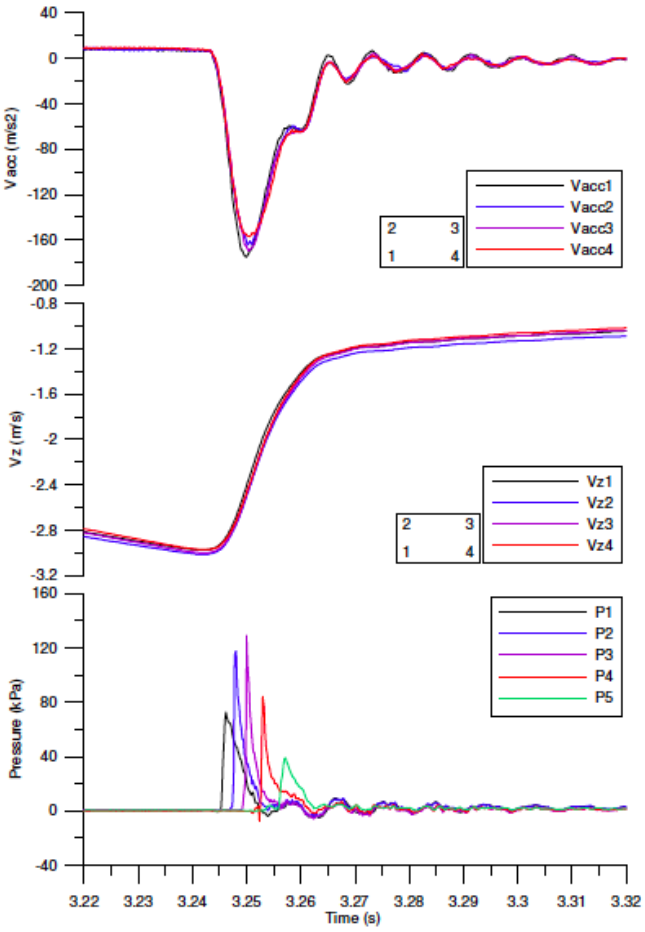

Figure 6.2 – Results from the experiment: time history of acceleration, velocity and pressure for 0.5 m drop height. (Yang et al. 2007)

For *Experiment 2* (fig. 6.3 b) the two circles represents the second sensor (100 mm from apex) and thirds sensor (150 mm from apex). For both cases the distance between the two sensors which peaks are illustrated is 50 mm.

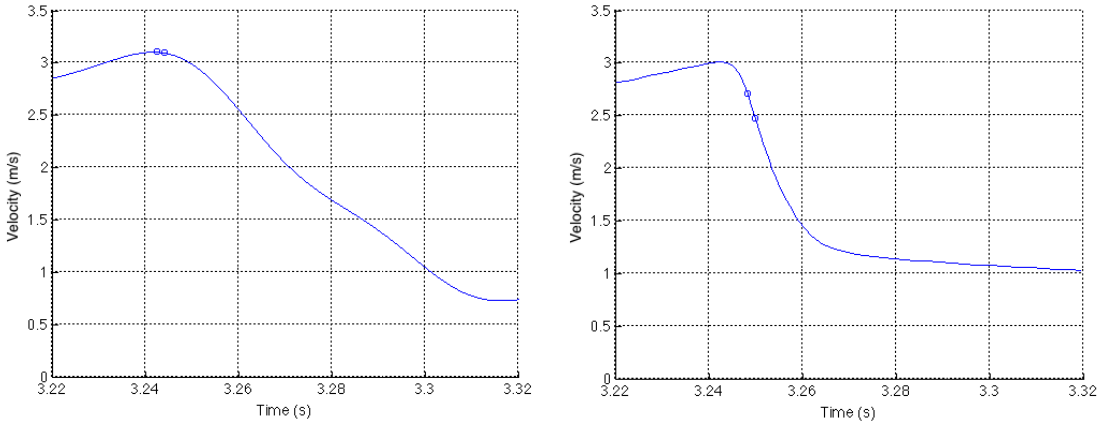

(a) **(b)**

Figure 6.3 – Velocity of the wedge with circles indicating first and last pressure peak for a) Experiment 1 and b) Experiment 2.

For *Experiment 1* the velocity remain constant during the peak pressures over the sensor rows. For *Experiment 2* the velocity has already been reduced to 2.71 m/s when peak pressure occurs at the second sensor row. When maximum pressure occurs at the third sensor row 0.0017 ms later it is further reduced by 0.2382 m/s.

It was reported by Yettou et al. (2005) that for a constant drop height, the deceleration is determined by the mass. The higher the mass, the smaller the deceleration. This is consistent with what is observed here. *Experiment 1* has mass that is 110 kg heavier than *Experiment 2*, which can explain a larger deceleration in the latter case. Yettou et al. (2005) reported that a changing velocity could affect the spatial pressure distribution.

It is drawn attention to the uncertainty present in the velocity for both experiments as it is not measured directly. In *Experiment 1* it is derived from position measurements while for *Experiment 2* it is integrated from acceleration measurements.

6.3.2 Pressure

From the plot in the bottom of figure 6.2 the pressure time history for each sensor in *Experiment 2* is shown. To obtain a meaningful comparison it is important to be aware of the sensor position. The first and last pressure peak is much lower than the two in the middle. In *Experiment 1*, the pressure peak values show less variation. This is a result of sensor position as different pressure distributions across the wedge surface will occur at different stages of impact. In the analysed results from *Experiment 1* the positions along the wedge surface from apex were 85, 95, 105, 115 and 125 mm. All these positions are closest to the sensor positioned at 100 mm distance from apex in *Experiment 2*. Considering the time history for each sensor from textitExperiment 2 it is decided that the sensors at 100 and 150 mm distance from apex are most qualified for a comparison. They will therefore be digitalized for further investigation. As the image quality of figure 6.2 is not high, the digitalization will be somewhat poor. This causes

the digitalized pressure plots from *Experiment 2* to appear more uneven than they are in reality.

6.3.2.1 Pressure peaks

Looking at the pressure time series in figure 6.2, it is discovered that the pressure peaks are much lower than in *Experiment 1*. Using Wagner (1932), the expected maximum pressure assuming constant velocity would be 390 kPa. This is with the velocity calculated from equality between potential and kinetic energy that gives an initial impact velocity of 3.13 m/s. The pressure peaks from *Experiment 2* only reach a value slightly above 120 kPa. It was first considered to use pressure time series from Wagner (1932) to compare the two experiments. As the pressure results from *Experiment 2* is so far away from this theoretical prediction it is decided to make the comparison visual. The pressure time series from *Experiment 1* and *Experiment 2* are therefore shown next to each other in figure 6.4. Please take note of the different scales on the vertical axes.

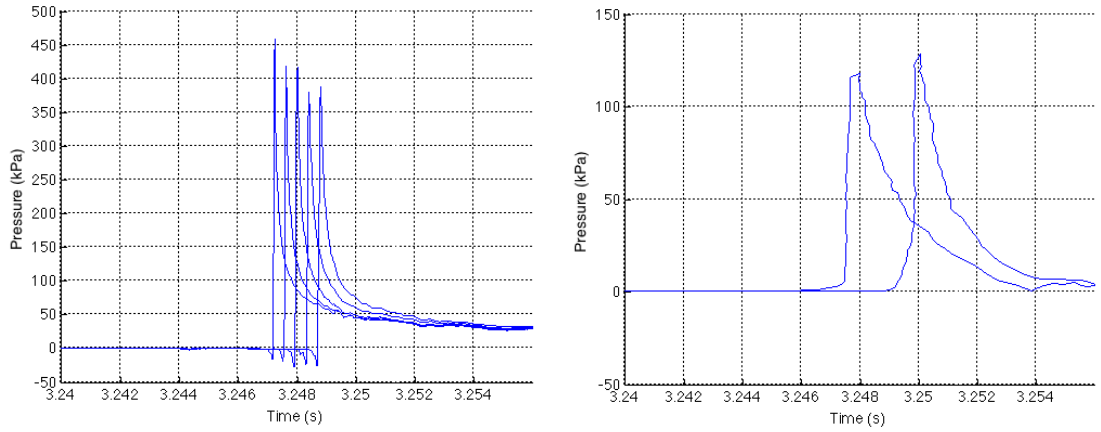

Figure 6.4 – Time history of measured pressure for a) Experiment 1 and b) Experiment 2.

It was found previously in this thesis that the average maximum pressure for *Experiment 1* at 0.5 m drop height was 402 kPa. For *Experiment 2* the average maximum pressure is found to be 123 kPa. The peak pressure from *Experiment 1* is consistent with the peak pressure from the similarity solution (Dobrovol'skaya 1969) and the asymptotic theory (Wagner 1932), assuming constant impact velocity. In the previous section it was found that the velocity under the occurrence of the pressure peaks was approximately 0.4 m/s lower for *Experiment 2*. Using Wagner's theory (1932) the value of the maximum pressure can be estimated as

$$p_{\max} = \frac{1}{2}\rho V^2 C_{p_{\max}} \tag{6.1}$$

where ρ is the density of water, V is the impact velocity and $C_{p_{\max}}$ is the maximum pressure coefficient given as

$$C_{p_{\max}} = \frac{\pi^2}{4}\cot^2\beta. \tag{6.2}$$

Here β is the deadrise angle of the wedge. Using these formulations with the velocities at the first peak for both experiments, that is 3.1 and 2.7 m/s, the following peak pressures are estimated:

$$\begin{array}{ll} Experiment1: & p_{\max} = 381kPa \\ Experiment2 & p_{\max} = 291kPa \end{array}$$

From the above calculation it is clear that a small reduction in impact velocity have a large influence on the peak pressure. Decreasing pressure amplitude with decreasing velocity was also reported by Yettou et al. (2005). Even so, the value from *Experiment 2* is still only 42.3 % of this estimate.

The large deviation from the expected maximum value by Wagner's theory for *Experiment 2* is explained by three-dimensional effects. In fact, the tank used in *Experiment 2* allows a fully three-dimensional flow, as the gap between the wedge and the tank wall is in the order of meters. In a fully three-dimensional case the pressure can be reduced by up to 50 % compared to the pressure for a two-dimensional case. This is sufficient to explain the lower value of the peak pressure measured in *Experiment 2* as the Wagner estimate is for two-dimensional flow.

6.3.2.2 Slamming pressure duration

The duration of the slamming pressure is defined as pressure above 50% of maximum pressure. For *Experiment 2* the mean duration of the slamming pressure for the two chosen pressure sensors is 0.82 ms. The mean duration for *Experiment 1* at 0.5 m drop height is 0.18 ms which is only 22% of the duration for *Experiment 2*. This indicates that three-dimensional effects can cause a longer duration of the slamming pressure.

6.4 VERIFICATION OF THREE-DIMENSIONAL EFFECTS

Yettou et al. (2006) presented an analytical solution to symmetrical water impact problems on two-dimensional wedges. In their solution, they included three-dimensional effects, using a correction factor based on the work of Zhao et al. (1996). By applying the moment theorem the following expression for the velocity at any time t during impact can be defined:

$$V(t) = \frac{V_0}{1 + \frac{M_a}{M}}. \tag{6.3}$$

Here V(t) is the instantaneous velocity of the wedge upon impact, V_0 is the initial impact velocity, M is the mass and M_a is the added mass of the wedge. The added mass is defined by Zhao et al. (1996) as

$$M_a = C_a\rho(Y(t))^2 \tag{6.4}$$

where

$$C_a = \frac{f_{3D}\pi}{2}\left(1 - \frac{\beta}{2\pi}\right). \tag{6.5}$$

Y(t) is the horizontal coordinate of the intersection between the free surface and the wedge, β is the deadrise angle and f_{3D} is a factor taken three-dimensional effects into account. The factor f_{3D} is calculated by Zhao et al. (1996) and varies between 0.5 and 1. $f_{3D} = 0.5$ corresponds to a completely three-dimensional case. It was observed in section 6.3.1 that the velocity decreased more for *Experiment 2* than for *Experiment 1*. By using the known velocity change from section 6.3.1 together with eq. (6.3) the value of f_{3D} can be found for *Experiment 2*.

By the use of eq. (6.3), (6.4) and (6.5) the factor f_{3D} is found to be 0.5. This means that from the test set-up in *Experiment 2* a three-dimensional drop test is performed. It was not stated to be a three-dimensional experiment in the report, but it is now clear that this is the case. It explains the large differences in results as *Experiment 1* is a two-dimensional experiment.

6.5 FINAL COMMENT ON COMPARISON

It was not specified in the report by Yang et al. (2007) that their experiment was performed in three-dimensional flow conditions. It is evident that this reduces the value of the comparison. If any explanations for the differences between theoretical predictions and measurements were to be found, the experiments should have similar flow conditions. What has been revealed from this comparison is the consequences of three-dimensional effects. The pressure peaks from Yang et al. (2007) are much lower than for the MARINTEK experiment. In the MARINTEK experiment, the pressure peaks were underestimated by Wagner's theory (1932). The low pressure peaks from Yang et al. (2007) argue that three-dimensional effects are not affecting the pressure results from MARINTEK.

7

APPLICATION OF THEORETICAL MODELS

In chapter 2, some recognized theories on slamming were shortly presented. They vary in applicability range, computer intensity and complexity. For the theory to fit the experiment, the theoretical applicability limits must be met by the experimental set-up and behaviour. In the analysis carried out in chapter 4, Wagner's theory (1932) was used for comparison. At the time the choice was made to use this theory, all involved features of the MARINTEK experiment were not yet known. At this point they are, and a new evaluation of what theoretical model are best suited to reproduce the involved features can be made. In this search for an appropriate theoretical model, efficiency will be valued.

The theories evaluated in this chapter are all based on potential flow of an incompressible fluid. The experiment that the theoretical model is aimed for here is a two-dimensional experiment and the three-dimensional theories from chapter 2 are disregarded.

A common restriction for theoretical models of slamming on wedges is the size of the deadrise angle. In the experiment under consideration the deadrise angle is 10°. It can therefore be defined as a blunt body. In figure 7.1 a comparison of the pressure distribution predicted by the similarity solution, the boundary element method and the asymptotic solution is illustrated. The results are based on the assumption of a constant impact velocity. It can be observed that the three theories are almost consistent in determining the pressure distribution for this angle. The estimates of maximum pressure coefficient agree very well for all three theories. In the lower part of the distribution, the asymptotic theory lies above the other two.

Of the theories in figure 7.1, the asymptotic solution has the lowest limit for applicable deadrise angles. The small deviations in the spatial pressure distribution show that 10° is still within the range of deadrise angles the asymptotic theory can provide valid estimates for. For the maximum pressure the theories provide equal results. When the asymptotic theory has been compared to experiments throughout time, different results on how well it predicts the maximum pressures have been found. Often the reasons for the deviation have proved to be the size of the pressure gauges and the sampling frequency. A changing velocity during the drop has also often been disregarded. Takemoto (1984) and Yamamoto et al. (1984) included these factors in their comparison and found a good agreement between experimental results and the asymptotic solution for deadrise angles $3° < \beta < 15°$.

The similarity solution by Dobrovol'skaya (1969) and the non-linear boundary element method by Zhao and Faltinsen (1993) allow larger angles. When the asymptotic theory is applied to large deadrise angle the results will not be consistent with neither the

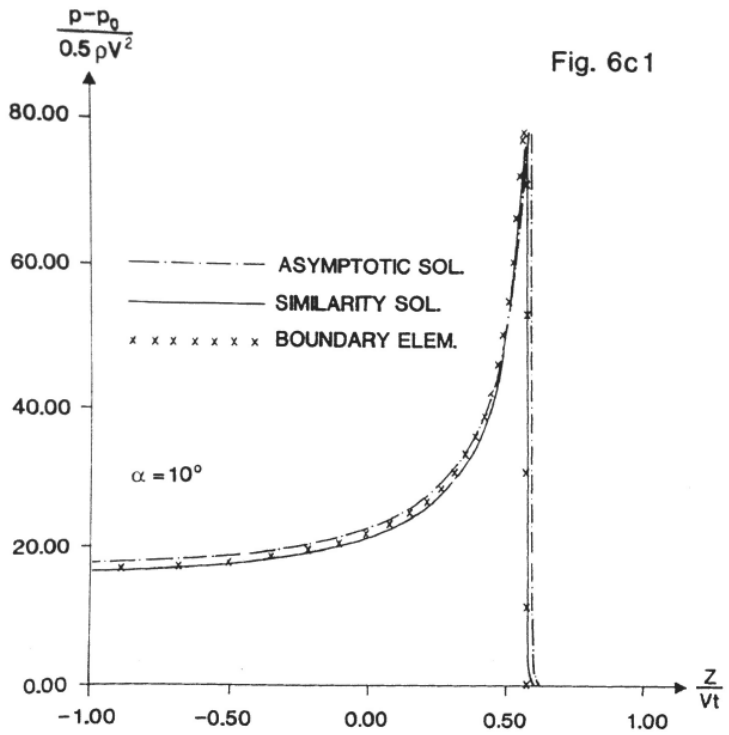

Figure 7.1 – Predictions of pressure distribution on a wedge with constant impact velocity. (Faltinsen 1997)

similarity solution nor the BEM. This is because the flat plate approximation used in the asymptotic solution no longer holds when the body becomes sharper. The spatial pressure distribution will therefore be expected to deviate from the theories that are designed to handle larger deadrise angles.

Figure 7.1 shows the pressure on a wedge with constant velocity. A constant water entry velocity is not a given. Chezhian (2003) found that when the mass of the body is smaller than the maximum slamming load, the body will decelerate. If the mass is larger than the maximum slamming force, the body will continue to accelerate until the submergence has increased the added mass and hydrostatic force enough to start a deceleration. The non-linear boundary element method by Zhao and Faltinsen (1993) is a theoretical model that can handle a varying velocity with time. For this experiment it is observed that the change in velocity during the time where pressure is measured is very small. The largest change in velocity between the pressure peaks is found for 0.25 m drop height as 0.03 m/s. With this slight velocity change it can be acceptable to assume a constant impact velocity and a theory that can handle a variation in velocity is not required.

Gravity is neglected in the asymptotic solution and the similarity solution. Neglecting gravity is true only when the fluid accelerations are large compared to the gravitational acceleration. After a while the fluid acceleration will decrease and gravity can no longer be neglected. If this happens then the theories that neglect gravity will overestimate the pressure. Gravity is included in the generalized Wagner method by Zhao et al. (1996) and can be included in the boundary element method by Zhao and Faltinsen (1993). Because of this, these theories are not limited to a small time scale. For estimates of the

maximum pressure, the assessed time scale is small. To get a better theoretical model for a larger part of the pressure time series it is considered beneficial to use a theory that can include gravity.

Evaluating the efficiency of the theoretical models, it is evident that the asymptotic solution will give a quick and conservative estimate. It is therefore suited for first estimates, but if a more detailed and precise estimate is needed it will not be recommended. The similarity solution can provide an accurate gravityless solution, but it is computer intensive. Especially for small deadrise angles it is numerically demanding. The non-linear boundary element method is also a numerically demanding model. For practical engineering purposes the simplified boundary element method presented as the generalized Wagner theory is a less computer intensive and more robust model.

The pressure is not the only important slamming paramater that should be captured by a theoretical model. In table 7.1 estimates of slamming parameters by the asymptotic theory, the similarity solution and the non-linear boundary element method is presented. The estimates are collected from Zhao and Faltinsen (1993) and all presented values are for deadrise anlge $\beta = 10°$.

Table 7.1 – Slamming parameters estimated by the similarity solution, the asymptotic theory and the boundary element method for water entry of a 10° wedge with constant impact velocity V. $C_{p_{\max}}$ = maximum pressure coefficient, $z_{\max}/Vt$ = z-coordinate of maximum pressure, ΔS_s = spatial extent of slamming pressure, $c = 0.5\pi Vt\cot\beta$, F_3 = total vertical hydrodynamic force on the wedge.

	Asymp.	Simil.	BEM
$C_{p_{\max}}$	79.36	77.847	80.2
$z_{\max}/Vt$	0.5708	0.5556	0.555
$\Delta S_s/c$	0.1002	0.09088	0.0941
$F_3/\left(\rho V^3 t\right)$	231.973	213.980	220.8

From the comparison in table 7.1 one can see that the maximum pressure is well predicted by the asymptotic solution. For the force estimates, the asymptotic theory is less accurate and clearly overestimates the value. Force measurements are an important feature of the analysed experiment. Wagner's (1932) asymptotic solution was used for comparison of maximum force in chapter 4. The estimate showed values much higher than the experimental values. Considering this, it appears the asymptotic solution is not suited for predicting the hydrodynamic vertical force on the wedge.

As the force estimates from the asymptotic solution showed values high above the experimental results, the boundary element method with the lowest force estimate is assessed. The non-linear boundary element method is less efficient than the generalized Wagner method, so the latter is preferred. It is similar to Wagner's theory, with the main difference being that the exact body boundary condition is satisfied at each time step instead of the flat plate approximation. Avoiding the flat plate approximation is expected to diminish the observed overestimation of the experimental force measurements.

On the basis of the above argumentation it is concluded that the generalized Wagner theory by Zhao et al. (1996) will be preferred for reproducing the phenomena of the analysed experiment from chapter 4. It is noted that this depends on the amount

and quality of information needed. Wagner's theory (1932) was used to generate the integrated pressure used for comparison with force measurements in chapter 4. Using the generalized Wagner theory for this purpose would be beneficial. It would have made the comparison in the tail of the force measurements more reliable, as gravity can be included.

For estimates of maximum pressures, the classical Wagner theory (1932) is still considered a good choice. From the investigation in this chapter, it is concluded that the theory is not the problem when maximum pressures are found to deviate from the prediction by Wagner. All applicability limits of the theory is met by the experiment when considering the pressure peaks. This argues, again, that it is measurement errors causing the observed differences.

8

CONCLUSIONS

Differences between measured data from the MARINTEK experiment and theoretically predicted impact loads are the reason why the work in this thesis has been carried out. To find explanations for the differences has been the motivation behind the analyses made. The applicability of theoretical models, measurement techniques and other experiments have been studied for this reason. Some conclusions have been made on what effects are most and least likely to cause the deviations.

Wagner's theory have been used for comparison, and is concluded to be suited for comparison of peak pressures. However, the maximum pressure along each sensor row decreases with increased distance from apex. The spatial distribution of the pressure coefficient showed values different from the predictions by Wagner. Experimental values were below the theoretical estimates. It is concluded that these results are not caused by a velocity change, as they occur for the largest drop height where the velocity is constant during these measurements. Both hydroelasticity and three-dimensional effects are assessed, but the experimental results do not show behaviour that can confirm the occurrence of any of the two. Evaluation of possible error sources for the pressure measurements show that the total decrease in peak pressure is inside a predicted error range. In addition to the standard deviation measured, this error range include error estimates for small disturbances in the free surface as well as errors in the velocity measurements. It is therefore concluded that the most likely explanation for the observed pressure behaviour is measurement errors.

Negative pressure drops are reoccurring before the rise of the pressure peaks for all drop heights. It was first assumed that the negative pressures are generated by a temperature shock in the sensor. The time scale of the negative pressures is very small, in the same range as the pressure rise time. No effect of the negative pressures is observed in the peak pressure value or in the pressure tail. It is therefore concluded that the best explanation is air trapped in the curvature of the sensor front. The conclusion is supported by the presence of a pressure rise before the negative drop. This can be explained by the trapped air being compressed initially (causing the rise in pressure), and when the cavity collapses this causes the negative pressure.

The above observations are reoccurring for all drop heights. A large discrepancy between force measurements and integrated pressure is only observed for the lowest drop height. An explanation for this behaviour has not been found. It is suspected that it is measurement errors. The question is why the measurement errors cause a large discrepancy for 0.1 m drop height, while there is no discrepancy for 0.5 m drop height. Relative to the maximum pressure, the estimated total error on the pressure is larger for 0.5 m drop height. This argues that errors in the pressure measurements are not the only explanation for the discrepancy. It is suspected that the force measurements for

the lowest drop height is above the real values. This assumption of a force measurement error is based on the maximum forces compared to the Wagner (1932) estimates.

The error estimate made for the peak pressures agrees well with the variation of peak pressure found in the repeatability analysis. Comparing the standard deviation from the repeatability analysis to the error estimate showed that the error estimate is conservative. Force measurements show very good repeatability for 0.5 and 0.25 m drop height. Pressure peaks are very sensitive to small changes in local details (Faltinsen 2010), and as expected they show a stochastic nature. The force is not as sensitive, which is reflected by its satisfactory repeatability. For 0.1 m drop height, the repeatability is not satisfying. The standard deviation is 15 times the value for the other heights. This supports the hypothesis of an error in the force measurements for the lowest drop height.

Very few reports of drop tests with a 10° wedge are available, and the experiment by Yang et al. (2007) was the best option. The comparison of drop test results between the MARINTEK experiment and a drop test performed by Yang et al. (2007) showed little agreement. It is concluded that this is due to the test set-up in Yang et al., which is three-dimensional. This comparison suggests that three-dimensional effects lead to a large decrease in peak pressure, which is expected (Bereznitski 2001). From the high pressure peaks in the MARINTEK experiment, this finding argues that three-dimensional effects are ruled out. This is consistent with the results of Yettou et al. (2006).

To verify the conclusions made for the observed features of the MARINTEK experiment, more information is needed. If video recordings or flow visualization was available it could possibly increase the understanding of what is happening. Without this, the best possible conclusion is measurement errors.

8.1 SUGGESTIONS FOR FURTHER STUDY

With the amount of information available from the MARINTEK experiment at this point, the possibilities for a further study are limited. Information in the form of video recordings or flow visualization cannot be obtained, as no visual presentation of the experiment was recorded. The following information may be available and could help obtain better explanations on the observed features of the experiment:

- A visual presentation of a similar drop test experiment from the same test rig to increase the understanding of what is happening.
- Data from a similar drop test programme at the same test rig at MARINTEK with different pressure and force sensor types than in this experiment. This could reveal possible sensor errors.
- Flow visualization of a drop test where the same Kulite sensors are used to confirm the hypothesis of trapped air causing the negative pressures.
- Data from a drop test of a 10° wedge in two-dimensional flow conditions to see if a comparison can reveal any error sources or explanations of the observed features.

Measurement errors are the best explanation found for the deviations from theoretical predictions. It is therefore suggested to perform a more in depth error analysis for force and pressure measurements. It is suspected that there is some error occurring for the force measurements at 0.1 m drop height, and this should be investigated further.

9

REFERENCES

Armand, J. L. and Cointe, R. (1986) Hydrodynamic impact analysis of a cylinder. *Proceedings of the Fifth International Offshore Mechanics and Arctic Engineering Symposium*, Vol. 1, pp 609-634.

Bereznitski, A. (2001) Slamming: the role of hydroelasticity. *International Shipbuilding Progress*, Vol. 48, pp 333-351.

Chezhian, M. (2003) *Three-dimensional analysis on slamming.* Ph. D. Norwegian University of Science and Technology.

Cointe, R. (1991) Free surface flows close to a surface-piercing body. *In* Miloh, T (ed.) *Mathematical Approaches in Hydrodynamics.*, Philadelphia, PA: Society for Industrial and Applied Mathematics, pp 319-334.

Das, S. (2009) Transducers: Sensor Models. *In Mechatronic Modeling and Simulation Using Bond Graphs.*, CRC Press, pp 227-302.

Dobrovol'skaya, Z. N. (1969) On some problems of fluid with a free surface. *Journal of Fluid Mechanics*, Vol. 36(4), pp 805-829.

Elbestawi, M. A. (1998) Force Measurement. *In* Webster, J. G. (ed.) *The Measurement, Instrumentation and Sensors Handbook.*, CRC Press LCC.

Eren, H. (2014) Measurements, Instrumentation and Sensors. *In* Webster, J. G. and Eren, H (eds.) *Measurement, Instrumentation, and Sensors Handbook, Second Edition: Spatial, Mechanical, Thermal, and Radiation Measurement.*, CRC Press, pp 1-1 - 1-14.

Faltinsen, O. M. (1990) *Sea Loads on Ships and Offshore Structures.* New York: Cambridge University Press.

Faltinsen, O. M. (1997) *Lecture notes for Hydrodynamics for Marine Structures 1.* Norwegian University of Science and Technology.

Faltinsen, O. M. and Zhao, R. (1998) Water entry of ship sections and axisymmetric bodies, *In* AGARD. *Report 827 High Speed Body Motions in Water*, pp 24-1-24-1. Neuilly-Sur-Seine, Cedex, France: AGARD/NATO.

Faltinsen, O. M. (1999) Water entry of a wedge by hydroelastic orthotropica plate theory. *Journal of Ship Research*, Vol. 43(3), pp 180-193.

Faltinsen, O. M. (2000) Hydroelastic slamming. *Journal of Marine Science and Technology*, Vol. 5(2), pp 49-65.

Faltinsen, O.M. and Chezhian, M. (2005) A generalized Wagner method for Three-Dimensional Slamming. *Journal of Ship Research*, Vol. 49, pp 279-287.

Faltinsen, O. M. (2010) *Hydrodynamics of High-Speed Marine Vehicles.* New York: Cambridge University Press.

Greco, M. (2012). *TMR4215: Sealoads: lecture notes.* NTNU, Trondheim.

Kapsenberg, G. K. (2011) Slamming of ships: where are we now?. *Philosophical Transactions of the Royal Society A: Mathematical, Physical and Engineering Sciences*, Vol. 369, pp 2892-2919.

Lewis, S.G., Hudson, D.A., Turnock, S.R. and Taunton, D. J. (2010) Impact of a free-falling wedge with water: synchronized visualization, pressure and acceleration measurements. *Fluid Dynamics Research*, Vol. 42, pp 1-30.

Meyerhoff, W. K. (1970) Added mass of thin rectangular plates calculated from potential theory. *Journal of Ship Research*, Vol. 14, pp 100-111.

Pinney, C. P. and Baker, W. E. (1998) Velocity Measurements. *In* Webster, J. G. (ed.) *The Measurement, Instrumentation and Sensors Handbook.*, CRC Press LLC.

Sayeed, T. M., Peng, H and Veitch, B. (2010) Experimental investigation of slamming loads on a wedge. *In* Proceedings of MARTEC 2010. *The International Conference on Marine Technology*, BUET, Dhaka, Bangladesh, 2010.

Scolan, Y. M. and Korobkin, A. A. (2001) Three-dimensional theory of water impact, Part 1, Inverse Wagner problem. *Journal of Fluid Mechanics*, Vol. 440, pp 293-326.

Smith, S. W. (2002) *The Scientist and Engineers Handbook to Digital Signal Processing.* [Online] http://www.dspguide.com/pdfbook.htm.

Steen, S. (2014) *TMR7 Experimental Methods in Marine Hydrodynamics.* Trondheim: Akademika forlag.

Takemoto, H. (1984) Some considerations on water impact pressure. *Jornal of the Society of Naval Architects of Japan*, Vol. 156, pp 314-322.

Tveitnes, T., Feirlie-Clarke, A. C. and Veryani, K. (2008) An experimental investigation into the constant velocity water entry of wedge-shaped sections. *Ocean Engineering*, Vol. 35, pp 1463-1478.

Van Nuffel, D., Vepa, K. S., De Baere, I., Degrieck, J., Derouck, J and Van Paepegem, W. (2013) Study on the Parameters Influencing the Accuracy and Reproductibility of Dynamic Pressure Measurements at the Surface of a Rigid Body During Water Impact. *Experimental Mechanics*, Vol. 53 (2013), pp 131-144.

Von Karman, T. (1929) *The impact of seaplane floats during landing.* NACA, Technical Note 321, Washington, DC.

Wagner, H. (1932) Uber struss-und Gleitvorgange ander Oberflasche von Flussikeiten. *Zeitschr. f. Angewandte Mathematik und Mechanik*, Vol. 12(4), pp 193-235.

Wang, J. (2014) *Water entry of Freefall Wedges - Wedge Motions and Cavity dynamics.* Ph. D. Norwegian University of Science and Technology.

Yamamoto, Y., Ohtsubo, H. and Kohno, Y. (1984) Water impact of wedge model. *Jornal of the Society of Naval Architects of Japan*, Vol. 155, pp 236-245.

Yang, S. H., Lee, H. H., Park, T. H., Lee, Y. W. and Lee, I. H. (2007) Experimental and numerical study on the water entry of symmetric wedges and a stern section of modern

containership. *Proceedings of the 10th International Symphosium of Practical Design of Ships and Other Floating Structures*, Houston, Texas, USA, pp 518-526.

Yettou, E. M., Desrocher, A., Champoux, Y. (2005) Experimental study on the water impact of a symmetrical wedge. *Fluid Dynamic Research*, Vol. 38, pp 47-66.

Yettou, E. M., Desrochers, A., Champoux, Y. (2006) New analytical model for pressure estimation of symmetrical water impact of a rigid wedge at variable velocities. *Journal of Fluids and Structures*, Vol. 23 (2007), pp 501-522.

Zhao, R. and Faltinsen, O. M. (1993) Water entry of two-dimensional bodies. *Jornal of Fluid Mechanics*, Vol. 246 (1993), pp 593-612.

Zhao, R., Faltinsen, O., Aarsnes, J. (1996) Water Entry of Arbitrary Two-Dimensional Sections with and Without Flow Separation. *In* Proceedings of the 21st Symposium on Naval Hydrodynamics, Trondheim, Norway. National Academy Press, Washington DC.

A

APPENDIX A

This appendix includes the Matlab code for generation of pressure time series from Wagner's(1932) theory developed in the project thesis.

A.1 Pressure distribution

A.1.1 findtau.m

findtau.m calculates the spatial pressure coefficient distribution for a wedge with a small deadrise angle (given as input) using asymptotic theory.

```
%-------------------------------------------------------------------------
% Purpose: Calculate pressure coefficient on wedge from asymptotic theory.
% Method: The formulas defined for the pressure coefficient are used
%         from input of the deadrise angle. Tau is found by iteration.
% ------------------------------------------------------------------------
%   Variables      Description
%   bmax           z/Vt for spray root, y=c
%   angle          Deadrise angle in degrees
%   beta           Deadrise angle in radians
%   k              Counter for values of pressure and z/Vt
%   j              Counter in for loop
%   b              z/Vt
%   tau            Relation between y and c in pressure equations
%   newton         Iterative function to find tau
%   l              Vector with z/Vt values
%   p1             Function calculating pressure for y<=c
%   p2             Function calculating pressure for y>c
%   p              Vector with pressure coefficients
%-------------------------------------------------------------------------
clear all
clc

% Read input from user:
angle=input('Please enter wedge deadrise angle in degrees:');

%Calculating necessary parameters:
bmax=(0.5*pi-1);
beta=(angle*pi)/180;

k=0;

% Max value of j is set for a 10 degree deadrise angle here.
for j=-1:0.002:0.64;
b=j;
```

```
% Call on function newton() to iterate tau value
tau=newton(@f1,@f2,0.1,0.00001,300,beta,b);

k=k+1;
l(k)=b;

% If we are outside the jet root (y>c) pressure is:
if b > bmax
    p2=pressure2(tau,beta);
    p(k)=p2;
else

% Before and in spray root (y<=c), the pressure is:
p1=pressure(b,tau,beta);
p(k)=p1;
end
end

for i=0.64:0.002:0.8
    l(k)=i;
    p(k)=0;
    k=k+1;
end

% Check results for beta=10:

M=csvread('asymptotic_cp.csv');
x=M(:,1);
y=M(:,2);

figure
plot(l,p,'color','r')
axis ( [-1 1 0 100] )
hold on
plot(x,y,'color','g')
set(gca,'fontsize',14)
set(gcf,'color','white')
xlabel('z/Vt','FontSize',14)
ylabel('Pressure Coeff.','FontSize',14)
legend('Implemented code','Existing data');
```

A.1.2 newton.m

Calculation of τ with Newton's method.

```
%-------------------------------------------------------------------------
% Purpose: Calculate tau.
% Method:  Tau is calculated by using Newtons method.
%-------------------------------------------------------------------------
% -------------------------------------------------------------------------
%   Variables      Description
%   fun            f(tau)=f1
%   funder         f'(tau)=f2
%   xest           Start vaule of tau in iteration
%   err            Allowed error between two last iterations
%   imax           Max number of iterations before stopped
%   beta           Deadrise angles in radians
%   b              z/Vt
%-------------------------------------------------------------------------

function tau=newton(fun,funder,xest,err,imax,beta,b)

for i=1:imax
    x1=xest-feval(fun,xest,beta,b)/feval(funder,xest,beta);
    if abs((x1-xest)/xest)<err
        tau=x1;
        break
    end
    xest=x1;
end
if i==imax
    fprintf('Solution was not found in %i iterations.\n',imax)
    tau=('No answer');
end
```

A.1.3 f1.m, f2.m

Functions in Newton's method.

```
%-------------------------------------------------------------------------
% Function for input in Newtons method. f1=f(tau).
%-------------------------------------------------------------------------

function f=f1(x,beta,b)

m=0.5*pi*cot(beta)-cot(beta)*(1+b);
n=(((1/(4*pi))*tan(beta))*(-log(abs(x))-(4*sqrt(abs(x)))-abs(x)+5));
f=m+n;


%-------------------------------------------------------------------------
% Function for input in Newtons method. f2=f'(tau).
%-------------------------------------------------------------------------

function g=f2(x,beta)

g=0.25*pi*tan(beta)*(-(1/x)-(x/(2*(abs(x)^2/3)))-(x/abs(x)));
```

A.1.4 pressure.m, pressure2.m

Functions for pressure calculation.

```
%-------------------------------------------------------------------------
% Purpose: Calculating pressure coefficient (p1) for y<=c
% Method: Use b, tau and beta as input to calculate p1 as output.
%-------------------------------------------------------------------------

function p1=pressure(b,tau,beta)

a=cot(beta);
c=(1+b);
d=0.5*pi;
t=abs(tau);
p1=0.5*(pi^2)*(a^2)*((1/(a*sqrt(d^2-c^2)))-(1/(a*sqrt(pi*(d-c))))
+((2*sqrt(t))/((1+sqrt(t))^2)));



%-------------------------------------------------------------------------
% Purpose: Calculating pressure coefficient (p2) for y>c
% Method: Use tau and beta as input to calculate p2 as output.
%-------------------------------------------------------------------------

function p2=pressure2(tau,beta)

a=(cot(beta))^2;
c=pi^2;
d=sqrt(abs(tau));
e=1./(1+sqrt(abs(tau))).^2;

p2=a.*c.*d.*e;
```

A.2 maketimehistory.m

maketimehistory.m generates pressure time series at given sensor positions by using the spatial pressure distribution from findtau.m.

```
%-------------------------------------------------------------------------
% Purpose: Generate pressure time series for comparison with
%          experimental results.
% Method:  Using the pressure coefficient the pressure is found for
%          input of a sensor location by finding the pressure
%          at each time instant at this location for input drop height.
% Note:    The script for the pressure coefficient must be run before
%          this script can be run.
% -------------------------------------------------------------------------
%   Variables      Description
%   v              Water entry velocity
%   z1             Vector of vertical sensor coordinates
%   t              Time
%   m              Counter for pressure matrices
%   zs1-5          Relative entry depth for sensor row 1-5
%   l1-l5          Non-dimensional entry depth
%   pp1-5          Pressure time series for sensor row 1-5
%   pm1-pm13       Experimental pressure for sensor row 1-5
%-------------------------------------------------------------------------

% Water entry velocity: Fill in manually.
v=sqrt(2*9.81*0.5);

% Vertical coordinates of sensors for final drop test:
z1=[0.0148, 0.0165, 0.0182, 0.0200, 0.0217];

% Vertical coordinates of sensors for initial drop test:
%z1=[0.0108, 0.0116, 0.0125, 0.0134, 0.0142, 0.0151];
m=1;

% Find pressure coefficient and pressure for each time instant
for t=0.002:0.000035:0.012
    time(m)=t;
zs1(m)=z1(1)-(v*t);
zs2(m)=z1(2)-(v*t);
zs3(m)=z1(3)-(v*t);
zs4(m)=z1(4)-(v*t);
zs5(m)=z1(5)-(v*t);
l1=zs1(m)/(v*t);
l2=zs2(m)/(v*t);
l3=zs3(m)/(v*t);
l4=zs4(m)/(v*t);
l5=zs5(m)/(v*t);
[minDifferenceValue, indexAtMin] = min(abs(l - l1));
pp1(m)=p(indexAtMin)*500*v^2;
[minDifferenceValue, indexAtMin] = min(abs(l - l2));
pp2(m)=p(indexAtMin)*500*v^2;
[minDifferenceValue, indexAtMin] = min(abs(l - l3));
pp3(m)=p(indexAtMin)*500*v^2;
[minDifferenceValue, indexAtMin] = min(abs(l - l4));
pp4(m)=p(indexAtMin)*500*v^2;
[minDifferenceValue, indexAtMin] = min(abs(l - l5));
pp5(m)=p(indexAtMin)*500*v^2;
m=m+1;
end
```

B

APPENDIX B

This appendix contains the Matlab scripts used in chapter 4 for the experimental analysis. 98XX indicate test numbers , where XX varies from 01 to 12.

B.1 analyse.m

analyse.m loads the chosen .mat file containing all data from a test. Froude scaling and geometrical similiraty is applied with a scaling ratio of 50. Filtering of force and position measurements is also performed.

```
%-------------------------------------------------------------------------
% Purpose: Scale measurements from full scale to model scale.
% Method: Load measurements and scale with scaling factor 50.
% ------------------------------------------------------------------------
%   Variables      Description
%   fm             Sampling frequency - Model scale
%   Posm           Position - Model scale
%   Timem          Time - Model scale
%   pm(x)          Pressure at sensor x - Model scale
%   ForcePanelm    Force - Model scale
%   A              Pressure Matrix - Model scale
%   fs             Sampling frequency - Full scale
%   Pos            Position - Full scale
%   Time           Time - Full scale
%   mXXXX          Pressure at sensor XXXX - Full scale
%   ForcePanel     Force - Full scale
%   ffilt          Filtered force - Model scale
%   pfilt          Filtered position - Model scale
%-------------------------------------------------------------------------

clc
clear all
load('test9810.mat')
% Scale variables to model scale
fm=fs*sqrt(50);
Posm=Pos/50;
Timem=Time/sqrt(50);
pm1=m1029/50;
pm2=m1020/50;
pm3=m1019/50;
pm4=m1018/50;
pm5=m1017/50;
pm6=m1000/50;
pm7=m1015/50;
pm8=m1014/50;
pm9=m1013/50;
```

```
pm10=m1012/50;
pm11=m1010/50;
pm12=m1009/50;
pm13=m1008/50;
pm14=m1005/50;
pm15=m1003/50;
ForcePanelm=ForcePanel/125000;
A=[pm1;pm2;pm3;pm4;pm5;pm6;pm7;pm8;pm9;pm10;pm11;pm12;pm13;pm14;pm15];

% Filtering of force measurements
Fd=double(ForcePanelm);
[b,a] = butter(4,0.024,'low');
ffilt=filtfilt(b,a,Fd);
[b,a] = butter(4,[0.014 0.018],'stop');
ffilt=filtfilt(b,a,ffilt);

% Low pass filtering of position measurements
Posd=double(Posm);
[b,a] = butter(4,0.001,'low');
pfilt=filtfilt(b,a,Posd);
```

B.2 dispvelc.m

dispvelc.m use the LP-filtered position measurements for numerical derivation to obtain the velocity. Time instances of initial impact, pressure peak over first sensor row and pressure peak over last sensor row is found and marked in the plot of the velocity that is generated. - analyse.m must be run first.

```
%-------------------------------------------------------------------------
% Purpose: Derive velocity from position measurements.
% Method: Numerical derivation and filtering.
% ------------------------------------------------------------------------
%   Variables      Description
%   pfilt          LP-filtered position measurements
%   h              Derivation time step
%   Timem          Time
%   pm1-pm15       Pressure
%   v              Velocity
%   vnull          Velocity at initial impact
%   tnull          Time of initial impact
%   I1,I2          Index variables
%   t1             Time of pressure peak first & last row
%   s1             Velocity at t1
%   ForcePanel     Force - Full scale
%-------------------------------------------------------------------------

% Derivation of velocity
h=Timem(2)-Timem(1);
v=diff(pfilt)/h;

% Check velocity when apex hits water
[minDifferenceValue, indexAtMin] = min(abs(pfilt - 0));
vnull=v(indexAtMin);
tnull=Timem(indexAtMin);

% Time when maximum velocity
ii=find(v==min(v));
tmaks=Timem(ii);

% Plot velocity
I1=find(pm1==max(pm1));
I2=find(pm14==max(pm14));
t1=[Timem(I1), Timem(I2)];
s1=[v(I1), v(I2)];
hold on
plot(Timem(1:499999),-v,'b')
scatter(t1,-s1,100,'r');
scatter(tnull,-vnull,70,'*k')
set(gca,'fontsize',14)
set(gcf,'color','white')
xlabel('Time (s)','FontSize',14)
ylabel('Velocity (m/s)','FontSize',14)
grid on
```

B.3 maxp.m

maxp.m loads the 98XX_max.mat files containing maximum pressure over each sensor for each drop test 98XX. The mean and standard deviation of the maximum pressure is calculated over all sensors and tests at each drop height.

```
%-------------------------------------------------------------------------
% Purpose: Find mean maximum pressure each drop height with stand. dev.
% Method: Load max from each test, use func. mean and std.
% ------------------------------------------------------------------------
%   Variables      Description
%   m1-m12         Vectors of max pressure for test 1-12
%   m01            Matrix of maximum pressure for 0.1 m drop height
%   m025           Matrix of maximum pressure for 0.25 m drop height
%   m05            Matrix of maximum pressure for 0.5 m drop height
%   m01m           Mean maximum pressure for 0.1 m drop height
%   m025m          Mean maximum pressure for 0.25 m drop height
%   m05m           Mean maximum pressure for 0.5 m drop height
%   e01            Std. deviation of max. pressure for 0.1 m drop height
%   e025           Std. deviation of max. pressure for 0.25 m drop height
%   e05            Std. deviation of max. pressure for 0.5 m drop height
%-------------------------------------------------------------------------

clc
clear all

% Load maximum pressure for all tests over all sensors
load('9801_max.mat')
load('9802_max.mat')
load('9803_max.mat')
load('9804_max.mat')
load('9806_max.mat')
load('9807_max.mat')
load('9808_max.mat')
load('9809_max.mat')
load('9810_max.mat')
load('9811_max.mat')
load('9812_max.mat')

% Calculate mean and standard deviation for each drop height
m01=[m10,m11,m12];
m01m=mean(m01);
e01=(std(m01)/m01m)*100;
m025=[m1,m2,m3,m4];
m025m=mean(m025);
e025=(std(m025)/m025m)*100;
m05=[m6,m6,m8,m9];
m05m=mean(m05);
e05=(std(m05)/m05m)*100;
```

B.4 spatial2.m

spatial2.m loads the 98XX_psens.mat files containing the pressure over each sensor for test 98XX at the time instances where peak pressure occur over each sensor row. Mean and standard deviation is found over each sensor row, and is plotted with errorbars as a function of the distance of the sensors from apex.

```
%-------------------------------------------------------------------------
% Purpose: Plot spatial distribution of pressure.
% Method: Load spatial pressure distribution for all tests and calc.
%         mean and std for all sensors - plot with errorbars.
% ------------------------------------------------------------------------
%   Variables      Description
%   s1-s12         Matrix of pressure at sensors at tests 1-12 at times 1-5
%   s01            Matrix of pressure distribution for 0.1 m drop height
%   s025           Matrix of pressure distribution for 0.25 m drop height
%   s05            Matrix of pressure distribution for 0.5 m drop height
%   s01m           Mean of s01
%   s025m          Mean of s025
%   s05m           Mean of s05
%   e01            Standard deviation of s01
%   e025           Standard deviation for s025
%   e05            Standard deviation for s05
%   P1-P5          Sensor positions at time instants 1-5
%   C1-C5          Mean pressure distribution at time instants 1-5
%   CP             Peak pressure at sensors
%   E1-E5          Std of pressure distribution at time instants 1-5
%-------------------------------------------------------------------------

clc
clear all

% Load pressure coefficients
load('9801_psens.mat')
load('9802_psens.mat')
load('9803_psens.mat')
load('9804_psens.mat')
load('9806_psens.mat')
load('9807_psens.mat')
load('9808_psens.mat')
load('9809_psens.mat')
load('9810_psens.mat')
load('9811_psens.mat')
load('9812_psens.mat')

% Calculate mean and std for each sensor
s01=[s10; s11; s12];
s01m=mean(s01,1);
e01=std(s01,0,1);
s025=[s1; s2; s3; s4];
s025m=mean(s025,1);
e025=std(s025,0,1);
s05=[s6; s7; s8; s9];
s05m=mean(s05,1);
e05=std(s05,0,1);

% Prepare plot
P1=85;
C1=s05m(1);
E1=e05(1);
```

```
P2=[85, 95];
C2=[s05m(2),s05m(3)];
E2=[e05(2),e05(3)];
P3=[85, 95, 105];
C3=[s05m(4),s05m(5),s05m(6)];
E3=[e05(4),e05(5),e05(6)];
P4=[85,95,105,115];
C4=[s05m(7),s05m(8),s05m(9),s05m(10)];
E4=[e05(7),e05(8),e05(9),e05(10)];
P5=[85,95,105,115,125];
C5=[s05m(11),s05m(12),s05m(13),s05m(14),s05m(15)];
E5=[e05(11),e05(12),e05(13),e05(14),e05(15)];
CP=[s05m(1),s05m(3),s05m(6),s05m(10),s05m(15)];

% Plot spatial distribution
figure
hold on
grid on
errorbar(P1,C1,E1,'r');
errorbar(P2,C2,E2,'-b');
errorbar(P3,C3,E3,'-m');
errorbar(P4,C4,E4 ,'-c');
errorbar(P5,C5,E5,'-g');
plot(P5,CP,'-k','LineWidth',2)
axis([80,140,-10,700]);
set(gca,'fontsize',14)
set(gcf,'color','white')
xlabel('Position along wedge surface (mm)','FontSize',14)
ylabel('Pressure (kPa)','FontSize',14)
legend('t1','t2','t3','t4','t5','Peak Pressure')
```

B.5 Pressurecoeff.m

Pressurecoeff.m use the 98XX_psens.mat files from the time instance where the pressure peak occur over the fifth sensor row. The maximum pressure is made non-dimensional, i.e. maximum pressure coefficients. The maximum pressure coefficients vs. distance of sensor position from apex is plotted.

```
%-------------------------------------------------------------------------
% Purpose: Plot spatial distribution of pressure coefficient.
% Method: Load spatial pressure dist. for all tests and calc. mean and std
%         for all sensors - plot with errorbars.
% ------------------------------------------------------------------------
%   Variables      Description
%   s1-s12         Matrix of pressure at all sensors at all tests at time t
%   s01            Matrix of pressure coefficient for 0.1 m drop height
%   s025           Matrix of pressure coefficient for 0.25 m drop height
%   s05            Matrix of pressure coefficient for 0.5 m drop height
%   s01m           Mean of s01
%   s025m          Mean of s025
%   s05m           Mean of s05
%   e01            Standard deviation of s01
%   e025           Standard deviation for s025
%   e05            Standard deviation for s05
%   v01            Square of velocity, 0.1 m drop height
%   v025           Square of velocity, 0.25 m drop height
%   v05            Square of velocity, 0.5 m drop height
%   P              Sensor positions
%   C1-C5          Matrix for mean pressure coeff. at each drop height
%   E1-E5          Matrix of std. for each drop height
%-------------------------------------------------------------------------

clc
clear all

% Loading spatial pressure distribution
load('9801_psens.mat')
load('9802_psens.mat')
load('9803_psens.mat')
load('9804_psens.mat')
load('9806_psens.mat')
load('9807_psens.mat')
load('9808_psens.mat')
load('9809_psens.mat')
load('9810_psens.mat')
load('9811_psens.mat')
load('9812_psens.mat')

% Calculate square of velocity
v01=0.1*9.81;
v025=0.25*9.81;
v05=0.5*9.81;

% Calculate mean and std for each sensor
s01=[s10; s11; s12]./v01;
s01m=mean(s01,1);
e01=std(s01,0,1);
s025=[s1; s2; s3; s4]./v025;
s025m=mean(s025,1);
e025=std(s025,0,1);
s05=[s6; s7; s8; s9]./v05;
```

```
s05m=mean(s05,1);
e05=std(s05,0,1);

% Prepare plot
P=[85,95,105,115,125];
C5=[s05m(11),s05m(12),s05m(13),s05m(14),s05m(15)];
E5=[e05(11),e05(12),e05(13),e05(14),e05(15)];
C25=[s025m(11),s025m(12),s025m(13),s025m(14),s025m(15)];
E25=[e025(11),e025(12),e025(13),e025(14),e025(15)];
C1=[s01m(11),s01m(12),s01m(13),s01m(14),s01m(15)];
E1=[e01(11),e01(12),e01(13),e01(14),e01(15)];

% Plot spatial distribution
figure
hold on
grid on
errorbar(P,C1,E1,'r');
errorbar(P,C25,E25,'-b');
errorbar(P,C5,E5,'-m');
axis([80,120,0,130]);
set(gca,'fontsize',14)
set(gcf,'color','white')
xlabel('Position along wedge surface (mm)','FontSize',14)
ylabel('Pressure coefficient, Cp','FontSize',14)
legend('h = 0.1 m','h = 0.25 m','h = 0.5 m')
```

B.6 decay.m

decay.m calculates the duration of the slamming pressure for each sensor. This is done by finding all indices of each pressure vector that contains pressure values above 50% of the maximum pressure. After the time duration is found the mean and standard deviation for all sensors are found. The duration of the slamming force is found in the same manner. Note: analyse.m must be run first.

```
%-------------------------------------------------------------------------
% Purpose: Find duration of slamming pressure and force.
% Method: Track indices of pressure/force > 50% max pressure/force.
% ------------------------------------------------------------------------
%   Variables      Description
%   slamt          Vector for duration for each sensor
%   i              Counter for sensor number
%   Timem          Time - Model scale
%   A              Pressure Matrix - Model scale
%   x              Vector for pressure for sensor i/ force measurement
%   M              Max pressure/force
%   M2             50% max pressure
%   I              Indices of pressure above M2
%   slamtm         Mean slamming duration for test
%   stand          Standard deviation of slamming durations
%   fd             Force duration
%-------------------------------------------------------------------------

% Find slamming duration for each sensor
slamt=zeros(1,15);
for i=1:15
    x=A(i,:);
    M=max(x);
    M2=0.5*M;
    I=find(x>M2);
    slamt(i)=Timem(I(length(I)))-Timem(I(1));
end

% Find mean slamming duration
slamtm=(mean(slamt))*1000;
stand=(std(slamt))*1000;

% Find duration of slamming force
x=ffilt;
M=max(x);
M2=0.5*M;
I=find(x>M2);
fd=Timem(I(length(I)))-Timem(I);
```

B.7 minp.m

minp.m loads the 98XX_min.mat files containing minimum pressure over each sensor for each drop test 98XX. The mean and standard deviation of the minimum pressure is calculated over all sensors and tests at each drop height.

```
%-------------------------------------------------------------------------
% Purpose: Find mean minimum pressure each drop height with stand. dev.
% Method: Load min from each test, use func. mean and std.
% ------------------------------------------------------------------------
%   Variables      Description
%   min1-12        Vectors of minimum pressure each sensor and test
%   m01            Matrix of minimum pressure for 0.1 m drop height
%   m025           Matrix of minimum pressure for 0.25 m drop height
%   m05            Matrix of minimum pressure for 0.5 m drop height
%   m01m           Mean minimum pressure for 0.1 m drop height
%   m025m          Mean minimum pressure for 0.25 m drop height
%   m05m           Mean minimum pressure for 0.5 m drop height
%   e01            Std. deviation of max. pressure for 0.1 m drop height
%   e025           Std. deviation of max. pressure for 0.25 m drop height
%   e05            Std. deviation of max. pressure for 0.5 m drop height
%-------------------------------------------------------------------------

clc
clear all

% Load minimum pressure for all tests over all sensors
load('9801_min.mat')
load('9802_min.mat')
load('9803_min.mat')
load('9804_min.mat')
load('9806_min.mat')
load('9807_min.mat')
load('9808_min.mat')
load('9809_min.mat')
load('9810_min.mat')
load('9811_min.mat')
load('9812_min.mat')

% Calculate mean and standard deviation for each drop height
m01=[min10,min11,min12];
m01m=mean(m01);
e01=(std(m01)/m01m)*100;
m025=[min1,min2,min3,min4];
m025m=mean(m025);
e025=(std(m025)/m025m)*100;
m05=[min6,min6,min8,min9];
m05m=mean(m05);
e05=(std(m05)/m05m)*100;
```

B.8 threedim.m

threedim.m loads the 98XX_max.mat files with maximum pressure values for test 98XX. The mean maximum pressure over each column is found to check for possible three-dimensioanl effects closer to the edges.

```
%-------------------------------------------------------------------------
% Purpose: Check for three-dimensional effects
% Method:  Find mean max pressure for each sensor column
% ------------------------------------------------------------------------
%   Variables      Description
%   m1-m12         Vectors of max pressure from test 1-12
%   (x)            1-3
%   (y)            0.1, 0.25, 0.5
%   c(x)(y)        Max pressure of column x at drop height y
%   c(x)(y)m       Mean max pressure of column x at drop height y
%-------------------------------------------------------------------------

% Load maximum pressures

load('9801_max.mat')
load('9802_max.mat')
load('9803_max.mat')
load('9804_max.mat')
load('9806_max.mat')
load('9807_max.mat')
load('9808_max.mat')
load('9809_max.mat')
load('9810_max.mat')
load('9811_max.mat')
load('9812_max.mat')

% Find mean over each 'column'
% Column 1: Sensor 1029-1008
c101=[m10(1),m10(4),m10(7),m10(10),m10(13),m11(1),m11(4),m11(7),m11(10),
    m11(13),m12(1),m12(4),m12(7),m12(10),m12(13)];
c101m=mean(c101,2);
c1025=[m1(1),m1(4),m1(7),m1(10),m1(13),m2(1),m2(4),m2(7),m2(10),m2(13),
    m3(1),m3(4),m3(7),m3(10),m3(13),m4(1),m4(4),m4(7),m4(10),m4(13)];
c1025m=mean(c1025,2);
c105=[m6(1),m6(4),m6(7),m6(10),m6(13),m7(1),m7(4),m7(7),m7(10),m7(13),
    m8(1),m8(4),m8(7),m8(10),m8(13),m9(1),m9(4),m9(7),m9(10),m9(13)];
c105m=mean(c105,2);
% Column 2: Sensor 1020-1005
c201=[m10(2),m10(5),m10(8),m10(11),m10(14),m11(2),m11(5),m11(8),m11(11),
    m11(14),m12(2),m12(5),m12(8),m12(11),m12(14)];
c201m=mean(c201,2);
c2025=[m1(2),m1(5),m1(8),m1(11),m1(14),m2(2),m2(5),m2(8),m2(11),m2(14),
    m3(2),m3(5),m3(8),m3(11),m3(14),m4(2),m4(5),m4(8),m4(11),m4(14)];
c2025m=mean(c2025,2);
c205=[m6(2),m6(5),m6(8),m6(11),m6(14),m7(2),m7(5),m7(8),m7(11),m7(14),
    m8(2),m8(5),m8(8),m8(11),m8(14),m9(2),m9(5),m9(8),m9(11),m9(14)];
c205m=mean(c205,2);
% Column 3: Sensor 1019-1003
c301=[m10(3),m10(6),m10(9),m10(12),m10(15),m11(3),m11(6),m11(9),m11(12),
    m11(15),m12(3),m12(6),m12(9),m12(12),m12(15)];
c301m=mean(c301,2);
c3025=[m1(3),m1(6),m1(9),m1(12),m1(15),m2(3),m2(6),m2(9),m2(12),m2(15),
    m3(3),m3(6),m3(9),m3(12),m3(15),m4(3),m4(6),m4(9),m4(12),m4(15)];
c3025m=mean(c3025,2);
```

```
c305=[m6(3),m6(6),m6(9),m6(12),m6(15),m7(3),m7(6),m7(9),m7(12),m7(15),
    m8(3),m8(6),m8(9),m8(12),m8(15),m9(3),m9(6),m9(9),m9(12),m9(15)];
c305m=mean(c305,2);
```

B.9 hydroelasticity.m

hydroelasticity.m check for hydroelastic behaviour for 0.1 m drop height (test 9810). Pressure time series generated by maketimeseries.m is loaded for final and initital drop tests. These pressure time series are synchronized and plotted together with the experimental results for comparison. Force measurements from inital and final drop tests are compared as well as position measurements.

```
%-------------------------------------------------------------------------
% Purpose: Check for indications of hydroelastic behaviour.
% Method:  Compare time series of inital and final drop tests.
%          Compare initial integrated pressure to Wagner.
% ------------------------------------------------------------------------
%   Variables      Description
%   NFA            Matrix of pressure, initial test
%   NFTimem        Time - inital test
%   NFPos          Position - initial test
%   pm31-33        Pressure vectors, inital test
%   Timem          Time - Model scale
%   pp1-pp6        Pressure vectors, Wagner generated
%   time           Time - Wagner generated
%   pm4-pm13       Pressure vectors, final test
%   P1             Averaged pressure, initial test
%   b,a            LP-filter variables
%   pfilt          LP-filtered position, final test
%   pfilt2         LP-filtered position, inital test
%   pXXXX          Pressure - Full scale
%   ForcePanel     Force - Full scale
%-------------------------------------------------------------------------

% !! NOTE: Run analyse.m for test 9810 before start this script !!
% Load pressure from initial drop test
load('NoPanel01.mat')
% Load Wagner estimate for inital drop test
load('WagP_NoPanel.mat')

% Prepare plot
pm31=NFA(31,:);
pm32=NFA(32,:);
pm33=NFA(33,:);
pm34=NFA(34,:);
pm35=NFA(35,:);
pm36=NFA(36,:);

% Plot inital time series vs. Wagner time series
figure(1)
h1=plot(time,pp1/1000,'r');
hold on
plot(time,pp2/1000,'r')
plot(time,pp3/1000,'r')
plot(time,pp4/1000,'r')
plot(time,pp5/1000,'r')
plot(time,pp6/1000,'r')
h2=plot(NFTimem,pm31,'b');
hold on
plot(NFTimem,pm32,'b')
plot(NFTimem,pm33,'b')
plot(NFTimem,pm34,'b')
plot(NFTimem,pm35,'b')
```

```
plot(NFTimem,pm36,'b')
grid on
set(gca,'fontsize',14)
set(gcf,'color','white')
xlabel('Time (s)','FontSize',14)
ylabel('Pressure (kPa)','FontSize',14)
legend([h1 h2],{'Wagner', 'Experimental'})
axis([0.002 0.011995 -20 125])

% Load Wagner estimate for final drop test
load('WagForce_01.mat')

% Plot final time series vs. Wagner time series
figure(2)
h1=plot(time,pp1/1000,'r');
hold on
plot(time,pp2/1000,'r')
plot(time,pp3/1000,'r')
plot(time,pp4/1000,'r')
plot(time,pp5/1000,'r')
h2=plot(Timem,pm1,'b');
hold on
plot(Timem,pm4,'b')
plot(Timem,pm7,'b')
plot(Timem,pm10,'b')
plot(Timem,pm13,'b')
grid on
set(gca,'fontsize',14)
set(gcf,'color','white')
xlabel('Time (s)','FontSize',14)
ylabel('Pressure (kPa)','FontSize',14)
legend([h1 h2],{'Wagner', 'Experimental'})
axis([0.002 0.011995 -20 125])

%Compare initial force measurements to Wagner force
P1=[pp1;pp2;pp3;pp4;pp5;pp6];
P1=mean(P1,1)/1000;
P2=mean(NFA,1);

% Plot force comparison
figure(3)
grid on
hold on
plot(NFTimem,(P2*3.6),'r')
plot(time,(P1*3.6),'b');
set(gca,'fontsize',14)
set(gcf,'color','white')
xlabel('Time (s)','FontSize',14)
ylabel('Force (N)','FontSize',14)
legend('Measured integrated pressure','Wagner integrated pressure')
axis([2.51 2.52 -9 205])

% Load position measurements from inital drop test
load('NoPanelPos.mat')

% Compare initial position measurements to final
NFpos=NFPosm+0.1;

% Filter initial position measurements
Posd=double(NFpos);
[b,a] = butter(4,0.001,'low');
```

```
pfilt2=filtfilt(b,a,Posd);

% Plot comparison
plot(Timem,pfilt,'b')
hold on
plot(NFTimem-6.1691,pfilt2,'r')
set(gca,'fontsize',14)
set(gcf,'color','white')
xlabel('Time (s)','FontSize',14)
ylabel('Position (m)','FontSize',14)
legend('Final drop test','Initial drop test')
```

B.10 integral.m

integral.m compares the integrated pressure measurements with measured force. It also loads pressure time series from the code maketimeseries.m that was presented in appendix X. A comparison is made between integrated pressure measurements, force measurements and integrated pressure generated from Wagner's(1932) theory. Note: analysis.m must be run first.

```
%-------------------------------------------------------------------------
% Purpose: Integrate measured pressure to compare with force measures.
% Method:  Find average pressure over panel area.
% ------------------------------------------------------------------------
%   Variables      Description
%   Timem          Time - Model scale
%   time           Time, Wagner generated
%   ffilt          LP-filtered force measurement
%   A              Pressure Matrix - Model scale
%   P6             Average pressure over panel
%   pp1-pp5        Pressure vectors, Wagner generated
%   P7             Average pressure, Wagner generated
%-------------------------------------------------------------------------

% Comparison of force measurements and integrated pressure
P6=mean(A,1);
figure(1)
hold on
plot(Timem,ffilt*1000,'b');
plot(Timem,P6*3.6,'r')
set(gca,'fontsize',14)
set(gcf,'color','white')
xlabel('Time (s)','FontSize',14)
ylabel('Force (N)','FontSize',14)
legend('Measured integrated pressure','Measured force')
grid on

% Comparison force measurements, integrated pressure, Wagner integrated

% Read input from user:
height=input('Enter analysed drop height (0.1 or 0.5):');

% Load generated Wagner pressure for chosen drop height
if height==0.1
    load('WagForce_01.mat')
elseif height==0.5
    load('WagForce_05.mat')
else
    disp('Height not valid')
    stop
end

% Plot
P7=[pp1;pp2;pp3;pp4;pp5];
P7=mean(P7,1)/1000;
figure(2)
hold on
plot(Timem,(P6*3.6),'r')
plot(time-2.5065,P7*3.6,'b')
plot(Timem,ffilt*1000,'g')
set(gca,'fontsize',14)
```

```
set(gcf,'color','white')
xlabel('Time (s)','FontSize',14)
ylabel('Force (N)','FontSize',14)
legend('Measured integrated pressure', 'Wagner integrated pressure',
       'Measured force')
```

B.11 Forcean.m

Forcean.m loads the ffilt_XX.mat files containing the filtered force measurements from test 98XX. The mean maximum force is found for each drop height. Maximum force from Wagner's(1932) theory is calculated for each drop test.

```
%-------------------------------------------------------------------------
% Purpose: Find mean max each drop height and Wagner estimate of Fmax.
% Method:  Loading max values of filtered values, calc mean and std.
%          Caluculate Wagner max force
% ------------------------------------------------------------------------
%   Variables      Description
%   rho            Density of water
%   v              Impact velocity
%   beta           Deadrise angle
%   xa,xb,b        Calculation variables
%   f              Wagner mac force per unit length
%   fmax01         Wagner max force for 0.1 m drop height
%   fmax025        Wagner max force for 0.25 m drop height
%   fmax05         Wagner max force for 0.5 m drop height
%   f1-f4          Variables storing max force from tests
%   F              Vector of max forces
%   F01            Mean max force for 0.1 m drop height
%   F025           Mean max force for 0.25 m drop height
%   F05            Mean max force for 0.5 m drop height
%-------------------------------------------------------------------------

% Find wagner maximum for each drop height

% 0.1 m drop height
rho=1000;
v=sqrt(2*9.81*0.1);
beta=(10/180)*pi;
xa=cos(beta)*(75/1000);
xb=cos(beta)*(135/1000);
b=asin(xa/abs(xb));
f=((rho*(v^2)*xb*pi)/(2*tan(beta)))*((pi/2)-b);
fmax01=fmax*(60/1000);

% 0.25 m drop height
v=sqrt(2*9.81*0.25);
f=((rho*(v^2)*xb*pi)/(2*tan(beta)))*((pi/2)-b);
fmax025=f*(60/1000);

% 0.5 m drop height
v=sqrt(2*9.81*0.5);
f=((rho*(v^2)*xb*pi)/(2*tan(beta)))*((pi/2)-b);
fmax05=f*(60/1000);

% Load filtered force measurements
load('ffilt_01.mat')
load('ffilt_02.mat')
load('ffilt_03.mat')
load('ffilt_04.mat')
load('ffilt_06.mat')
load('ffilt_07.mat')
load('ffilt_08.mat')
load('ffilt_09.mat')
load('ffilt_10.mat')
load('ffilt_11.mat')
```

```
load('ffilt_12.mat')

% Mean max force 0.1 m drop height
f1=max(ffilt10);
f2=max(ffilt11);
f3=max(ffilt12);
F=[f1; f2; f3];
F01=mean(F);

% Mean max force 0.25 m drop height
f1=max(ffilt01);
f2=max(ffilt02);
f3=max(ffilt03);
f4=max(ffilt04);
F=[f1; f2; f3; f4];
F025=mean(F);

% Mean max force 0.5 m drop height
f1=max(ffilt06);
f2=max(ffilt07);
f3=max(ffilt08);
f4=max(ffilt09);
F=[f1; f2; f3; f4];
F05=mean(F);
```

C

APPENDIX C

This appendix contains the Matlab scripts used in chapter 5 for investigation of repeatability and behaviour of local quantities. 98XX indicate test numbers, where XX varies from 01 to 12.

C.1 repeatability.m

repeatability.m load the 98XX_pf.mat files containing the filtered force and pressure measurements from each test. The pressure time series are synchronized in time using the peak pressure at first sensor row. Force measurements are synchronized by peak force. Shaded errorbar plots are generated.

```
%-------------------------------------------------------------------------
% Purpose: Check repeatability of force and pressure measurements
% Method:  Load measurements and synchronize.
%          Plot with shadederrorbar for mean and std.
% ------------------------------------------------------------------------
%   Variables      Description
%   m1-m4          Max measurements
%   I1-I4          Index of maxima
%   P1-P4          Synchronized pressure vectors
%   dt             Time step
%   t              Time
%   PP1-PP5        Matrix of pressure for each sensor from all equal tests
%   M1-M5          Mean pressure for each sensor
%   E1-E5          Std. of pressure over each sensor
%   F1-F3          Synchronized force measurements
%   FF             Vector of synchronized force from all equal tests
%   MF1            Mean force
%   EF1            Std of force
%-------------------------------------------------------------------------

clc
clear all

% Load pressure and force measurements
load('9806_pf.mat')
load('9807_pf.mat')
load('9808_pf.mat')
load('9809_pf.mat')
load('9810_pf.mat')
load('9811_pf.mat')
load('9812_pf.mat')
load('9801_pf.mat')
load('9802_pf.mat')
load('9803_pf.mat')
```

```
load('9804_pf.mat')

% Prepare plot for 0.5 m drop height

% Synchronize pressure time series from tests
m1=max(P9806(1,:));
m2=max(P9807(1,:));
m3=max(P9808(1,:));
m4=max(P9809(1,:));
I1=find(P9806(1,:)==m1);
I2=find(P9807(1,:)==m2);
I3=find(P9808(1,:)==m3);
I4=find(P9809(1,:)==m4);
P1=P9806(:,(I1-50000):(I1+150000));
P2=P9807(:,(I2-50000):(I2+150000));
P3=P9808(:,(I3-50000):(I3+150000));
P4=P9809(:,(I4-50000):(I4+150000));
dt=1/50000;
t=0:dt:((200001*dt)-dt);

%Caulculate mean and standard deviation
PP1=[P1(1,:); P2(1,:); P3(1,:);P4(1,:)];
PP2=[P1(2,:);P2(2,:);P3(2,:);P4(2,:)];
PP3=[P1(3,:);P2(3,:);P3(3,:);P4(3,:)];
PP4=[P1(4,:);P2(4,:);P3(4,:);P4(4,:)];
PP5=[P1(5,:);P2(5,:);P3(5,:);P4(5,:)];
M1=mean(PP1,1);
M2=mean(PP2,1);
M3=mean(PP3,1);
M4=mean(PP4,1);
M5=mean(PP5,1);
E1=std(PP1,1);
E2=std(PP2,1);
E3=std(PP3,1);
E4=std(PP4,1);
E5=std(PP5,1);
%Plot
figure(1)
hold on
A=shadedErrorBar(t,M1,(E1),{'-b', 'LineWidth', 2});
B=shadedErrorBar(t,M2,(E2),{'-g', 'LineWidth', 2});
C=shadedErrorBar(t,M3,(E3),{'-r', 'LineWidth', 2});
D=shadedErrorBar(t,M4,E4,{'-c', 'LineWidth', 2});
E=shadedErrorBar(t,M5,E5,{'-y', 'LineWidth', 2});
legend([A.mainLine,B.mainLine,C.mainLine,D.mainLine,E.mainLine],
 'Sensor1029 - Row1','Sensor1018 - Row2', 'Sensor1015 - Row3',
 'Sensor1012 - Row4', 'Sensor1008 - Row5');
set(gca,'fontsize',14)
set(gcf,'color','white')
xlabel('Time (s)','FontSize',14)
ylabel('Pressure (kPa)','FontSize',14)

% Prepare plot for 0.1 m drop height

% Synchronize pressure time series from tests
m1=max(P9810(1,:));
m2=max(P9811(1,:));
m3=max(P9812(1,:));
I1=find(P9810(1,:)==m1);
I2=find(P9811(1,:)==m2);
I3=find(P9812(1,:)==m3);
```

```
P1=P9810(:,(I1-50000):(I1+150000));
P2=P9811(:,(I2-50000):(I2+150000));
P3=P9812(:,(I3-50000):(I3+150000));
dt=1/50000;
t=0:dt:((200001*dt)-dt);

%Caulculate mean and standard deviation
PP1=[P1(1,:); P2(1,:); P3(1,:)];
PP2=[P1(2,:);P2(2,:);P3(2,:)];
PP3=[P1(3,:);P2(3,:);P3(3,:)];
PP4=[P1(4,:);P2(4,:);P3(4,:)];
PP5=[P1(5,:);P2(5,:);P3(5,:)];
M1=mean(PP1,1);
M2=mean(PP2,1);
M3=mean(PP3,1);
M4=mean(PP4,1);
M5=mean(PP5,1);
E1=std(PP1,1);
E2=std(PP2,1);
E3=std(PP3,1);
E4=std(PP4,1);
E5=std(PP5,1);
%Plot
figure(2)
hold on
A=shadedErrorBar(t,M1,(E1),{'-b', 'LineWidth', 2});
B=shadedErrorBar(t,M2,(E2),{'-g', 'LineWidth', 2});
C=shadedErrorBar(t,M3,(E3),{'-r', 'LineWidth', 2});
D=shadedErrorBar(t,M4,E4,{'-c', 'LineWidth', 2});
E=shadedErrorBar(t,M5,E5,{'-y', 'LineWidth', 2});
legend([A.mainLine,B.mainLine,C.mainLine,D.mainLine,E.mainLine],
 'Sensor1029 - Row1','Sensor1018 - Row2', 'Sensor1015 - Row3',
 'Sensor1012 - Row4', 'Sensor1008 - Row5');
set(gca,'fontsize',14)
set(gcf,'color','white')
xlabel('Time (s)','FontSize',14)
ylabel('Pressure (kPa)','FontSize',14)

% Prepare plot for force measurements for 0.5 m drop height

%Synchronize force records
m1=max(F9806(1,:));
m2=max(F9807(1,:));
m3=max(F9808(1,:));
m4=max(F9809(1,:));
I1=find(F9806(1,:)==m1);
I2=find(F9807(1,:)==m2);
I3=find(F9808(1,:)==m3);
I4=find(F9809(1,:)==m4);
F1=F9806(:,(I1-50000):(I1+150000));
F2=F9807(:,(I2-50000):(I2+150000));
F3=F9808(:,(I3-50000):(I3+150000));
F4=F9809(:,(I4-50000):(I4+150000));
%Calculate mean and standard deviation
FF=[F1(1,:); F2(1,:); F3(1,:);F4(1,:)];
MF1=mean(FF,1);
EF1=std(FF,1);
%Plot
figure(3)
hold on
shadedErrorBar(t,MF1,(EF1),{'-b', 'LineWidth', 2});
```

```
set(gca,'fontsize',14)
set(gcf,'color','white')
xlabel('Time (s)','FontSize',14)
ylabel('Force (N)','FontSize',14)

% Prepare plot for force measurements for 0.1 m drop height

%Synchronize force records
m1=max(F9810(1,:));
m2=max(F9811(1,:));
m3=max(F9812(1,:));
I1=find(F9810(1,:)==m1);
I2=find(F9811(1,:)==m2);
I3=find(F9812(1,:)==m3);
F1=F9810(:,(I1-50000):(I1+100000));
F2=F9811(:,(I2-50000):(I2+100000));
F3=F9812(:,(I3-50000):(I3+100000));
%Calculate mean and standard deviation
FF=[F1(1,:); F2(1,:); F3(1,:)];
MF1=mean(FF,1);
EF1=std(FF,1);
dt=1/50000;
t=0:dt:((150001*dt)-dt);
%Plot
figure(4)
hold on
shadedErrorBar(t,MF1,(EF1),{'-b', 'LineWidth', 2});
set(gca,'fontsize',14)
set(gcf,'color','white')
xlabel('Time (s)','FontSize',14)
ylabel('Force (N)','FontSize',14)
```

C.2 linearity.m

linearity.m loads the 98XX_max.mat files containing maximum pressures, ffilt_XX.mat files containing filtered time series, dur98XX.mat files containing slamming pressure duration, fdur98XX.mat files containing slamming force duration and rise98XX.mat files containing rise time of pressure. Variation with drop height and accorss rows are found and plotted for all the loaded quantities.

```
%-------------------------------------------------------------------------
% Purpose: Check linear dependence on drop height.
% Method:  Load measurements and synchronize.
%          Plot with shadederrorbar for mean and std.
% ------------------------------------------------------------------------
%   Variables      Description
%   h              Vector of drop heights
%   (y)            1-5
%   (x)            0.1, 0.25, 0.5
%   r(x)(y)        Peak pressure at row x at drop height y
%   r(x)(y)m       Mean peak pressure at row x at drop height y
%   y(y)           Vector with peaks for row y at all heights
%   v1-v3          Square velocity times half of water density
%   c(y)           Vector with max Cp for row y at all heights
%   f(y)           Max force for drop height y
%   f              All max forces
%   x              Drop heights for force plot
%   d(x)(y)        Slamming pressure duration at row x at drop height y
%   d(x)(y)m       Mean slamming pressure dur. at row x at drop height y
%   d(y)           Vector with peaks for row y at all heights
%   f2             Vector of all slam. force durations
%   ri(x)(y)       Rise time pressure at row x at drop height y
%   ri(x)(y)m      Mean rise time pressure at row x at drop height y
%   ri(y)          Vector with rise time for row y at all heights
%-------------------------------------------------------------------------

clc
clear all

% Load maximum pressure
load('9801_max.mat')
load('9802_max.mat')
load('9803_max.mat')
load('9804_max.mat')
load('9806_max.mat')
load('9807_max.mat')
load('9808_max.mat')
load('9809_max.mat')
load('9810_max.mat')
load('9811_max.mat')
load('9812_max.mat')

% Scatter plot of peak pressure vs. drop height

h=[0.1, 0.25, 0.5];
% Find mean over each row - 0.1 m
r101=[m10(1),m10(2),m10(3),m11(1),m11(2),m11(3),m12(1),m12(2),m12(3)];
r101m=mean(r101,2);
r201=[m10(4),m10(5),m10(6),m11(4),m11(5),m11(6),m12(4),m12(5),m12(6)];
r201m=mean(r201,2);
r301=[m10(7),m10(8),m10(9),m11(7),m11(8),m11(9),m12(7),m12(8),m12(9)];
```

```
r301m=mean(r301,2);
r401=[m10(10),m10(11),m10(12),m11(10),m11(11),m11(12),m12(10),m12(11),m12(12)];
r401m=mean(r401,2);
r501=[m10(13),m10(14),m10(15),m11(13),m11(14),m11(15),m12(13),m12(14),m12(15)];
r501m=mean(r501,2);
% Find mean over each row - 0.25 m
r1025=[m1(1),m1(2),m1(3),m2(1),m2(2),m2(3),m3(1),m3(2),m3(3),m4(1),m4(2),m4(3)];
r1025m=mean(r1025,2);
r2025=[m1(4),m1(5),m1(6),m2(4),m2(5),m2(6),m3(4),m3(5),m3(6),m4(4),m4(5),m4(6)];
r2025m=mean(r2025,2);
r3025=[m1(7),m1(8),m1(9),m2(7),m2(8),m2(9),m3(7),m3(8),m3(9),m4(7),m4(8),m4(9)];
r3025m=mean(r3025,2);
r4025=[m1(10),m1(11),m1(12),m2(10),m2(11),m2(12),m3(10),m3(11),m3(12),m4(10),
    m4(11),m4(12)];
r4025m=mean(r4025,2);
r5025=[m1(13),m1(14),m1(15),m2(13),m2(14),m2(15),m3(13),m3(14),m3(15),m4(13),
    m4(14),m4(15)];
r5025m=mean(r5025,2);
% Find mean over each row - 0.5 m
r105=[m6(1),m6(2),m6(3),m7(1),m7(2),m7(3),m8(1),m8(2),m8(3),m9(1),m9(2),m9(3)];
r105m=mean(r105,2);
r205=[m6(4),m6(5),m6(6),m7(4),m7(5),m7(6),m8(4),m8(5),m8(6),m9(4),m9(5),m9(6)];
r205m=mean(r205,2);
r305=[m6(7),m6(8),m6(9),m7(7),m7(8),m7(9),m8(7),m8(8),m8(9),m9(7),m9(8),m9(9)];
r305m=mean(r305,2);
r405=[m6(10),m6(11),m6(12),m7(10),m7(11),m7(12),m8(10),m8(11),m8(12),m9(10),
    m9(11),m9(12)];
r405m=mean(r405,2);
r505=[m6(13),m6(14),m6(15),m7(13),m7(14),m7(15),m8(13),m8(14),m8(15),m9(13),
    m9(14),m9(15)];
r505m=mean(r505,2);
% Make scatter plot
x=[0.1, 0.25, 0.5];
y1=[r101m,r1025m,r105m];
y2=[r201m,r2025m,r205m];
y3=[r301m,r3025m,r305m];
y4=[r401m,r4025m,r405m];
y5=[r501m,r5025m,r505m];
figure(1)
hold on
scatter(x,y1,100,'ro')
scatter(x,y2,100,'g+')
scatter(x,y3,100,'b*')
scatter(x,y4,100,'kd')
scatter(x,y5,100,'ms')
legend('Row 1','Row 2','Row 3','Row 4','Row 5')
set(gca,'fontsize',14)
set(gcf,'color','white')
xlabel('Drop height (m)','FontSize',14)
ylabel('Max Pressure (kPa)','FontSize',14)
axis([0 0.7 0 500])
grid on

% Scatter plot of maximum pressure coefficient vs. drop height

v1=2*9.81*0.1*500;
v2=2*9.81*0.25*500;
v3=2*9.81*0.5*500;
v=[v1,v2,v3];
% Define pressure coefficients each drop height
c1=y1./v;
```

```
c2=y2./v;
c3=y3./v;
c4=y4./v;
c5=y5./v;
% Plot
figure(2)
hold on
scatter(x,c1*1000,100,'ro')
scatter(x,c2*1000,100,'g+')
scatter(x,c3*1000,100,'b*')
scatter(x,c4*1000,100,'kd')
scatter(x,c5*1000,100,'ms')
legend('Row 1','Row 2','Row 3','Row 4','Row 5')
set(gca,'fontsize',14)
set(gcf,'color','white')
xlabel('Drop height (m)','FontSize',14)
ylabel('Cp = Pmax/(0.5*rho*V^2)','FontSize',14)
axis([0 0.7 0 100])
grid on

% Scatter plot pf maximum force vs. drop height

% Load filtered force measurements
load('ffilt_01.mat')
load('ffilt_02.mat')
load('ffilt_03.mat')
load('ffilt_04.mat')
load('ffilt_06.mat')
load('ffilt_07.mat')
load('ffilt_08.mat')
load('ffilt_09.mat')
load('ffilt_10.mat')
load('ffilt_11.mat')
load('ffilt_12.mat')
% Max each drop height
f01=[max(ffilt10),max(ffilt11),max(ffilt12)];
f025=[max(ffilt01),max(ffilt02),max(ffilt03),max(ffilt04)];
f05=[max(ffilt06),max(ffilt07),max(ffilt08),max(ffilt09)];
f=[f01,f025,f05];
x=[0.1,0.1,0.1,0.25,0.25,0.25,0.25,0.5,0.5,0.5,0.5];
% Plot
figure(3)
hold on
scatter(x,f*1000,100,'b*')
set(gca,'fontsize',14)
set(gcf,'color','white')
xlabel('Drop height (m)','FontSize',14)
ylabel('Max Force (N)','FontSize',14)
axis([0 0.7 0 400])
grid on

% Scatter plot of slamming pressure duration vs. drop height

% Load slamming pressure duration
load('dur9801.mat')
load('dur9802.mat')
load('dur9803.mat')
load('dur9804.mat')
load('dur9806.mat')
load('dur9807.mat')
load('dur9808.mat')
```

```
load('dur9809.mat')
load('dur9810.mat')
load('dur9811.mat')
load('dur9812.mat')

% Find mean over each row - 0.1 m
d101=[d10(1),d10(2),d10(3),d11(1),d11(2),d11(3),d12(1),d12(2),d12(3)];
d101m=mean(d101,2);
d201=[d10(4),d10(5),d10(6),d11(4),d11(5),d11(6),d12(4),d12(5),d12(6)];
d201m=mean(d201,2);
d301=[d10(7),d10(8),d10(9),d11(7),d11(8),d11(9),d12(7),d12(8),d12(9)];
d301m=mean(d301,2);
d401=[d10(10),d10(11),d10(12),d11(10),d11(11),d11(12),d12(10),d12(11),d12(12)];
d401m=mean(d401,2);
d501=[d10(13),d10(14),d10(15),d11(13),d11(14),d11(15),d12(13),d12(14),d12(15)];
d501m=mean(d501,2);
% Find mean over each row - 0.25 m
d1025=[d01(1),d01(2),d01(3),d02(1),d02(2),d02(3),d03(1),d03(2),d03(3),d04(1),
    d04(2),d04(3)];
d1025m=mean(d1025,2);
d2025=[d01(4),d01(5),d01(6),d02(4),d02(5),d02(6),d03(4),d03(5),d03(6),d04(4),
    d04(5),d04(6)];
d2025m=mean(d2025,2);
d3025=[d01(7),d01(8),d01(9),d02(7),d02(8),d02(9),d03(7),d03(8),d03(9),d04(7),
    d04(8),d04(9)];
d3025m=mean(d3025,2);
d4025=[d01(10),d01(11),d01(12),d02(10),d02(11),d02(12),d03(10),d03(11),d03(12),
    d04(10),d04(11),d04(12)];
d4025m=mean(d4025,2);
d5025=[d01(13),d01(14),d01(15),d02(13),d02(14),d02(15),d03(13),d03(14),d03(15),
    d04(13),d04(14),d04(15)];
d5025m=mean(d5025,2);
% Find mean over each row - 0.5 m
d105=[d06(1),d06(2),d06(3),d07(1),d07(2),d07(3),d08(1),d08(2),d08(3),d09(1),
    d09(2),d09(3)];
d105m=mean(d105,2);
d205=[d06(4),d06(5),d06(6),d07(4),d07(5),d07(6),d08(4),d08(5),d08(6),d09(4),
    d09(5),d09(6)];
d205m=mean(d205,2);
d305=[d06(7),d06(8),d06(9),d07(7),d07(8),d07(9),d08(7),d08(8),d08(9),d09(7),
    d09(8),d09(9)];
d305m=mean(d305,2);
d405=[d06(10),d06(11),d06(12),d07(10),d07(11),d07(12),d08(10),d08(11),d08(12),
    d09(10),d09(11),d09(12)];
d405m=mean(d405,2);
d505=[d06(13),d06(14),d06(15),d07(13),d07(14),d07(15),d08(13),d08(14),d08(15),
    d09(13),d09(14),d09(15)];
d505m=mean(d505,2);
% Make scatter plot
x=[0.1, 0.25, 0.5];
d1=[d101m,d1025m,d105m];
d2=[d201m,d2025m,d205m];
d3=[d301m,d3025m,d305m];
d4=[d401m,d4025m,d405m];
d5=[d501m,d5025m,d505m];
figure(4)
hold on
scatter(x,d1*1000,100,'ro')
scatter(x,d2*1000,100,'g+')
scatter(x,d3*1000,100,'b*')
scatter(x,d4*1000,100,'kd')
```

```
scatter(x,d5*1000,100,'ms')
legend('Row 1','Row 2','Row 3','Row 4','Row 5')
set(gca,'fontsize',14)
set(gcf,'color','white')
xlabel('Drop height (m)','FontSize',14)
ylabel('Slamming Duration (ms)','FontSize',14)
axis([0 0.7 0 0.4])

% Scatter plot of slamming force duration

% Load slamming force duration
load('fdur9801.mat')
load('fdur9802.mat')
load('fdur9803.mat')
load('fdur9804.mat')
load('fdur9806.mat')
load('fdur9807.mat')
load('fdur9808.mat')
load('fdur9809.mat')
load('fdur9810.mat')
load('fdur9811.mat')
load('fdur9812.mat')

f2=[fd10,fd11,fd12,fd1,fd2,fd3,fd4,fd6,fd7,fd8,fd9];
x=[0.1,0.1,0.1,0.25,0.25,0.25,0.25,0.5,0.5,0.5,0.5];
% Make scatter plot
figure(5)
hold on
scatter(x,f2*1000,100,'b*')
set(gca,'fontsize',14)
set(gcf,'color','white')
xlabel('Drop height (m)','FontSize',14)
ylabel('Slamming force duration (ms)','FontSize',14)
axis([0 0.7 0 10])

% Scatter plot pf rise time of pressure vs. drop height

% Load rise time
load('rise9801.mat')
load('rise9802.mat')
load('rise9803.mat')
load('rise9804.mat')
load('rise9806.mat')
load('rise9807.mat')
load('rise9808.mat')
load('rise9809.mat')
load('rise9810.mat')
load('rise9811.mat')
load('rise9812.mat')

% Find mean over each row - 0.1 m
ri101=[rise10(1),rise10(2),rise10(3),rise11(1),rise11(2),rise11(3),rise12(1),
    rise12(2),rise12(3)];
ri101m=mean(ri101,2);
ri201=[rise10(4),rise10(5),rise10(6),rise11(4),rise11(5),rise11(6),rise12(4),
    rise12(5),rise12(6)];
ri201m=mean(ri201,2);
ri301=[rise10(7),rise10(8),rise10(9),rise11(7),rise11(8),rise11(9),rise12(7),
    rise12(8),rise12(9)];
ri301m=mean(ri301,2);
ri401=[rise10(10),rise10(11),rise10(12),rise11(10),rise11(11),rise11(12),
```

```
    rise12(10),rise12(11),rise12(12)];
ri401m=mean(ri401,2);
ri501=[rise10(13),rise10(14),rise10(15),rise11(13),rise11(14),rise11(15),
    rise12(13),rise12(14),rise12(15)];
ri501m=mean(ri501,2);
% Find mean over each row - 0.25 m
ri1025=[rise1(1),rise1(2),rise1(3),rise2(1),rise2(2),rise2(3),rise3(1),
    rise3(2),rise3(3),rise4(1),rise4(2),rise4(3)];
ri1025m=mean(ri1025,2);
ri2025=[rise1(4),rise1(5),rise1(6),rise2(4),rise2(5),rise2(6),rise3(4),
    rise3(5),rise3(6),rise4(4),rise4(5),rise4(6)];
ri2025m=mean(ri2025,2);
ri3025=[rise1(7),rise1(8),rise1(9),rise2(7),rise2(8),rise2(9),rise3(7),
    rise3(8),rise3(9),rise4(7),rise4(8),rise4(9)];
ri3025m=mean(ri3025,2);
ri4025=[rise1(10),rise1(11),rise1(12),rise2(10),rise2(11),rise2(12),
    rise3(10),rise3(11),rise3(12),rise4(10),rise4(11),rise4(12)];
ri4025m=mean(ri4025,2);
ri5025=[rise1(13),rise1(14),rise1(15),rise2(13),rise2(14),rise2(15),
    rise3(13),rise3(14),rise3(15),rise4(13),rise4(14),rise4(15)];
ri5025m=mean(ri5025,2);
% Find mean over each row - 0.5 m
ri105=[rise6(1),rise6(2),rise6(3),rise7(1),rise7(2),rise7(3),rise8(1),
    rise8(2),rise8(3),rise9(1),rise9(2),rise9(3)];
ri105m=mean(ri105,2);
ri205=[rise6(4),rise6(5),rise6(6),rise7(4),rise7(5),rise7(6),rise8(4),
    rise8(5),rise8(6),rise9(4),rise9(5),rise9(6)];
ri205m=mean(ri205,2);
ri305=[rise6(7),rise6(8),rise6(9),rise7(7),rise7(8),rise7(9),rise8(7),
    rise8(8),rise8(9),rise9(7),rise9(8),rise9(9)];
ri305m=mean(ri305,2);
ri405=[rise6(10),rise6(11),rise6(12),rise7(10),rise7(11),rise7(12),
    rise8(10),rise8(11),rise8(12),rise9(10),rise9(11),rise9(12)];
ri405m=mean(ri405,2);
ri505=[rise6(13),rise6(14),rise6(15),rise7(13),rise7(14),rise7(15),
    rise8(13),rise8(14),rise8(15),rise9(13),rise9(14),rise9(15)];
ri505m=mean(ri505,2);
% Make scatter plot
x=[0.1, 0.25, 0.5];
ri1=[ri101m,ri1025m,ri105m];
ri2=[ri201m,ri2025m,ri205m];
ri3=[ri301m,ri3025m,ri305m];
ri4=[ri401m,ri4025m,ri405m];
ri5=[ri501m,ri5025m,ri505m];
figure(6)
hold on
scatter(x,ri1*1000,100,'ro')
scatter(x,ri2*1000,100,'g+')
scatter(x,ri3*1000,100,'b*')
scatter(x,ri4*1000,100,'kd')
scatter(x,ri5*1000,100,'ms')
legend('Row 1','Row 2','Row 3','Row 4','Row 5')
set(gca,'fontsize',14)
set(gcf,'color','white')
xlabel('Drop height (m)','FontSize',14)
ylabel('Rise Time (ms)','FontSize',14)
axis([0 0.7 0 0.35])
```